Master thesis

Quantifying Greenhouse Gas Emissions of Offshore Wind Farm Decommissioning

Sustainable Energy Technology

F.J. van Gaalen

Delft University of Technology

TU Delft

Master thesis

Quantifying Greenhouse Gas Emissions of Offshore Wind Farm Decommissioning

by

F.J. van Gaalen

To obtain the degree of Master of Science
at the Delft University of Technology

Student number:	4724992
Project Duration:	January, 2024 - October, 2024
Thesis committee:	Prof. dr. D.A. von Terzi
	Dr. Ir. M.B. Zaayer
	Dr. F. Yin
Daily supervisor:	Dr. V.V. Dighe

TU Delft

Preface

Six years ago, my career at Delft University of Technology started with the Bachelor's program in Mechanical Engineering. During this study, my interest and passion for sustainability grew, which eventually led to my decision to pursue the Master's program in Sustainable Energy Technology. In particular, I focused on the technology behind two of the largest renewable energy sources: solar and wind energy. Additionally, I have explored one of the main challenges of renewable energy, namely intermittency and the associated necessity of energy storage.

The crucial role of the North Sea in the production of offshore wind energy sparked my interest and motivated me to investigate a topic that will become increasingly important: the decommissioning of offshore wind farms. In this research, I specifically focused on the emissions generated during this phase, in order to also identify the environmental challenges of offshore wind energy.

The past years, and particularly the last nine months, have shaped me both personally and professionally. I am grateful for the numerous opportunities, experiences, and friendships that have fostered my growth, both inside and outside the university.

First, I would like to express my gratitude to my supervisors, Michiel Zaayer and Vinit Dighe, for their invaluable guidance and clear communication. Your feedback and insights have strengthened the effectiveness of our meetings and allowed me to continuously improve my research. I am especially thankful to Michiel for his extensive, detailed feedback on my thesis draft. I would also like to express my appreciation to my colleagues at TNO for their warm welcome, stimulating conversations and shared knowledge on wind energy. Special thanks go to Kamiel Jansen and Jesse Bloothoofd for their valuable contributions to this research. Finally, I would like to thank my family and friends for their unconditional support and encouragement throughout my thesis project. Your support has been essential in helping me reach this milestone, and I am deeply grateful for that.

The result of this thesis project is a piece of work that I am very proud of. Through this research, I aim to contribute to reducing emissions during the decommissioning of offshore wind farms, moving towards a climate-neutral future without greenhouse gas emissions.

Floortje van Gaalen
Amsterdam, October 2024

Abstract

The decommissioning of offshore wind farms (OWFs) presents a significant challenge due to the environmental impact associated with the process, particularly in terms of greenhouse gas (GHG) emissions. This research aims to develop a model for quantifying and analysing the GHG emissions associated with large-scale OWF decommissioning. It examines key variables, including vessel types, decommissioning activities, transport strategies, and weather conditions, to assess their impact on total emissions.

Using a GHG inventory-based approach, the research applies both deterministic and probabilistic methods to assess emissions across various decommissioning scenarios. The model integrates operational logistics with emission factors, providing a flexible framework that adapts to different OWF projects. The research specifically examines the decommissioning of OWF Lincs Limited.

The results of this study highlight the potential for emissions reduction through optimised vessel strategies, transport methods, and campaign scheduling. While operational activities dominate emissions, the research underscores the importance of addressing external factors, such as weather and campaign timing, to minimise environmental impact. The developed model offers valuable insights to stakeholders aiming to implement effective GHG emission reduction strategies in future OWF decommissioning projects.

Keywords
Offshore wind farms (OWFs), decommissioning, greenhouse gas (GHG), direct emissions, offshore activities, GHG inventory model, vessels

Contents

List of Figures

List of Tables

Nomenclature

Abbreviations

Abbreviation	Definition
AC	Alternating current
AHP	Analytic hierarchical process
AHTS	Anchor handling tug supply
AR	Assessment report
AWJ	Abrasive water jet
CEM	Continuous emission measurement
CH_4	Methane
CLB	Cable laying barge
CLV	Cable laying vessel
C	Carbon
CF_4	Tetrafluoromethane
CO	Carbon monoxide
CO_2	Carbon dioxide
CTV	Crew transport vessel
DSA	Deterministic sensitivity analysis
DC	Direct current
DCBV	Derrick crane barge vessel
DP	Decommissioning programme
DWSC	Diamond wire saw cutting
EC	Export cables
ECA	Emission control area
EoL	End-of-Life
EVT	Extreme value theory
FOU	Foundation
GBS	Gravity-based structures
GHG	Greenhouse gas
GSA	Global sensitivity analysis
GUI	Graphical user interface
GW	Gigawatt
GWP	Global warming potential
HCl	Hydrogen chloride
HCV	Higher calorific value
HF	Hydrogen fluoride
HFC	Hydrofluorocarbon
HFO	Heavy fuel oil
HHV	Higher heating value
HLV	Heavy lift vessel
HS	High speed
HVAC	High voltage alternating current
HVDC	High voltage direct current
IAC	Inter-array cables
IMO	International maritime organisation
IOA	Input-Output Analysis
IPCC	Intergovernmental Panel on Climate Change
JUB	Jack-up barge

Abbreviation	Definition
JUV	Jack-up vessel
LCA	Life cycle Analysis
LCV	Lower calorific value
LSA	Local sensitivity analysis
LHV	Lower heating value
LNG	Liquefied natural gas
MCDA	Multi-criteria decision analysis
MDO	Marine diesel oil
MGO	Marine gas oil
MM	Meteorological mast
MS	Medium speed
MW	Megawatt
N	Nitrogen
NF_3	Nitrogen trifluoride
NH_3	Ammonia
NMVOCs	Non methane volatile organic compounds
NO_x	Nitrogen oxides
N_2O	Nitrous oxide
O&M	Operation & maintenance
OAT	One-at-a-time
OSS	Offshore substation
OSV	Offshore support vessel
OWE	Offshore wind energy
OWF	Offshore wind farm
PFC	Perfluorocarbon
PM	Particulate matter
RDV	Rock dumping vessel
ROV	Remotely operated vehicle
SF_6	Sulphur hexafluoride
SOV	Service operation vessel
SO_2	Sulphur dioxide
SO_x	Sulphur oxides
SP	Scour protection
SPMT	Self-propelled modular transporter
SPL	Scour protection layer
SS	Slow speed
SSCV	Semi-submersible crane vessel
SWATH	Small water area twin hull
TB	Tug boat
TLP	Tension-leg platform
TNO	Netherlands Organisation for Applied Scientific Research
TTW	Tank-to-Wheel
ULSFO	Ultra low sulphur fuel oil
UWiSE	Unified Wind Farm Simulation Environment
VLSFO	Very low sulphur fuel oil
WSM	Weighted sum model
WT	Wind turbine
WTIV	Wind turbine installation vessel
WTT	Well-to-Tank
WTW	Well-to-Wheel
W2WV	Walk-to-work-vessel

Symbols

Symbol	Definition	Unit
FC	Fuel consumption	**[tonne/hr]**
EF_f	Fuel-based emission factor	**[kg/tonne]**
EF_e	Energy-based emission factor	**[kg/kWh]**
GWP	Global warming potential	**[-]**
LCV	Lower calorific value	**[MJ/kg]**
η	Thermal efficiency	**[%]**
$T_{transit}$	Transiting duration	**[hr]**
T_{idle}	Idling/operating duration	**[hr]**
W	Effective engine energy	**[kWh]**
μ	Mean or location parameter (mu)	**[context-dependent]**
σ	Standard deviation or scale parameter (sigma)	**[context-dependent]**
π	Pi	**[-]**
H_s	Significant wave height	**[m]**

1 Introduction

This chapter provides an introduction to the study and consists of six sections. First, section 1.1 will provide general background information, introducing the topic of the study. Next, section 1.2 will indicate the gap in research and thereby analysing the problem. Afterwards, section 1.3 will provide the aim of the study, the main research question, and sub-questions. Section 1.4 will subsequently describe the scope of the study, followed by a research approach in section 1.5 and then finally description of the thesis outline in section 1.6.

1.1. Background

Climate change is a pressing issue, driving the growing interest and research in various renewable energy technologies in order to tackle this global challenge. To further motivate this interest, several international agreements have been established. One of these is the Paris Climate Agreement. This is a legally binding international convention on climate change, which was created in 2015. This agreement aims to limit global warming to well below 2 °C above pre-industrial levels, ideally even at 1.5 °C (Nations, 2024). Among others, has this agreement accelerated the transition from fossil-based energy sources to renewable and clean sources. Solar and wind power are the fastest growing renewable energy sources, where wind seems to be the most reliable and practical. In addition, wind power, especially offshore wind power, produces the fewest emissions of all energy source (Dinh & McKeogh, 2018). Offshore wind power has several advantages over onshore, consisting of lower visual impact, less turbulence and lower noise constraints allowing higher turbine rotor speeds and larger turbines. Due to these advantages, the offshore wind industry has been expanding in the past decades. Europe plays an important role within the wind energy sector, as wind farms are installed in 11 different countries, with most of them in the North Sea. The North Sea is home to the largest offshore wind farm (OWF) in the world with a capacity of 1218 megawatt (MW) and 174 turbines by 2020 (Chirosca et al., 2022). European policy documents indicate that an increase in offshore wind of 450 gigawatt (GW) is needed by 2050, of which 85% will be developed in the North Sea (WindEurope, 2019).

The life of an OWF can be divided into six different life cycle phases, which are the development, manufacturing, installation, operation and maintenance (O&M), decommissioning and end-of-life (EoL) phase (Dinh & McKeogh, 2018) (Joustra et al., 2020). The decommissioning phase is becoming increasingly important at the moment as many wind farms in the North Sea region are scheduled to be decommissioned in the next decade. At the moment only a few OWFs have been decommissioned, which are described in subsection 2.2.1 and presented in table 2.1. Therefore, the experience and knowledge in this area is limited (Spielmann et al., 2021). The decommissioning phase itself can also be divided into three different sub-phases, which are called pre-decommissioning, dismantling and post-decommissioning (Topham & McMillan, 2017). Subsequently, the dismantling sub-phase can be divided into several stages. These stages consist of preparing and removing all components of an OWF. Whether all these stages are performed depends on the scope.

According to Topham, Gonzalez, et al. (2019), OWF decommissioning faces two primary challenges: cost and environmental impact. The environmental impact includes factors such as seabed disturbance, air quality, effects on marine life, ecological consequences, and emissions. When considering emissions, a distinction can be made between air pollutants and greenhouse gases (GHGs) (NAEI, 2022). Quantifying GHG emissions from these processes is crucial, particularly due to the GHG Protocol, a global standard widely used for measuring and managing GHG emissions in both the private and public sectors (Institute & for Sustainable Development, 2004). Various methodologies exist to quantify GHG emissions throughout the life cycle of an OWF, with different approaches capturing distinct emission scopes. Direct emissions, classified as scope 1 (NationalGrid, 2023), refer to emissions directly produced by decommissioning activities, such as fuel consumption by vessels. In contrast, indirect emissions (scope 2 and scope 3) include those from supporting processes, such as electricity generation for equipment (scope 2) and supply chain activities like material production and recycling (scope 3).

1.2. Problem definition

The global shift towards renewable energy has led to a substantial increase of OWFs, particularly in regions such as the North Sea. As the first generation of OWFs reaches the end of their operational life, decommissioning these large-scale infrastructures presents several challenges. Several studies, such as those by Gillian Smits (2015), Adedipe et al. (2021) and Milne et al. (2021), have developed cost models for OWF decommissioning processes. In addition to these holistic cost models, the Netherlands Organisation for Applied Scientific Research (TNO) has developed a high-fidelity simulation tool for optimising the processes in OWF decommissioning based on cost and time. This tool developed by TNO is called Unified Wind Farm Simulation Environment (UWiSE) decommissioning (TNO, 2023). However, limited attention has been given to the environmental impacts of decommissioning, specifically the GHG emissions associated with the various activities involved. The activities involved in OWF decommissioning are complex, and no comprehensive models currently exist that integrate both logistics planning and emission calculations. This gap in research highlights the need for a more comprehensive understanding of the emissions generated during OWF decommissioning for the continued growth of the offshore wind industry.

1.3. Research question

This research aims to address the current gap regarding emissions from OWF decommissioning by developing a GHG emissions assessment model. The main objective of the study is summarised in the following main research question.

How can GHG emissions associated with the decommissioning of a large-scale OWF be effectively quantified and assessed?

This main question will be answered through research, which will be conducted using the following research questions:

1. *How can the decommissioning phase be characterised and how does the phase affect GHG emissions?*
    (a) What operational procedures and technologies will be employed in the decommissioning of large-scale OWFs?
    (b) What parameters of the decommissioning process must be taken into account to ensure a thorough quantification of GHG emissions?
2. *What approaches can be utilised to measure GHG emissions based on the specified parameters during the decommissioning of an OWF?*
    (a) What are the existing methods and their mathematical principles for measuring GHG emissions, as identified through literature review?
    (b) What operational criteria and limitations must the model adhere to for effective implementation?

(c) Which methodology for quantifying GHG emissions is best suited for the decommissioning of OWFs?

3. *How could a tool designed to calculate emissions from various activities involved in decommissioning of an OWF be conceptualised, particularly in terms of its appearance and functional design features?*
4. *What preliminary insights can be drawn from the tool in terms of its capability to assess GHG emission reduction strategies for future offshore wind farm decommissioning projects?*

1.4. Research scope

This section outlines the scope of this research. First, the focus is on direct GHG emissions generated during OWF decommissioning, which are also referred to as Scope 1 emissions, as mentioned in Section 1.1. Consequently, indirect emissions (Scope 2 and 3) are excluded from this study. Second, the scope is limited to offshore activities related to OWF decommissioning. This is due to the reliance on output data from TNO's UWiSE Decommission tool (TNO, 2023), which is restricted to offshore processes. As a result, onshore activities are not included in this research.

1.5. Research approach

The process of this research is presented in the flow diagram in figure 1.1. This flow diagram is based on the main question and research questions mentioned in section 1.3.

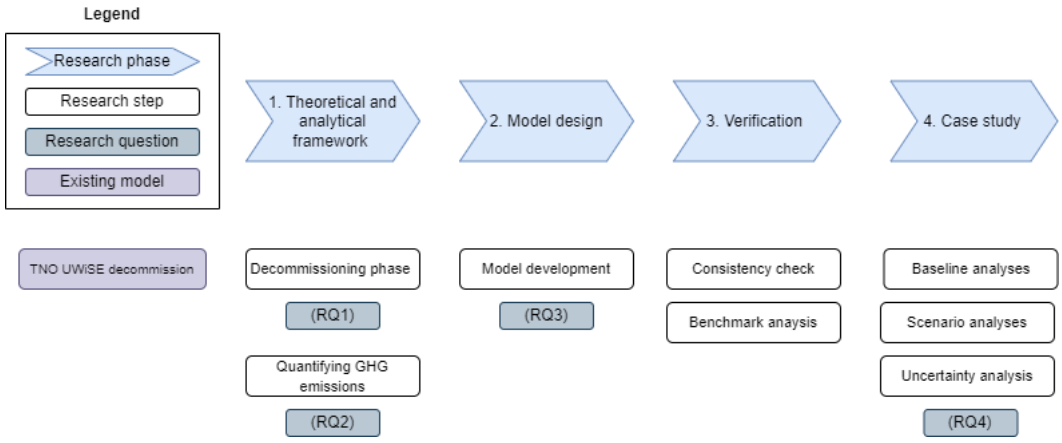

Figure 1.1: Research process flow diagram

The first phase of the research is the construction of the theoretical and analytical foundation. This is accomplished by conducting literature research, followed by analyses performed upon the retrieved information. This will identify all offshore operational procedures and technologies where direct GHG emissions are released during OWF decommissioning. In addition, it will also provide the most suitable approach for quantifying GHG emissions of OWF decommissioning. Therefore, this phase answers the first two research questions.

The second phase of the research is to design the model. This GHG emission assessment model will quantify emissions during the OWF decommissioning phase and will be developed in Python. For the development of the model, both the output from the already existing decommissioning tool called UWiSE, and the output from the first phase are required. Together, this will add up to a model that can quantify direct GHG emissions during offshore operations in OWF decommissioning.

The third phase of the study will verify the model built in the second phase. The verification starts with a consistency check to ensure that the model provides realistic results. Subsequently, a benchmark will be performed using an existing LCA tool, named Brightway (Brightway, 2024).

The final phase of this study comprises a case study, including a baseline emission analysis, scenario analysis, and uncertainty analysis. The purpose of the baseline emission analysis is to quantify and map vessel- and activity-related emissions. The scenario analysis aims to evaluate the impact of weather conditions and transport strategies. Finally, uncertainty analysis is designed to assess the effect of input uncertainties on the output, identifying which parameters have the greatest impact. The analysis includes both deterministic and probabilistic sensitivity assessments, as well as uncertainty propagation. This phase provides preliminary insights on reduction strategies for future OWF decommissioning projects, thereby answering the fourth research question.

While a case study from the North Sea region is used as an example, the findings are expected to have broader global relevance. This because the challenges and processes involved in OWF decommissioning are similar across different regions, making the results applicable on an international scale.

Eventually, the four process phases discussed in the text above, answer the research questions. This collectively provides an answer to the main question.

1.6. Report outline

This section provides the outline of the remainder of this report. First, chapter 2 establishes the theoretical and analytical framework, covering offshore wind energy, decommissioning process, UWiSE Decommission tool and approaches for quantifying GHG emissions. Subsequently, chapter 3 presents the model design for both deterministic and probabilistic approaches, along with the mathematical formulation. After that, chapter 4 provides the verification of the developed model, which includes consistency checks and a benchmark analysis. Then, chapter 5 applies the model to a case study, incorporating baseline emission analyses, scenario assessments and uncertainty propagation. Finally, chapter 6 concludes the research, summarising the key findings and offering recommendations for future research.

2

Theoretical and analytical framework

This chapter provides both the theoretical and analytical framework for the research, focusing on the decommissioning phase of an OWF and its impact on GHG emissions. Section 2.1 introduces offshore wind energy (OWE) through an overview of OWFs and their life cycle phases. In section 2.2, the decommissioning phase of an OWF is elaborated, addressing the first research question. This section starts with an introduction of the phase, followed by a detailed description of its sub-phases and stages. Subsequently, the vessels, fuels, and strategies involved in decommissioning are outlined, along with the removal and cutting techniques. Finally, the key parameters influencing GHG emissions will be identified. Section 2.3 will then explain TNO's existing tool, UWiSE Decommission. Finally, section 2.4 examine how GHG emissions released from OWF decommissioning can be quantified, addressing the second research question. First, GHG emissions will be introduced, followed by an overview of approaches to quantifying them and finally a multi-criteria decision analysis (MCDA) for the selection of the most suitable methodology for this research.

2.1. Offshore wind energy

This section will provide information on OWE. First, subsection 2.1.1 introduces OWFs, followed by an overview of the life cycle phases of OWFs in subsection 2.1.2.

2.1.1. Offshore wind farms

This subsection will provide key information on OWFs. First, the sector will be introduced, highlighting both the opportunities and challenges. Subsequently, an overview of the different systems, subsystems and components of which an OWF consists will be provided.

Global warming remains a major global concern, and renewable energy sources are crucial solutions to mitigate its effects. Over the past decades, several international protocols, such as the Kyoto Protocol, the Paris Climate Agreement and the European 2030 Climate and Energy Framework, have been established to address this issue (Jalili et al., 2022). The European Union aims to be the first climate-neutral continent (Eckardt, 2022). According to the International Energy Agency, the energy sector contributes significantly to global emissions, with nearly half of total emissions in 2018 attributed to this sector (Jalili et al., 2022). Therefore, the transition from fossil-based energy to renewable and renewable sources such as solar, wind and bio energy has been initiated. Among these, wind energy, particularly offshore wind energy, has proven to be one of the most reliable and practical solutions.

The electricity produced by wind power has increased tremendously in recent decades for this reason, to a capacity of 129 GW in 2014 in Europe. Therefore wind power is the fastest developing renewable energy technology of all existing ones (Huang et al., 2017). From this, the European Energy Association has outlined the prediction that wind power capacity within Europe will rise further to a total of 320 GW by 2030. This will cover 24% of Europe's total electricity demand by then (Bonou et al., 2016). Wind energy can be generated both on land and offshore. Land-based wind energy, as already mentioned in section 1.1, has limitations on both view and noise. As a result, in certain countries, the development

limit of onshore wind energy has been reached. In contrast, OWE has virtually no visual, turbulence and noise restrictions, allowing higher turbine rotor speeds and larger turbines. Other advantages of offshore over onshore wind energy include more full-load hours, longer lifetime and higher energy production. The higher energy production results from the fact that offshore has higher and more stable wind speeds (Dinh & McKeogh, 2018). Another pleasant fact is the high availability of space at sea, which makes large-scale projects possible (Vis et al., 2016). All the advantages of offshore over onshore wind power are the reason that moving to offshore is said to be the driving force of wind energy technology development. These advantages resulted in a massive growth of the wind power industry with a remarkable increasing number of OWFs further offshore. The first OWF was installed in Denmark in 1991, and since then the offshore wind industry has grown to an installed capacity in Europe of 18.5 GW, hereby becoming the world's leader in this industry (Topham, Gonzalez, et al., 2019). Leading countries include United Kingdom, Germany, Denmark, Belgium and the Netherlands (Spielmann et al., 2021). The annual and cumulative capacity between 1991 to 2015 within Europe, non-Europe and globally can be seen in figure 2.1 (Kaldellis & Apostolou, 2017).

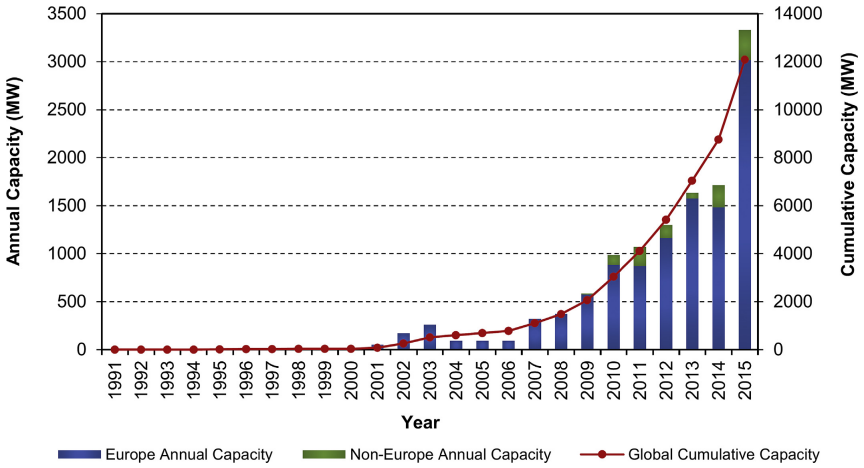

Figure 2.1: Offshore wind energy evolution (Kaldellis & Apostolou, 2017)

Further substantial growth of OWFs is expected (Huang et al., 2017). In fact, recently the expected growth within Europe has been announced to be 150 GW and 460 GW in 2030 and 2050, respectively (Jalili et al., 2022).

OWE presents both opportunities and challenges. First, the opportunities will be discussed. Wind speeds are generally 20% higher at sea than on land due to lower surface resistance, and the ocean climate is more stable, resulting in a higher number of full-load hours annually. These factors create the potential for reduced energy costs, although this remains uncertain due to the high upfront costs associated with offshore installations. Furthermore, the steadier wind speeds at sea can lead to reduced wear on wind turbine components, thereby extending the service life of offshore wind substructures. Other potential benefits include the continuity of a sustainable electricity supply, creation of jobs and new opportunities within the supply chain, synergies with or replacement of offshore oil and gas platforms, and an overall improvement in environmental quality (Dinh & McKeogh, 2018). Additionally, OWFs can have positive ecological effects, with research indicating that foundation structures like monopiles create new habitats for marine species (Perveen et al., 2014). However, OWE also faces significant challenges. Wind variability complicates grid integration, and the unpredictable nature of wind makes forecasting difficult. Additionally, the installation, operation and maintenance (O&M), and decommissioning phases are challenging due to the large, heavy components involved and the likelihood of adverse weather conditions. Negative ecological impacts also exist, such as risks to bird life through collisions, habitat loss, and interference with migration routes, as well as noise pollution from construction, which can affect marine mammals and fish. Finally, current costs are high and difficult to predict (Dinh & McKeogh, 2018). The opportunities and challenges mentioned are among the most critical for OWE, although many others exist.

An OWF consists of several offshore systems, which can be divided into sub-systems and further into components, each made from different materials. The five main systems in an OWF are the wind turbine (WT), the offshore substation (OSS), the meteorological mast (MM), the transmission system, and scour protection (SP). These systems serve different functions and can vary in design and structure. A detailed breakdown of the sub-systems, components, and materials is provided in table A.1 in appendix A. A study by Bonou et al. (2016) concluded that metals, particularly steel, dominate the material composition of OWF infrastructure. The paragraph below provides a concise overview of the purpose and structure of the five main systems.

First, the WT is the primary system responsible for generating electricity. It consists of several subsystems: the rotor, nacelle, tower, and support structure. First, the rotor converts wind energy into mechanical energy, while the nacelle houses key components like the gearbox and generator (Eckardt, 2022). Subsequently, the tower provides essential structural support. Additionally, the support structure consists of the transition piece, which connects the wind turbine to the foundation, and the foundation itself. The foundation, which can either be fixed or floating, secures the WT to the seabed (Topham, McMillan, et al., 2019). Fixed foundations include gravity-based structures (GBS), monopiles, tripods, tripiles, suction buckets, and jackets. Floating foundations consist of tension-leg platforms (TLP), semi-submersible structures, spar-buoys, and pontoons (Chirosca et al., 2022). The choice of foundation depends on both the water depth and seabed conditions.
Subsequently, the OSS is essential for transforming electricity generated by the WTs to a higher voltage for efficient transmission to shore. It consists of a topside, where transformers and switchgear are located, and a support structure, typically a jacket foundation, which stabilises it on the seabed (Eckardt, 2022).
In addition, the MM is used to measure wind speeds and other environmental conditions, which helps optimise the performance of the OWF. It consists of similar subsystems as the OSS but is smaller and lighter (GL, 2014).
Moreover, the transmission system, which includes inter-array cables (IAC) and export cables (EC), is responsible for transporting electricity from the WTs to the OSS and then to shore. Depending on the distance to shore, the electricity is transmitted using either alternating current (AC) or high voltage direct current (HVDC) systems (Eckardt, 2022).
Finally, SP is used around the foundations of the WTs and OSS to prevent erosion of the seabed caused by water currents. Common methods of scour protection include concrete mattresses, natural stone, gravel, and geocontainers (Eckardt, 2022).

Appendix A provides more detailed description of these systems, consisting of the purpose and the potential variations in their design and functionality.

At present, the majority of OWFs are equipped with WTs with a capacity of 2 to 4 MW, predominantly installed on monopile foundations (Gillian Smits, 2015). A trend in the OWE is to move OWFs in deeper waters, where more consistent and energy-dense wind resources can be utilised. This shift enables greater nominal power output from WTs, but also necessitates the use of longer blades, larger generators, and taller towers. As a result, the increased weight of the topside structures requires monopiles with larger diameters to ensure stability (Topham, McMillan, et al., 2019). Consequently, OWFs are increasingly consuming more materials, particularly steel, to accommodate these structural demands.

2.1.2. Life cycle phases

This subsection will provide an overview of the life phases of an OWF. Each phase will be explained in detail, after which the focus of this research will be clearly outlined.

As mentioned in section 1.1, an OWF typically consists of six different life cycle phases, namely development and licensing, manufacturing of all components, installation, operation & maintenance, decommissioning and finally EoL. An overview of the life cycle phases of an OWF can be observed in figure 2.2, showing the different activities that take place in each phase. A description of the phases engaged in offshore processes such as the installation, O&M and decommissioning of an OWF will be provided below. In all of these phases, logistics strategies and methods as well as weather are important factors.

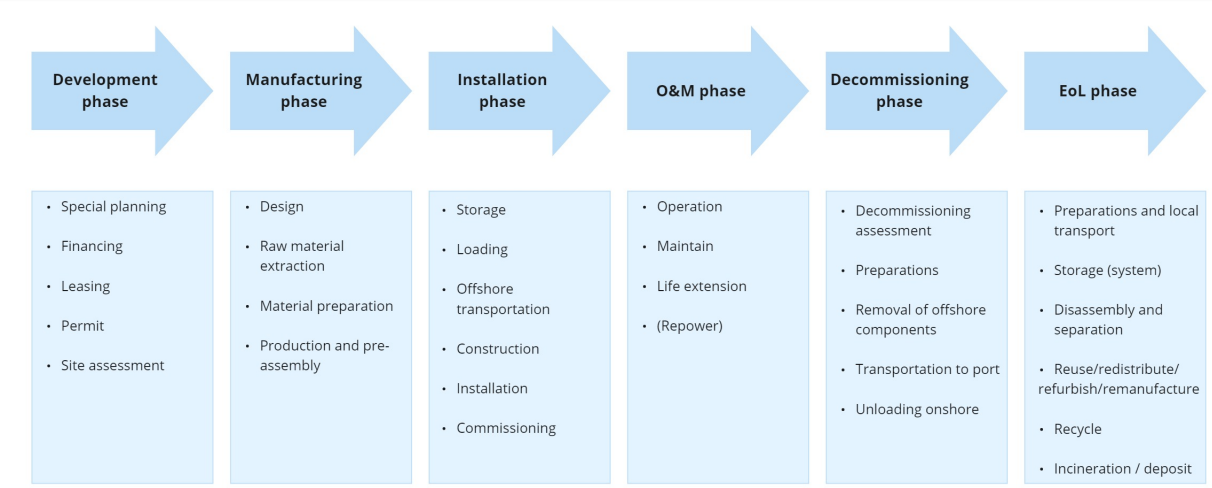

Figure 2.2: OWFs life cycle phases with associated activities, data retrieved from (Joustra et al., 2020)

To start, the installation of an OWF can be divided into three key steps. Step one is the construction of the sub sea infrastructure, step two is the installation of the towers, nacelles and rotor blades and finally step three is the connection to the power grid (Huang et al., 2017). Several types of methods are available for installing the WTs, namely the bunny-ear, full rotor star and part-by-part (Vis et al., 2016). However, by now only part-by-part method is actually used because of increasingly larger offshore WTs. Using the part-by-part method saves deck space on ships, and the work is less wind sensitive (Eckardt, 2022). When the installation of the OWF is completed, then the OWF will commission and thereby go into operation. The next phase of the OWF is O&M. During the operational phase of the OWF, which is linked to its life time, maintenance will take place. The expected operational life time of OWFs is between 20 and 25 years. However, due to harsh weather conditions and site-specific characteristics, there is much uncertainty surrounding the length of operational life (Jalili et al., 2023). During this time span, a number of scheduled and unscheduled maintenance tasks must be performed to keep the offshore WTs operational and maintain energy production. There is a difference in minor and major maintenance, and the types of vessels are adjusted accordingly (Dalgic et al., 2015). To maintain high efficiency of the OWF, maintenance of offshore WTs usually consists of scheduled maintenance 1 to 2 times and unscheduled maintenance 1 to 4 times per year per WT. At the end of the operational time of an OWF the last two phases, decommissioning and EoL, begin. In EoL phase, the primary goal is to address waste recycling and disposal to minimise environmental impact. This with the aim of returning the site to its original state (Huang et al., 2017). Several scenarios are possible before the end of life of an OWFs. The potential scenarios for the EoL phase are presented in figure 2.3.

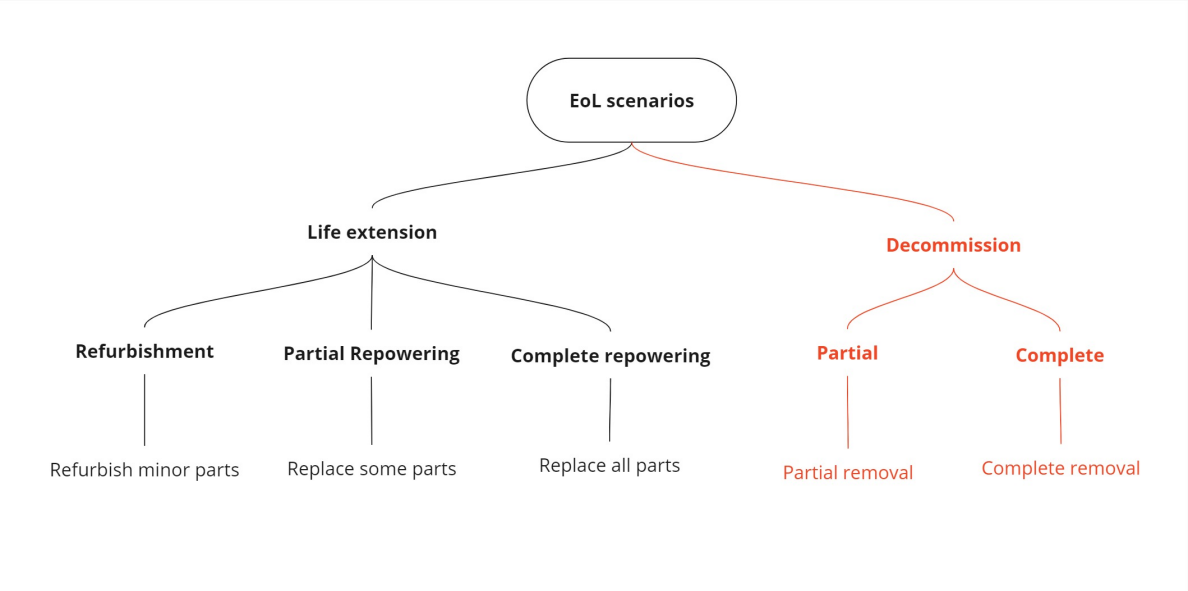

Figure 2.3: OWFs potential EoL scenarios, data retrieved from (Hall et al., 2020)

As shown in figure 2.3, at the end of the operational design life of an OWF, two main paths are possible: life extension or decommissioning. The decision on the final scenario at the end of the O&M phase depends on several factors, including the cost of immediate decommissioning, any maintenance or monitoring requirements, environmental considerations, and regulatory obligations (Hall et al., 2020). If life extension is chosen, further options are available, such as repowering or refurbishment. Repowering involves replacing the existing WTs with more powerful ones, achieving the same capacity with fewer turbines. This option is typically pursued when the location of the OWF proves ideal for continued wind energy generation. On the other hand, refurbishment entails replacing less critical components, such as the drive train and rotor, while retaining the foundation, tower, and cables where possible. In this option, existing projects are upgraded to enhance energy production (Topham & McMillan, 2017). Although life extension may postpone decommissioning, it remains an inevitable phase in the life cycle for all OWFs (Topham, Gonzalez, et al., 2019). Therefore, decommissioning, indicated by the red option in figure 2.3, is considered the most critical EoL scenario. As decommissioning is the focus of this research, the remaining life cycle phases will not be considered from this point onward. Decommissioning is often considered as the reverse of the installation phase (Topham, McMillan, et al., 2019) and can be either partial or complete. Partial decommissioning may occur under specific circumstances, such as when a structure can be repurposed or when full removal would pose an unacceptable risk to the marine environment. In the absence of these conditions, complete decommissioning is typically required, which generally refers to the removal of all structures above the water surface (Hall et al., 2020). As shown in figure 2.2, the decommissioning phase involves several activities. It begins with a decommissioning assessment, followed by preparatory activities. Next, the offshore components of the OWF are removed, transported to shore, and unloaded at the port. This marks the end of the decommissioning phase. However, the life cycle of the OWF components is not complete once they reach the port. First, preparations and land transportation will take place, then components will be stored. After that, components will be disassembled or material will be separated, depending on the waste management strategy applied (Joustra et al., 2020). The disposal of OWF components is conducted according to the waste hierarchy, as shown in figure 2.4.

Figure 2.4: Waste hierarchy (John, 2023)

The aim for the material received onshore from the OWF, to the extent possible, is to be reused, alternatively recycled or incinerated for energy recovery. If none of these alternatives is possible, for example due to the presence of an environmentally hazardous substance, the material will be disposed of in a landfill (Gjødvad & Ibsen, 2016). For each of the materials, listed in table A.1 in appendix A, a treatment is available. The different type of treatments for processing are recycling, incineration and disposal (Huang et al., 2017). This study concluded that glass fiber, rubber and plastic cannot be recycled. Hence, the most discussed issue of WT dismantling is indeed the processing of the turbine blades. These are in fact made of glass fiber reinforced composite, as shown in table A.1. The difficulties in processing the rotor blades are due to several factors. The materials of the blades consist of a complex structure composed of different parts and materials, this depending on the manufacturer and the year of production (Joustra et al., 2020).

The various life cycle phases of the OWF have been outlined briefly above. This study, however, focuses on quantifying the direct GHG emissions released from the decommissioning phase. As such, the other life cycle phases shown in figure 2.2 fall outside the scope of this research and will not be further discussed. From this point onward, the decommissioning phase will be examined in detail.

2.2. Decommissioning of offshore wind farms

In this section, the decommissioning phase of an OWF will be characterised and its impact on GHG emissions will be analysed. Therefore, this section will answer the first research question. The answer is supported by several subsections. First, subsection 2.2.1 introduces the decommissioning phase of an OWF. Subsequently, subsection 2.2.2 discusses the various sub-phases and stages involved in OWF decommissioning. Subsection 2.2.3 outlines the different vessels, fuels and transport strategies relevant to OWF decommissioning. Additionally, subsection 2.2.4 provides an overview of the removal and cutting techniques utilised. Finally, in subsection 2.2.5 the key parameters that influence GHG emissions within the decommissioning of an OWF will be given.

2.2.1. Introduction

This subsection introduces the decommissioning phase of an OWF. It begins with an explanation of the decommissioning programme (DP). Subsequently, the OWFs decommissioned to date will be outlined, highlighting the challenges that arise due to the limited experience in this area.

Of the different life cycle phases of OWFs highlighted in subsection 2.1.2, this research will focus on the decommissioning phase. Decommissioning is the final phase of a project's life cycle, and can be considered the opposite of the installation phase. In the decommissioning phase, the "polluter pays" principle applies, implying that the site of the OWF must be left in the same condition as before commissioning (Topham & McMillan, 2017). There are several life-limiting factors that can lead to the decommissioning of an OWF. These factors may be technological, economic, legal, commercial or organisational in nature. In order to carry out decommissioning properly, a decommissioning program (DP) exists. In Scotland, OWF owners must submit such a DP to get approval for the installation phase. This therefore means only once the DP is approved can the OWF be installed. In a DP, the owners/developers of OWFs must forecast detailed decommissioning costs, techniques and approaches (Jalili et al., 2023). The study, Topham and McMillan (2017), investigated several existing DPs, and observed that each DP, and therefore ultimately the decommissioning of each project, differs from each other. An important observation therefore is that the requirements and activities for decommissioning are unique to each site. Hence, there is not one single operational procedure because the location, time, type of structures, equipment used, market conditions and contractual conditions differ from each other. For that reason, this study also investigated which factors have the most impact on such a DP. The key aspects were found to be the reduction of time, cost and environmental impact.

Up to now, there is not much experience in decommissioning OWFs. Table 2.1 shows which OWFs have been decommissioned globally to date.

Table 2.1: Overview of decommissioned OWFs worldwide, data retrieved from (4C Offshore, 2024)

OWF Name	WTGs	Farm Capacity [MW]	Shore Distance [km]
Beatrice Demo	2	10	25
Blyth	2	4	1.5
Fukushima Forward II	2	12	20
Irene Vorrink	28	16.8	-
Kemin Ajoksen I&II	10	30	2.6
Lely	4	2	-
Utgrunden I	7	10.5	5
Vindeby	11	5	1.8
Yttre Stengrund	5	10	2

These decommissioned wind farms consisted of relatively small turbines (450-2000 kW) in shallow water (4-15m) close to shore. Only the Beatrice and Fukushima Forward wind farms were in somewhat deeper water further from shore. These former smaller OWFs consist of some turbines, their foundations and with the electricty being delivered directly to a substation on land. In contrast, the OWFs of this generation are considerable larger, incorporating MM and OSS to collect the power (Gillian Smits, 2015). The experience gained to date from decommissioning smaller OWFs cannot be transferred to

larger OWFs located further offshore in deeper water (Spielmann et al., 2021). There is therefore lack of knowledge for decommissioning of large-scale OWFs further offshore. However, decommissioning of offshore oil and gas facilities in the North Sea and Gulf of Mexico has been going on since 1990. This decommissioning uses certain techniques that would be easily adapted to offshore wind industry decommissioning. Those techniques include heavy lifting techniques for removing topsides, removing piles below the mud-line and removing foundations. Thus, knowledge can be gained from the experience that does exist in decommissioning offshore oil and gas installations. However, there are also many differences between the offshore decommissioning of these two industries. In fact, oil and gas installations are often single entities, located hundreds of miles from shore on hundreds of feet of deep water. In addition, the pipelines and rooms of these facilities are often polluted with hydrocarbons and radioactive residues. Due to characteristics of the oil and gas industry, decommissioning logistics are, in turn, very different from those of the offshore wind industry (Gillian Smits, 2015) (Winkler et al., 2022).

While the decommissioning of oil and gas platforms offers some insight, the increasing number of large-scale OWFs approaching decommissioning in the North Sea region presents unique challenges. The North Sea is a crucial European region due to its resources, sea routes, and key ports for maritime transport (Chirosca et al., 2022). The region has also experienced significant growth in OWFs, with many projects now approaching the end of their operational life. To illustrate the scale of decommissioning activities, figure 2.5 provides an overview of the specific locations of existing OWFs in the North Sea region.

Figure 2.5: Specific locations of OWFs in the North Sea region (Wikipedia, 2023)

Additionally, appendix B lists all 59 operational OWFs in the North Sea region (4C Offshore, 2024) (Wikipedia, 2023). The table includes details such as the name of each OWF, turbine type and quantity, year of commissioning, projected decommissioning year, distance to shore and type of foundation. As discussed in subsection 2.1.2, the operational lifespan of an OWF typically ranges from 20 to 25 years, though advancements in technology may extend this for future projects (Joustra et al., 2020). Based on these estimates, several OWFs in the North Sea region are expected to begin decommissioning between 2020 and 2030, with many more scheduled in the decades to follow. Figure 2.6 illustrates the number of WTs from the North Sea region expected to be decommissioned in each decade.

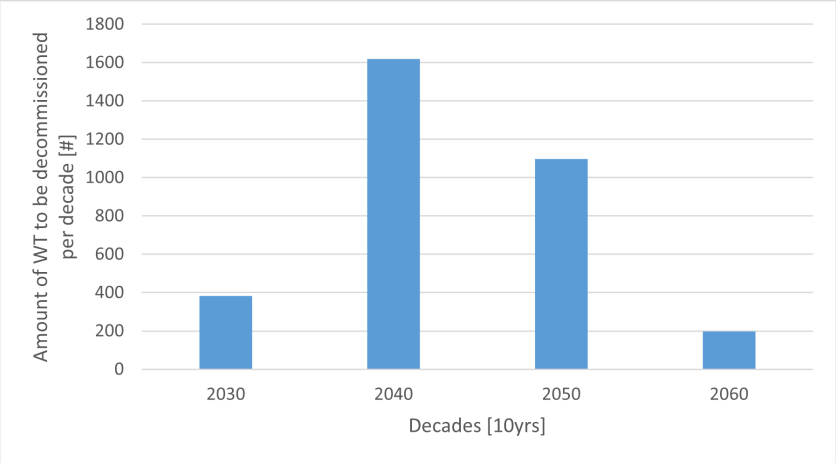

Figure 2.6: Amount of WT to be decommissioned per decade in the North Sea region, data retrieved from (4C Offshore, 2024)

This growing volume of decommissioning projects highlights the importance of researching the environmental impacts of these activities, further reinforcing the relevance of this study. Although there is little experience in decommissioning OWFs, it is clear that this process presents several challenges. The challenges in the decommissioning process are in fact similar to those in the installation phase. The different levels of planning, i.e., strategic, tactical and operational, present different challenges (Beinke et al., 2018). There are four major challenges in OWF decommissioning. Starting with the first challenge being the regulations, these are currently very limited and not specific to decommissioning OWFs. Existing regulations for oil & gas are taken as a starting point and, of course, general Health, Safety & Environment regulations must be followed (Gjødvad & Ibsen, 2016). Creating specific guidelines is highly recommended to ensure that owners can be held accountable (Winkler et al., 2022). The second challenge is process planning. Decommissioning process planning is far from simple as it varies from project to project. First, it is difficult to plan properly 10 years before decommissioning because of the substantial changes that may occur regarding technical feasibility. In addition, it is difficult to optimise both planning and costs due to high vessel costs and unpredictable weather. And the final factor that makes planning difficult is the lifetime of the WTs, which is a lot shorter than that of cables and foundations (Topham, Gonzalez, et al., 2019). The third challenge for decommissioning an OWF is the availability of vessels. Decommissioning requires specialised vessels with lifting and stability characteristics. The availability of these vessels is not very high due to the high demand for them, which consists of the predicted demand for new offshore wind installations, the O&M procedure of the already operational projects and in addition the decommissioning of oil and gas installations. Therefore, it is important that contractual arrangements are made well in advance. A large part of the cost of decommissioning consists of vessel rental, and in order to reduce it somewhat, the duration of activities must be carefully studied. However, the duration of activities is difficult to estimate because it is affected by daily rates, the availability of equipment, and unpredictable weather (Topham, Gonzalez, et al., 2019) (Topham & McMillan, 2017). The final challenge for decommissioning an OWF is the environmental impact. In this there are two main aspects. The first aspect is the debate over the need for either total or partial removal. The reason is that substructures can become habitats for marine wildlife, such as fish or shellfish (Hall et al., 2022). The second important aspect is to reuse or recycle as much material as possible, thus making the decommissioning as sustainable as possible (Topham, Gonzalez, et al., 2019).

2.2.2. Sub-phases and stages

In this subsection, the various sub-phases and stages of OWF decommissioning will be described. This answers research question 1a. First, the three main sub-phases will be outlined and discussed. Subsequently, the specific stages within these sub-phases that fall within the scope of this research will be examined in detail.

The decommissioning phase of OWFs can be decomposed into different sub-stages. Afterwards, the different stages and, in turn, processes within them will be described. The decommissioning phase will begin with preliminary work to plan the program and obtain the required permits. Subsequently, the process of removing parts of the OWF will begin. Finally, the monitoring stage ensures that the site has been left in the proper condition (Topham, Gonzalez, et al., 2019). Based on this, the decommissioning can be divided into three sub-phases, which are pre-decommissioning, dismantling and post-decommissioning (Topham & McMillan, 2017). This is a rough outline of the different parts within the decommissioning phase. This can be converted into a clearer decomposition structure of the different stages within OWF decommissioning. Based on the decomposition frameworks and additional information in various studies, Jalili et al. (2023), Topham and McMillan (2017), Winkler et al. (2022), Gjødvad and Ibsen (2016) and Eckardt (2022), an overview of all stages in the three sub-phases has been created. This is presented in figure 2.7.

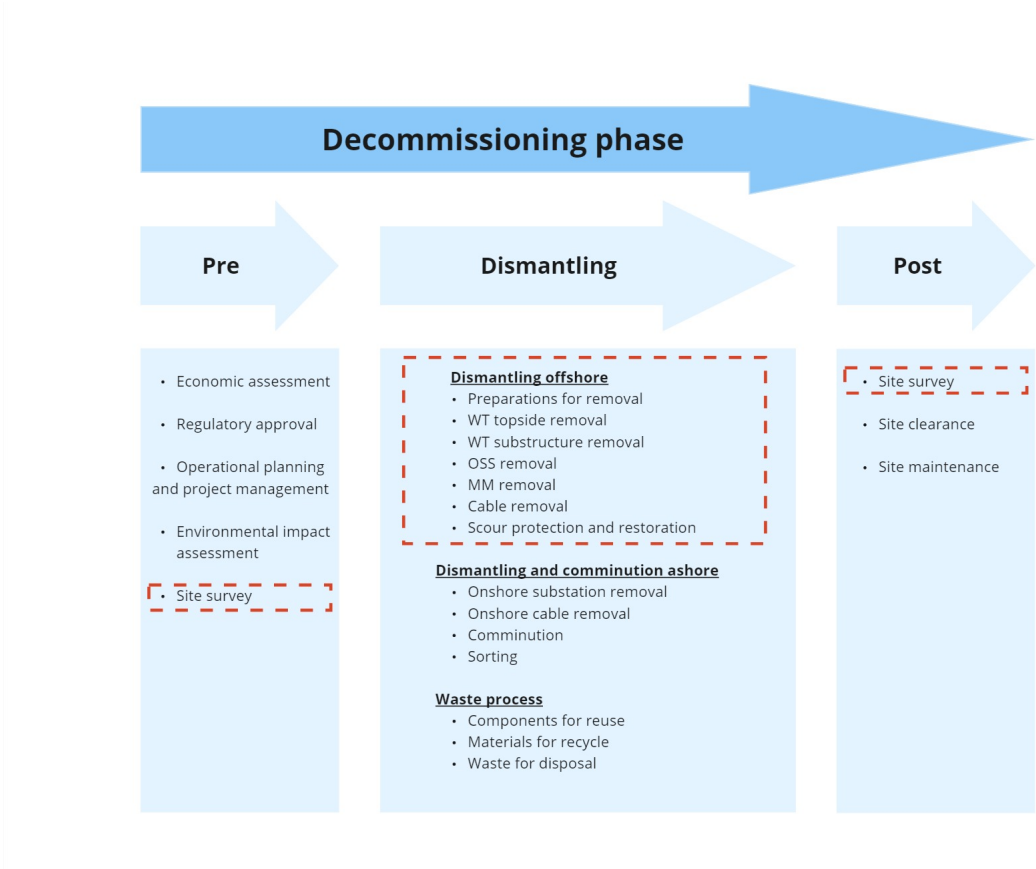

Figure 2.7: Sub-phases and stages within the decommissioning phase of an OWF

First, pre-decommissioning starts, which consists of the economic assessment, regulatory approval, operational planning and project management, environmental impact assessment and the site survey. Then the dismantling begins, which in itself can be further divided into offshore dismantling, onshore dismantling and waste treatment. Included in offshore dismantling are the preparations offshore and the removal of the topside of the WT, the sub structures of the WT, the OSS, the MM, the cables and the SP. The dismantling of each component at sea can be divided into the equipment operations and the transport of the dismantled components to land (Jalili et al., 2023). The onshore decommissioning includes the decommissioning of cables and onshore substation. In addition, all parts of the OWF are shredded and stored before being collected for the specific waste treatment that applies to each component or type of material. Within the waste treatment, first the components that can be reused are transported to the new site. Subsequently, the materials that can be recycled are transported to the factory where chemical processes for them will take place. Finally, the waste that needs to be disposed will be transported to a suitable location. Finally, the post decommissioning consists of a site survey,

clean-up and maintenance.

Figure 2.7 also shows the system boundaries of the study. It is clear that the focus in this study is on the direct GHG emissions released during the offshore fuel-consuming processes of decommissioning. What is therefore not included in the study are emissions released during other energy-consuming processes, onshore fuel and energy-consuming processes and processes during waste treatment. All stages that fall within the scope of the study, will be discussed in detail. For each stage all choices and possible processes will be presented in a flow chart. In preparing these flow charts for each stage, certain assumptions were made. These assumptions are in terms of type of vessel or equipment used. The assumptions are made based on the vessels and equipment that are most suitable for the type of operation and defined transportation strategy, according to the literature. However, it does not mean that this is the only type of vessel or equipment that can perform that operation. Additionally, it is important to note that the stages discussed are not presented in a fixed order, as the sequence of decommissioning activities can vary depending on the specific OWF configuration and site conditions. The following sections will discuss the stages of pre-decommissioning, dismantling, and post-decommissioning that fall within the system boundaries, as depicted in figure 2.7.

The pre-dismantling phase begins with a site survey, which is the only stage in this phase where direct GHG emissions result from offshore fuel-consuming processes. The steps within the site survey are shown in figure 2.8.

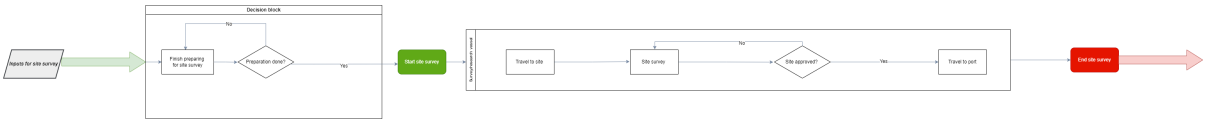

Figure 2.8: Process flow chart of the site survey in decommissioning phase of OWF

Once all preparations are complete, the site survey can begin, utilising a survey vessel to inspect each component at the site (Eckardt, 2022). After the vessel confirms that all components meet the necessary conditions, the vessel will return to the port. Subsequently, the second sub-phase, dismantling, will begin.

The dismantling phase starts with extensive preparations at the offshore site, which are critical before removal operations can start (Gjødvad & Ibsen, 2016). The preparations can be divided into the vessel-specific preparations, preparations at the port and preparations at the wind farm (Joustra et al., 2020). On-site preparations are the only ones that fall within the scope of this study, as these release direct GHG emissions from offshore fuel-consuming processes. What exactly happens in this preparation stage depends on the components to be removed, and the removal concept applied to them. In general, this stage amounts to the disconnection of electronic equipment and subsystems. The process flow chart of this stage is shown in figure 2.9.

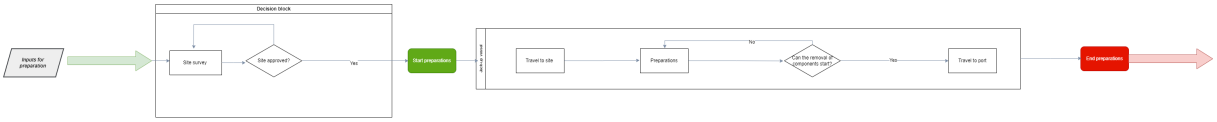

Figure 2.9: Process flow chart of the preparations in decommissioning phase of OWF

After that, removal of components of the OWF at sea can start. First, the topside of the WT will be removed. The topside of the WT includes the rotor, nacelle and tower, which will be removed (Jalili et al., 2023). There are different methods for the installation of the WT topside, and consequently different ways for its removal (Topham & McMillan, 2017). The main configurations for the installation and hence dismantling of the WT topside are the star configuration, bunny ear removal and the part-by-part removal method. The first two configurations require four lifting operations, while the third requires six (Hillers et al., 2023). The configuration used depends on the size and weight of the turbine, lifting capacity and vessel's deck space (Topham & McMillan, 2017). However, since the focus of this research is on large-scale OWFs in the North Sea, and these consist of large offshore WTs, only the part-by-part

removal configuration is considered (Jalili et al., 2023). In this configuration, all blades are removed in separate crane operations, which results in a total of six lifting operations. The advantages with this configuration are the fact that it saves deck space, and that the work is less sensitive to wind (Eckardt, 2022). A jack-up vessel (JUV) is normally used to perform the lifting of these parts. The process flow chart of this stage is shown in figure 2.10. In the decision block, the choice will have to be made whether to use a feeder or pendulum concept as the transportation strategy for the vessel logistics. The chosen transportation strategy will determine which type of vessel will transport the removed WT topside components to the port. When the feeder concept is chosen as the strategy, a transport ship will move the components to the port. There is generally no crane on the transport ship. Therefore, once arrived at the port, a large and a small auxiliary crane in tandem lift on land will be required to unload the vessel's deck (Eckardt, 2022). Since the focus of this study, as indicated in section 1.4, is on only the offshore fuel consuming activities, this activity is out of scope. With this reason, the on land cranes, and any direct GHG emissions associated with it, will not be considered in this study.

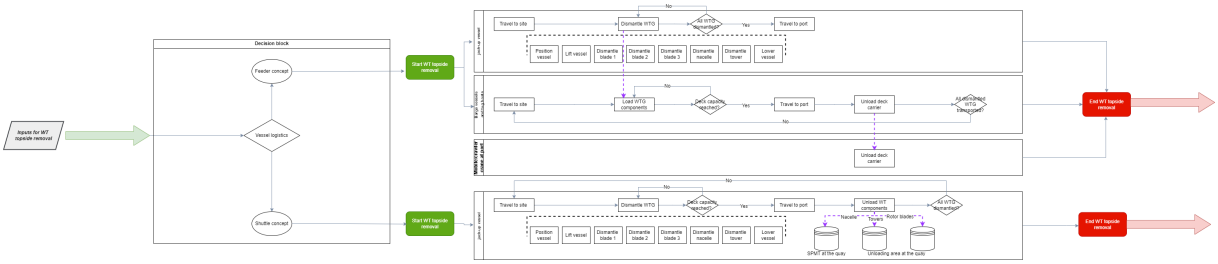

Figure 2.10: Process flow chart of the WT topside removal in decommissioning phase of OWF

Second, the substructure of the WT will be removed. The substructure of the WT includes the transition piece and foundation. During this stage, underwater pumping and cutting operations will take place. As a result, both a JUV, to lift these components, and a remotely operated vehicle (ROV), to support the subsea operations, will be used (Jalili et al., 2023). The operations performed depend on the type of foundation (Topham & McMillan, 2017). The process flow chart of this stage is shown in figure 2.11. In the decision block, choices will have to be made that affect the scope of decommissioning, namely whether the foundation will be partially or completely removed.If the foundation is partially removed, the choice is between removing it 1 meter below the seabed or 3 meters above it. Then there are also different cutting techniques for partial dismantling. The choices that are made here, and thus the operations that are eventually performed, depend on the type of foundation, as well as the seabed and the equipment available. In addition, similar to the decommissioning of WTs topside, the choice of whether to use a feeder or pendulum concept as transport strategy for vessel logistics is required. The chosen transportation strategy will determine which type of vessel will transport the removed WT substructure components to the port. When the feeder concept is chosen as the strategy, a transport ship will move the components to the port. There is generally no crane on the transport ship. Therefore, once arrived at the port, a large and a small auxiliary crane in tandem lift on land will be required to unload the vessel's deck (Eckardt, 2022). Since the focus of this study is on only the offshore fuel consuming activities, this activity is out of scope. For this reason, the on land cranes, and any direct GHG emissions associated with it, will not be considered in this study.

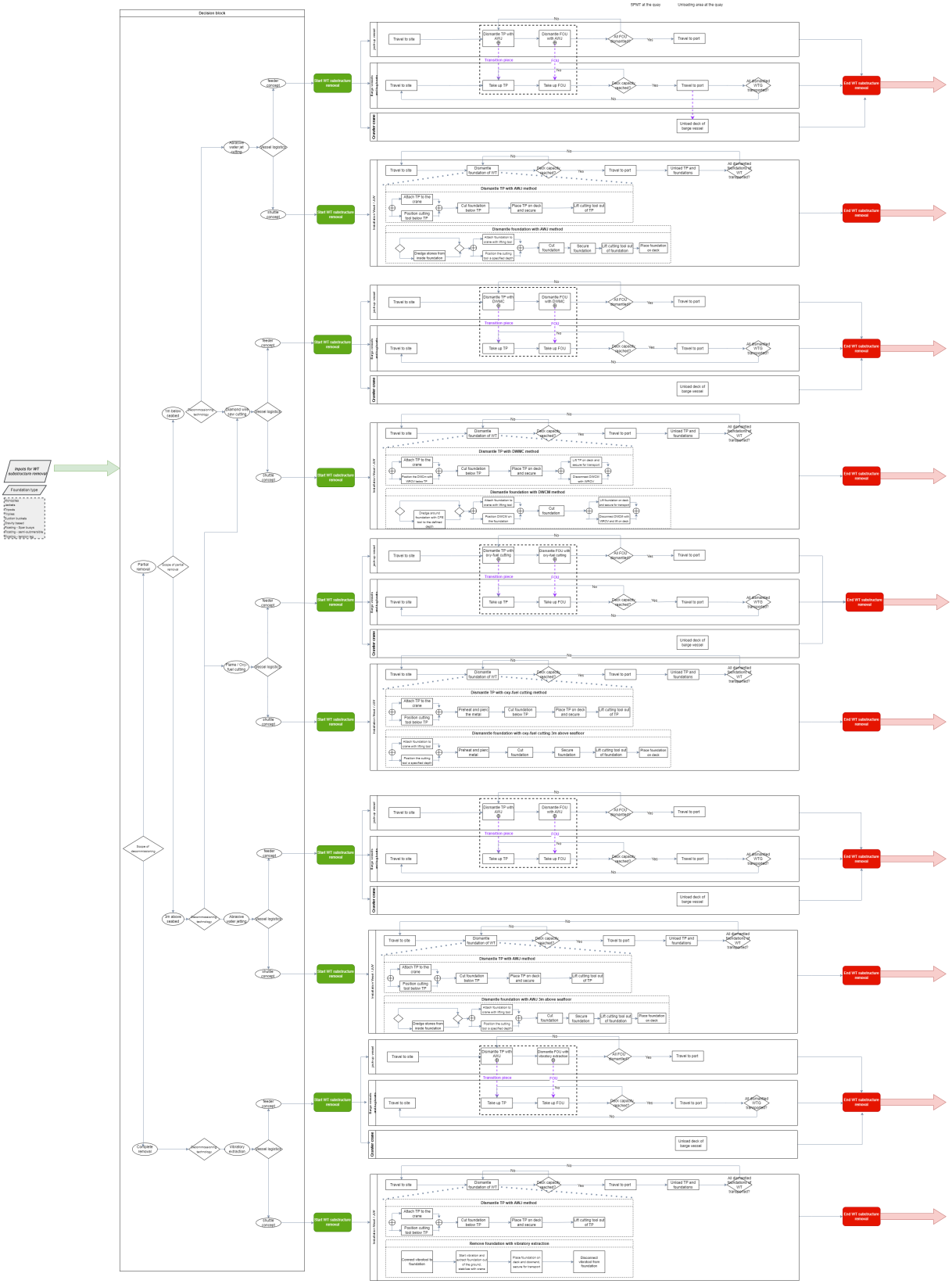

Figure 2.11: Process flow chart of the WT substructure removal in decommissioning phase of OWF

Third, the OSS will be removed. The OSS consists of the topside and substructure. The technique for dismantling the topside and substructure of the OSS is similar to that of the WT topside and substructure (Topham & McMillan, 2017). The components will also be lifted using a JUV (Jalili et al., 2023). The OSS is the most complex, large and heavy component of the OWF (Eckardt, 2022). The process flow chart of this stage is shown in figure 2.12. In the decision block, choices which will influence the scope of decommissioning are made. This includes decisions such as whether the foundation will be partially or completely removed. Subsequently, there are also different cutting techniques for partial dismantling. In this stage, it is not possible to choose between different transport strategies. As shown in the decision block, the removal of the OSS and its transport will be performed automatically with the feeder concept. This concept uses a transport vessel that generally lacks a crane. Visible in the flow chart, the topside and substructure of the OSS will therefore be removed from the vessel's deck, using a self-propelled modular transporter (SPMT). SPMT are self-propelled trolleys with several axles, often 4 to 8 axle lines per module. Hydraulically, surfaces can be raised and lowered by the SPMT. Large heavy components can be moved by the SPMT to storage or disassembly areas within the harbour (Eckardt, 2022). Since the focus of this study is on only the offshore fuel consuming activities, this activity is out of scope. For this reason, the SPMT, and any direct GHG emissions associated with it, will not be considered in this study.

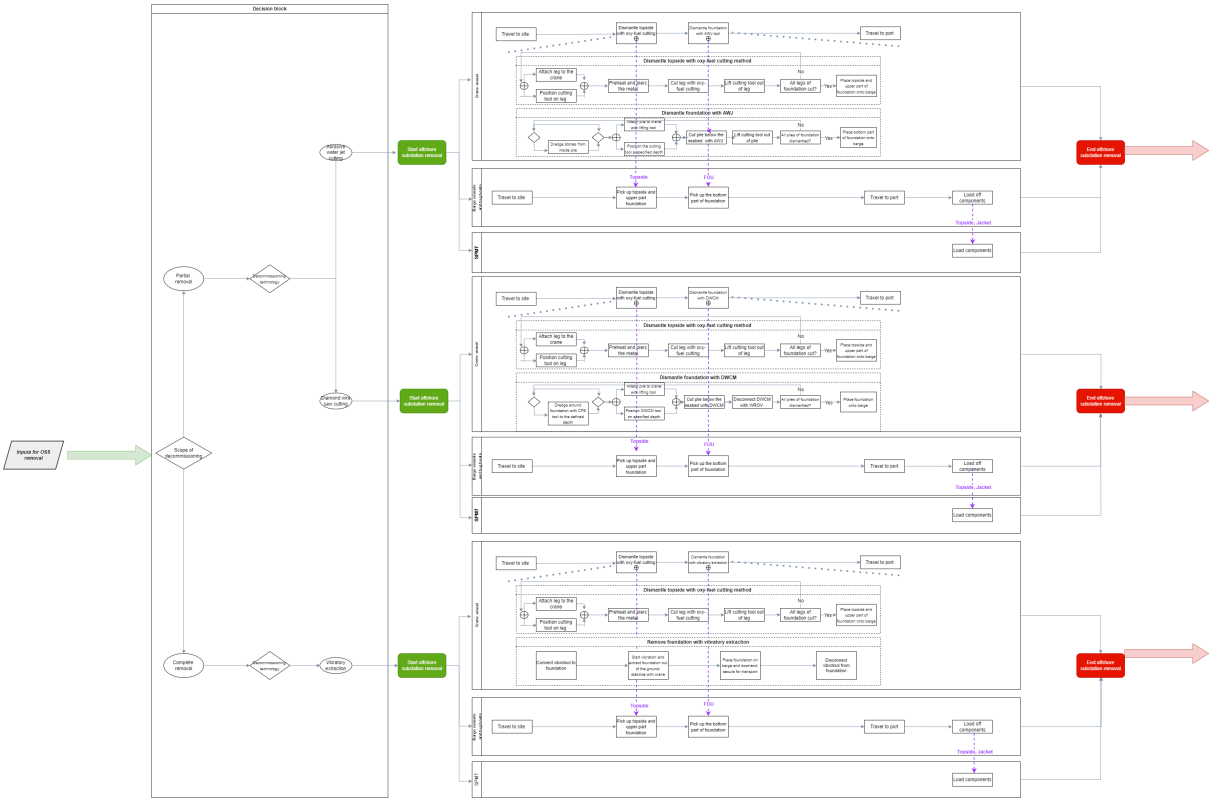

Figure 2.12: Process flow chart of the OSS removal in decommissioning phase of OWF

Fourth, the MM will be removed. The process and type of vessel used corresponds to those of the OSS dismantling. The only difference is that the topside and support structure of the MM are considerably lighter and smaller than those of the OSS. The process flow chart of this stage is shown in figure 2.13. Likewise, the decision block corresponds to that of the OSS.

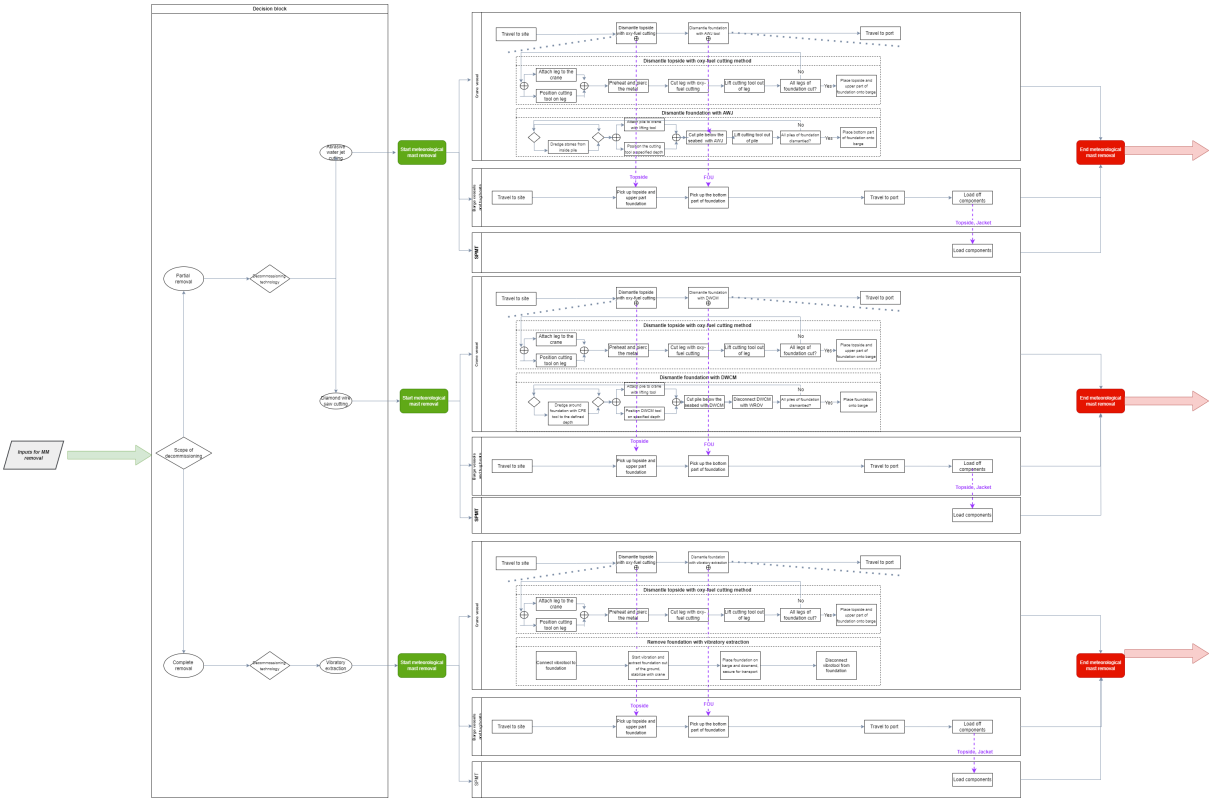

Figure 2.13: Process flow chart of the MM removal in decommissioning phase of OWF

Fifth, the submarine cables will be removed. The submarine cables consist of both IAC and EC. Typically, they are buried at a depth of more than one meter below the seabed. The process starts with locating the cables, where excavators and grabs can then be used to lift the cables from the ground and cut the necessary sections as close to the foundation as possible. The cables are then lifted onto the vessel and wrapped around a drum. The remaining ends are weighted and buried back in at approximately 1 meter (Topham & McMillan, 2017). For both the IAC and EC removal operation, a cable laying vessel (CLV) is used with subsea inspections performed by an ROV. The cable removal is expected to take place in a shorter time than the installation (Jalili et al., 2023). The process flow chart for removal of the IAC and EC are shown in figure 2.14 and 2.15 respectively. For both stages, a choice is to be made in the decision block that affects the scope of decommissioning, namely whether the cables will be removed or left in place. This will generally depend on whether the cable is buried or not, since the complete removal of covered cables is extremely costly (Topham & McMillan, 2017). However, there is a greater preference for leaving in situ for the EC than the IAC, as they are buried deeper. Removal of the EC will therefore involve higher costs and a bigger environmental disruption (Gillian Smits, 2015). As visible in the two flow charts, in addition to the CLV, a walk-to-work-vessel (W2WV) is used when removing the IAC, and when removing or leaving the EC in situ. A W2WV is designed to safely transfer personnel and equipment from the vessel to offshore platforms or wind turbines via a motion-compensated walkway.

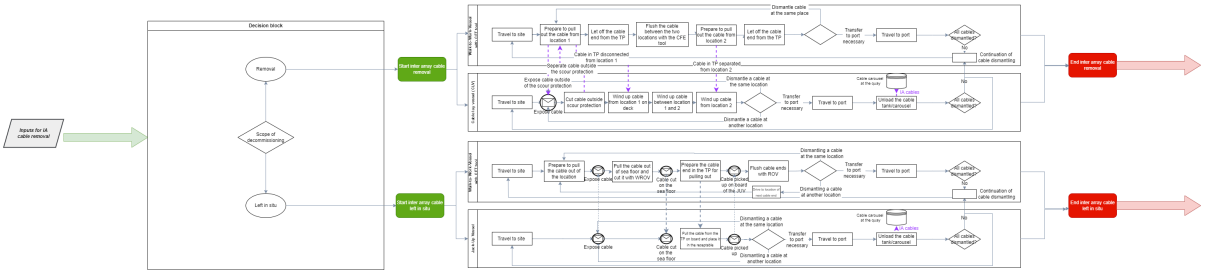

Figure 2.14: Process flow chart of the IAC removal in decommissioning phase of OWF

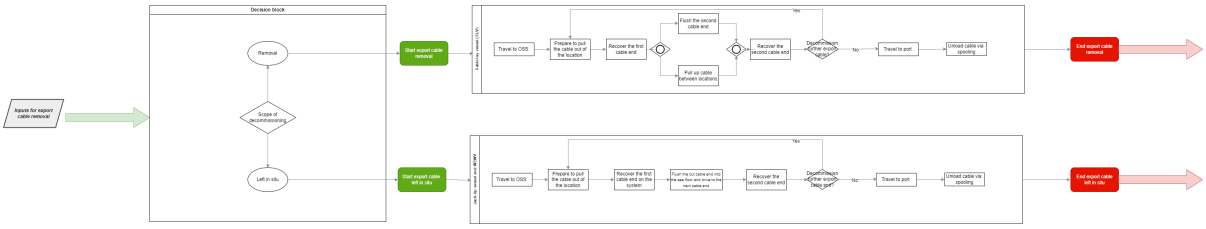

Figure 2.15: Process flow chart of the EC removal in decommissioning phase of OWF

Finally, the scour protection layer (SPL) will be removed. A derrick crane barge vessel (DCBV) will be used to remove the SPL. In addition, for inspection and support of the underwater assets, an ROV is also required (Jalili et al., 2023). If the SP consists of rock fill then the individual boulders are collected using a grab barge. In contrast, if the SP consists of reed mats, concrete platforms or other cable protection then a crane vessel is used (Topham & McMillan, 2017). The process flow chart of this stage is shown in figure 2.16. As with cable dismantling, the SP requires a choice of whether to remove it or leave it in place. This will generally depend on whether marine life has formed on the SP during the life time of the OWF. If that is the case then the SP is more likely to be left in place. This is an advantageous option from the environmental and cost point of view (Jalili et al., 2023) (Gillian Smits, 2015). If removal of the SPL is chosen in the decision block, then, as visible, different vessels will have to be used. This because also in this stage, the removal of the SPL and its transport will be performed automatically with the feeder concept. This concept uses a transport vessel that generally lacks a crane. Visible in the flow chart, the SPL will therefore be removed from the vessel's deck, using an excavator. Excavators are typically used on construction sites to lift large attachments (Eckardt, 2022). Since the focus of this study is on only the offshore fuel consuming activities, this activity is out of scope. With this reason, the excavator, and any direct GHG emissions associated with it, will not be considered in this study.

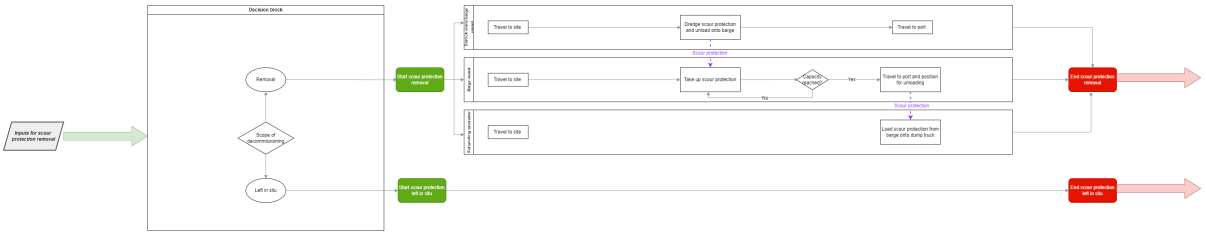

Figure 2.16: Process flow chart of the scour protection removal in decommissioning phase of OWF

Post-decommissioning

After the dismantling is complete, the post-dismantling phase includes a final site survey to confirm the removal of all relevant components. Similar to pre-decommissioning, the site survey is the only stage where direct GHG emissions will be released from fuel consuming processes at sea in post-decommissioning. The steps within the site survey are shown in figure 2.17. This process mirrors the initial site survey in pre-dismantling and involves similar steps. After each location has been verified to meet all required conditions and the vessel has returned to the port, the final sub-phase of decommissioning, and thereby the entire decommissioning phase, is considered complete.

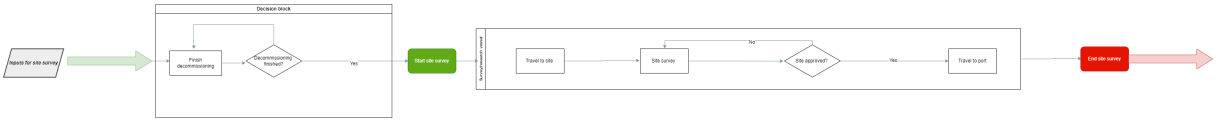

Figure 2.17: Process flow chart of the site survey in decommissioning phase of OWF

2.2.3. Vessels, fuels and transport strategies

This subsection provides an overview of the various vessels relevant to OWF decommissioning. Subsequently, the types of fuel used by these vessels will be discussed. The relationship between the decommissioning stages, vessel types, and fuel usage will then be examined. Finally, the two main transport strategies available for vessels will be explained.

For each stage within decommissioning, a description is given in subsection 2.2.2. The description includes the type of vessel typically used for the processes (Jalili et al., 2023). However, additional vessels exist beyond those specified in the description. To provide an overview, the vessels mentioned, along with other vessels relevant to decommissioning, are summarised in table 2.2. This table outlines key characteristics, including whether the vessels are self-propelled, the decommissioning stages in which they are typically used, and their associated fuel types. Detailed descriptions of these vessels can be found in appendix C.
For some processes it is already established which type of vessel will be involved. However, there are also enough processes where there are several possibilities in terms of vessels. Which type of vessel is finally chosen depends on several factors. First, the number of turbines and foundations in the OWF that need to be dismantled, as the amount of space on the deck of a vessel is important. Besides that, the weight of the components, which affects the crane capacity of a vessel. Furthermore, the water depth and seabed type of the location also play a role, as not all vessels can operate on all seabeds. Finally, the market availability of vessels is also a factor (Topham & McMillan, 2017). In addition to these stated factors, weather also affects the decommissioning process. Wave height and wind speed are the main variables affecting the weather during decommissioning (Hillers et al., 2023). Therefore, vessel operation limits will be matched to the wave and wind conditions of the site for each OWF project (Gillian Smits, 2015).

The marine shipping industry uses different types of fuels, each with their own characteristics and applications. The main options are diesel fuels, liquefied natural gas (LNG) and methanol. These three types of fuels will be described in more detail.
Diesel fuels are the most traditional, with the main types being Marine Gas Oil (MGO), Marine Diesel Oil (MDO) and Heavy Fuel Oil (HFO). MGO is a low-sulfur distillate fuel used primarily in emission control areas (ECAs), while MDO is a blend of residual and distillate fuels. Finally, HFO, a residual oil, can have a high sulfur content. Although variants, such as very low sulfur fuel oil (VLSFO) and ultra low sulfur fuel oil (ULSFO), have lower sulfur content to meet stricter regulations (van Lieshout et al., 2020) (Lindstad et al., 2020).
LNG has gained popularity because of its environmental benefits. It emits significantly less sulfur oxides (SO_x) and particulate matter (PM) than traditional diesel fuels. There were 175 LNG-fueled ships in operation in early 2020, and a growing number of ships are LNG-ready. The market share of LNG is expected to increase and, according to some forecasts, may reach 41% by 2050 (Faber et al., 2021) (Lindstad et al., 2020). However, the GHG benefits of LNG are slightly mitigated by methane leakage during combustion, which can reduce the overall environmental benefit (van Lieshout et al., 2020) (Wang & Wright, 2021).
Methanol is another alternative fuel that has been gaining interest in the shipping industry. It has a higher hydrogen-to-carbon ratio and negligible sulfur content, resulting in lower SO_x and PM emissions. Methanol also offers significant reductions in nitrogen oxides (NO_x) emissions due to the lower combustion temperatures in the cylinder. Despite these advantages, market penetration remains limited, with an estimated market share of 5% to 22% under various scenarios.
This report examines MDO/MGO, HFO and LNG as potential fuels for vessels. The first fuel type considered is MDO/MGO. These two fuels are grouped together because they are both diesel-based, differing in sulfur content, which makes them suitable for different regulations (van Lieshout et al., 2020). The second fuel is HFO, which remains widely used despite its high sulfur content, primarily due to its

cost-effectiveness (Lindstad et al., 2020). The final fuel considered is LNG, selected for its established market presence and environmental advantages (Wang & Wright, 2021). Methanol, though highly promising, is not yet widely used and, therefore, is excluded from this report.

Table 2.2 provides a summary of the key details for each vessel discussed above. For each vessel, the table indicates whether it is self-propelled, the specific decommissioning stages where it is applicable, and the corresponding fuel type. All vessels operate on MDO/MGO or HFO, as these remain the predominant fuels in the shipping industry today (Faber et al., 2021). As previously mentioned, the barge, CLB, DCB, JUB, and ROV do not have their own propulsion systems and, therefore, do not require fuel, which is reflected in the table.

Table 2.2: Overview vessels during OWF decommissioning, with respective stage and fuel type, data retrieved from (Huang et al., 2017), (Arvesen et al., 2013), (Jalili et al., 2023)

Vessel type	self-propelled	Stage	Fuel type
Anchor handling tug supply	x	FOU, OSS, MM removal	MDO/MGO
Barge		WT, FOU, OSS, MM removal	-
Cable laying barge		IAC & EC removal	-
Cable laying vessel	x	IAC & EC removal	MDO/MGO
Crane vessel	x	WT, FOU, OSS, MM removal	HFO
Crew transfer vessel	x	All	MDO/MGO
Deck carrier	x	WT, FOU, OSS, MM removal	HFO
Derrick crane barge		SP removal	-
Dredger	x	SP removal	MDO/MGO
Heavy lift vessel	x	WT, FOU, OSS, MM removal	HFO
Jack-up barge		WT, FOU, OSS, MM removal	-
Jack-up vessel	x	WT, FOU, OSS, MM removal	HFO
Multi-purpose vessel	x	All	MDO/MGO
Offshore support vessel	x	All	MDO/MGO
Rock dumping vessel	x	SPL removal	HFO
Remotely operated vessel		All	-
Semi-submersible crane vessel	x	WT, FOU, OSS, MM removal	HFO
Service operation vessel	x	All	MDO/MGO
Survey/research vessel	x	Survey in pre- & post-decom.	MDO/MGO
Tug boat	x	All	MDO/MGO
Walk-to-work-vessel	x	All	MDO/MGO

Once the appropriate vessel type has been selected, the transport strategy must also be determined. There are two primary strategies: the feeder and pendulum concept. The feeder strategy keeps the decommissioning vessel stationed at the OWF site, while smaller vessels transport the dismantled components to the port. The vessel used in this strategy is referred to as the feeder ship. In contrast, the pendulum strategy involves the decommissioning vessel shuttling between the OWF and port, performing both dismantling and transportation tasks. This vessel is often referred to as a multitask decommissioning, pendulum, or shuttle vessel (Topham & McMillan, 2017) (Hillers et al., 2023).In this study, the terms feeder and pendulum concepts are used to describe these two transportation strategies. As shown in figures 2.10 and 2.11, the choice between the feeder or pendulum concept is relevant only when dismantling WT topsides and substructures (Eckardt, 2022).

The choice of transportation strategy significantly impacts the logistical operations of the vessels. The feeder concept requires the use of two or three different vessel types, whereas the pendulum concept simplifies operations by utilising only one vessel type. However, the strategy does not influence the total number of vessels required. This number follows a specific rule: for individual offshore structures, such as OSS or MM, only one vessel is needed. For dismantling multiple similar units, several vessels of the same type operate in parallel to optimise vessel capabilities and minimise lease periods (Gillian Smits, 2015). Additionally, the deck configuration of the vessel also influences the number of vessels

required. Specifically, the maximum number of WT topsides that can fit on a vessel's deck depends on the decommissioning configuration method used. In this study, the part-by-part method is considered standard due to its advantages, particularly for large-scale wind farms. This method allows more dismantled WT components to be loaded onto the vessel's deck compared to other configurations, enhancing operational efficiency (Vis et al., 2016).

2.2.4. Removal and cutting techniques

This subsection outlines the removal and cutting techniques relevant to OWF decommissioning. First, an introduction to the different techniques will be provided, followed by a detailed explanation of both partial and complete removal techniques.

OWF decommissioning involves extensive cutting operations. The cutting operations are mainly employed at the time when the dismantling of substructures of WT, OSS or MM takes place. Figure 2.11, 2.12 and 2.13 illustrate that a foundation can be either partially or completely removed. In both cases, specific removal techniques are applied, which may involve cutting. There are two types of methods for cutting. The first method is internal pile cutting, in which the cutting tool is lowered into the pile after internal parts have been cleared and the seabed has been excavated (Gjødvad & Ibsen, 2016). Internal cutting can be more practical because the inside is not affected by water currents, in addition, it is accessible from the platforms at the pile top (Gillian Smits, 2015). The second method is external cutting, where the cutting tool is installed after dredging the soil around the piles (Gjødvad & Ibsen, 2016). External cutting is suitable if the surrounding seabed can be easily excavated to the required depth, and the foundation has no protrusions (Gillian Smits, 2015).

Besides the two methods of cutting, various techniques exist that can be applied either internally, externally, or both. The process flow charts make use of the most commonly used cutting techniques, which will be described in detail. If partial dismantling of the foundation is selected, three cutting techniques are available: abrasive water jet (AWJ) cutting, diamond wire saw cutting (DWSC), and oxy-fuel cutting. AWJ cutting involves the removal of steel using a high-pressure water jet that may contain abrasive minerals such as quartz, garnet, or corundum sand. Two types of AWJ processes exist: the first adds the abrasive to the water in a calculated ratio and accelerates the mixture, while the second uses subpressure to draw the abrasive in before it is accelerated by the water jet.This technique can be used to cut the foundation internally or externally, though internal cutting is preferred (Eckardt, 2022). The DWSC technique, by contrast, employs wires embedded with artificial diamonds attached to saw segments. These wires are accelerated to cut through hard materials such as rock, concrete, and steel. Although this method can be applied for cutting below the seabed, it may necessitate additional measures, such as dredging, to facilitate the process (Eckardt, 2022). The third technique, oxy-fuel cutting, is a thermal process in which steel is heated to its ignition temperature before being severed by a jet of gas. This method is particularly suited for cutting unalloyed and low-alloyed metals with substantial thicknesses (3-300mm) and is commonly employed for operations above the water surface (Eckardt, 2022).
If the foundation is to be completely removed, the vibratory extraction method is the sole option. This technique works by transmitting vibrations that reduce the soil's bearing capacity around the pile, effectively creating a pseudo-fluid state. This minimises skin friction, making it easier to extract the pile from the seabed with less force. The method is especially effective for removing driven piles and monopile foundations on sandy seabeds, and it can be applied both above and below the water surface, up to depths of 350 meters (Eckardt, 2022).

Besides these widely used cutting techniques, other techniques are also available in the form of cutting using linear shaped charge (explosives), blade sawing and laser cutting (Gillian Smits, 2015). These are less commonly used, each for its own reason. Of the cutting techniques mentioned above, diamond wire is generally the preferred option. This since it does not involve vibration, it is less polluting, it can be wrapped around almost any size or shape, and it is cost-effective. The only disadvantage of this technique is that it requires good access to the cutting area (Topham & McMillan, 2017). However, the preferred cutting technique finally depends on the specific situation, and is determined by the amount of damage a technique causes.

2.2.5. Key parameters influencing greenhouse gas emissions

This subsection discusses the key parameters that influence GHG emissions within the decommissioning of an OWF. This answers research question 1b. An overview of both case dependent and independent parameters will be given.

In the decommissioning of an OWF, multiple parameters directly influence the GHG emissions. A clear understanding of these parameters is essential to ensure a comprehensive quantification of emissions. The key parameters can be broadly divided into two categories: project-dependent and project-independent factors (Jalili et al., 2023).

Project-dependent parameters refer to specific characteristics of the OWF being decommissioned, each of which plays a crucial role in determining the overall GHG emissions. The first key parameter is the type of system being dismantled. Another important factor is the decommissioning scope, which influences the scale of the operations. Whether components are completely or partially removed, or left in situ, has a direct effect on fuel requirements and, consequently, the associated emissions. In addition, the selection of vessel types used during decommissioning is a critical consideration. Vessel type is intrinsically linked to fuel consumption. Besides, the type of fuel used affects the carbon intensity of the operation. Moreover, the transport strategy employed, either feeder or pendulum, further influences the emissions profile. Additionally, operational factors, such as the distance between the OWF and the port, can influence the total emissions significantly. Longer transit distances increase fuel consumption and thus emissions, making geographical location an important consideration in both vessel and transport strategy decisions. Finally, the removal technology selected for dismantling also contributes to variations in energy consumption and efficiency. In summary, these project-dependent parameters are fundamental in shaping the GHG emissions profile of the decommissioning process.

Project-independent parameters include external factors that influence GHG emissions, regardless of the specific characteristics of the OWF being decommissioned. The first critical parameter is the fuel consumption rate of the vessels. The consumption of fuel directly affects the volume of emissions produced. Another significant factor is the emission factor associated with the type of fuel being used. Emission factors are standardised measures that indicate the amount of GHGs released per unit of fuel consumed. They are crucial in estimating the overall environmental impact of the decommissioning process and can vary significantly between fuel types. Finally, vessel efficiency, often defined by parameters such as engine performance and energy output, plays a vital role in influencing GHG emissions. In summary, project-independent parameters, while external to the specific project details, have a significant impact in determining on the overall emissions produced across OWF decommissioning.

In conclusion, to thoroughly quantify GHG emissions during OWF decommissioning, it is essential to consider both the specific project conditions and the external factors that influence emissions. By addressing both project-dependent and project-independent parameters, a more accurate estimation of total emissions can be achieved. These parameters apply to each stage within the scope of the decommissioning process, which may consist of site surveys, decommissioning preparations and removal of WT topsides, WT substructures, OSS, MM, cables and SP. The specific parameters influencing each of these stages will vary depending on the decommissioning scope. A detailed discussion of these parameters is provided in the modelling framework outlined in chapter 3.

2.3. TNO's UWiSE Decommission tool

This section will explain the working principle of the UWiSE decommission tool. This will immediately indicate what is currently missing from the tool, which is the quantification of emissions during OWF decommissioning. Therefore, this section is the bridge to the third and final section of the theoretical framework.

In 2017, TNO developed a tool to simulate the logistics around offshore wind and solar farms (TNO, 2023). As indicated earlier in subsection 1.2, this tool is called the UWiSE tool. The UWiSE software was developed with the purpose of supporting the industry in optimising OWF construction and O&M activities to reduce maintenance costs of offshore wind projects. The software consists of a back-end in which discrete-event simulation takes place, and a front-end, which is graphical and interactive. There are several modules within the UWiSE tool, including Installation, O&M Planning, Dispatch, and Decommission (Mancini et al., 2023). Since the focus of this research is the decommissioning of an OWF, the decommission tool of UWiSE will be further explored.

As already indicated in subsection 2.2.1, there is currently limited experience in OWF decommissioning. However, despite the lack of experience, various studies, Jalili et al. (2023), Topham and McMillan (2017), Gillian Smits (2015), Winkler et al. (2022), Milne et al. (2021) and Adedipe et al. (2021), have been conducted, which developed models for the cost of OWF decommissioning. However, high-fidelity logistics modelling tools for decommissioning are currently not widely available. Besides using UWiSE, only simulations have been performed for the OWFs decommissioning using DecomTools (Hillers et al., 2023). The current version of UWiSE decommission tool supports the modelling of global decommissioning campaigns of offshore WTs, including but not limited to foundations, SP, substations, export and IA cables and MMs. The users of UWiSE can determine their scope and level of detail. This UWiSE Decommission tool receives certain inputs, that is followed by an intermediate stage called the user interface, terminating in certain outputs. This modelling workflow of the UWiSE decommissioning tool is shown in Figure 2.18.

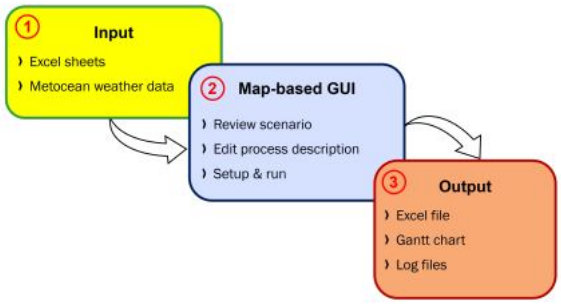

Figure 2.18: UWiSE Decommission modelling workflow (Mancini et al., 2023)

As shown in figure 2.18, the inputs comprise an excel input file and the metocean parameters table. The excel input file itself consists of information on the project, assets and resources. Once these files are uploaded, the second phase of the simulation workflow starts, which is performed entirely by graphical user interface (GUI). UWiSE GUi is organised in 4 tabs, named projects, inputs, process and simulations. This second phase of the modelling workflow is organised in three steps. The first step is input assessment, followed by process description, and finally tuning of simulation settings. The third and final stage of UWiSE involves processing the model output. For each simulation, UWiSE decommissioning generates a simulation log file, an excel summary output file, and an interactive Gantt chart (Mancini et al., 2023).

All the different stages and processes, which are explained is subsection 2.2.2, that can take place during decommissioning are thus optimised based on cost and time by the high-fidelity model. However, an important element is missing within this tool, which is the estimation of the environmental footprint due to decommissioning. This study aims to add this missing element to UWiSE Decommission.

2.4. Quantifying greenhouse gas emissions from offshore wind farm decommissioning

In this section, the approaches that can be utilised to measure GHG emissions based on the specified parameters during the decommissioning of an OWF will be described. Therefore, this will answer the second research question. The answer will be supported by several subsections. First, subsection 2.4.1 will give an introduction to GHG emissions, and explain which ones in particular will be addressed. Subsequently, subsection 2.4.2 will give an overview of all approaches that can quantify specifically those GHG emissions during OWF decommissioning. Then, the operational criteria and limitations which must be satisfied by the approach, and finally the evaluation of approaches and optimal approach will be given in the last subsection 2.4.3.

2.4.1. Introduction in greenhouse gas emissions

This subsection provides an introduction to GHG emissions, focusing on the direct GHG emissions released from offshore fuel-consuming processes in vessels during OWF decommissioning. First, the distinction between direct and indirect emissions will be clarified, followed by an explanation of the differences between air pollutants and GHGs. Additionally, the main GHGs relevant to offshore decommissioning will be introduced. Finally, the concept of quantifying the overall impact of these GHGs using global warming potential (GWP) will be outlined.

As briefly introduced in section 1.4, emissions can be categorised into direct and indirect emissions. It is important to distinguish these two categories, as they differ significantly in both their origin and impact on the environment. Therefore, a more detailed explanation will be provided here. Direct emissions, also referred to as Tank-to-Wheel (TTW), are generated directly by operational activities during on-site OWF decommissioning. For instance, The emissions from the combustion of fuel in vessels, helicopters, trucks, or machinery, which are directly involved in the decommissioning process. Indirect emissions, also known as Well-to-Tank (WTT), are generated during the upstream processes that support the decommissioning activities but are not part of ite. For instance, the emissions from the production, transportation, and refining of fuel, as well as the manufacturing of the transport vehicles used during decommissioning. It is important to clarify that emissions from the production or recycling processes of OWF components, are beyond the scope of this study. These emissions are associated with the overall life cycle of the OWF and not with the decommissioning activities specifically. Well-to-Wheel (WTW) is the sum of both WTT and TTW emissions. In other words, the indirect and direct emissions together (Kramel et al., 2021).

While the distinction between direct and indirect emissions provides a useful framework for understanding emissions at the operational level, a more comprehensive view is offered by the GHG Protocol, which categorises emissions into three scopes. These scopes allow for a more detailed assessment of emissions across the entire value chain of an organisation. Scope 1 covers direct emissions from an organisation's own sources, such as emissions from buildings, transportation, and production. Scope 2 includes indirect emissions from the generation of purchased electricity or heat. Scope 3 refers to all other indirect emissions, including those from business activities of other organisations that are outside of the company's direct control (NationalGrid, 2023).

The distinction between direct and indirect emissions is well established. When considering emissions, a distinction can be made between air pollutants and GHG. First, Air pollutants are harmful to human health and the environment. They contribute to issues like air quality degradation, acidification, and eutrophication. Examples of air pollutants are NO_x, SO_2, ammonia (NH_3), and particulate matter (PM) (NAEI, 2022). Although air pollutants are important environmental factors, they are not within the scope of this study. Therefore, their impact will not be further addressed, but remain important for future research and consideration. Second, GHGs are gases that capture heat in the Earth's atmosphere, leading to the greenhouse effect and global warming. These gases absorb infrared radiation, preventing it from escaping into space, which causes a rise in global temperatures. Without this effect, the Earth's average temperature would be significantly lower, around -18 °C, making life impossible. The increase in GHG concentrations due to human activities has intensified this natural process, contributing to climate change (EIA, 2022). Before delving into the specific types of GHGs, it is important

to distinguish between direct and indirect GHGs. This classification is different from the one used for direct and indirect emissions. Direct GHGs are those that directly contribute to the greenhouse effect by increasing the radiative forcing in the atmosphere. The study, Nations (1998), indicates that seven direct GHGs are inventoried, which are CO_2, CH_4, N_2O, hydrofluorocarbons (HFCs), perfluorocarbons (PFCs), suphur hexafluride (SF_6) and nitrogen trifluride (NF_3). HFCs, PFCs, SF_6 and NF_3 are collectively called the F-gases. CO_2 contributes the most to global warming, while CH_4 and N_2O combined account for less than 20% of the total contribution. F-gases generally contribute even less, often below 5%. In contrast, indirect GHGs do not directly contribute to the greenhouse effect but influence chemical reactions in the atmosphere that affect the concentration or lifetime of direct GHGs. Indirect GHGs can, for instance, promote ozone formation or alter atmospheric conditions, which in turn impact global warming. Examples include NO_x, carbon monoxide (CO), NMVOC and SO_2(NAEI, 2022). These substances overlap with air pollutants because they play a dual role, contributing to both pollution and influencing atmospheric processes that affect direct GHGs.

The distinction between direct and indirect emissions, as well as between air pollutants and GHG emissions, has been established. This provides the basis for investigating which direct GHGs are released from offshore fuel-consuming processes by vessels during OWF decommissioning. Indicated in subsection 2.2.3, this research assumes that vessels use one of the following fuels: MDO/MGO, HFO and LNG. The combustion of MDO/MGO, HFO and LNG during the transportation and offshore activities of OWF decommissioning releases a variety of emission types.The emission types of diesel fuel, MDO/MGO and HFO, are CO_2, NO_x, SO_x, PM and CH_4, in order of emitted amounts from major to minor. The emission types of LNG are the same, only in a slightly different sequence, namely CO_2, NO_x, CH_4, PM and with the smallest amount SO_x (Doedee, 2021). As indicated in Doedee (2021), in addition to CO_2, mainly air pollutants are emitted in large quantities. However, only GHGs are considered in this research. The three main direct GHGs emissions are CO_2, N_2O and CH_4, in order of the amount in which they are released (IPCC, 2000). Therefore, these are the three GHGs emissions on which this study will specifically focus.
Where CO_2 is emitted primarily by burning fossil fuels, carbon (C) in these fuels is released almost completely as CO_2. The amount of CO_2 ultimately emitted depends on the amount of carbon in the fuel, rather than the specific engine or combustion technology used. Furthermore, CH_4 is released when hydrocarbons in fuels are not fully combusted. These emissions are influenced by factors such as the CH_4 content of the fuel, engine type and post-combustion controls. Incomplete combustion, especially at low speeds or in poorly tuned engines, leads to higher CH_4 emissions. Finally, N_2O is produced during the combustion of fossil fuels at high temperatures, oxidising nitrogen (N) in the air or fuel. Although marine-vessel emissions of N_2O are generally small, the emissions can be affected by fuel type and engine characteristics. The presence of post-combustion catalysts can increase N_2O emissions, although these controls are not currently commonly used (IPCC, 2000).
According to Faber et al. (2021), the GHG emissions, including CO_2, CH_4, and N_2O, from total shipping (international, domestic, and fishing) increased from 977 million tonnes in 2012 to 1,076 million tonnes in 2018, representing a 9.6% rise. Specifically, CO_2 emissions rose from 962 million tonnes in 2012 to 1,056 million tonnes in 2018, marking a 9.3% increase. This study underscores the growing environmental impact of the shipping industry over this period.
In addition to measuring each of those emission types, CO_2, CH_4 and N_2O, the environmental footprint can also be measured in another way. That is, by measuring the amount of CO_2-equivalents. The amount of CO_2-equivalents emitted is calculated using a GWP value of a specific emission types (IPCC, 2021) (NationalGrid, 2023). The GWP is a measure that compares the warming impact of different GHGs to that of CO_2 over a specific time horizon. A higher GWP means that the gas retains more heat in the atmosphere than CO_2. This allows different gases and their contribution to climate change to be compared in a standardised way (EPA, 2024). The amount of CO_2-equivalents can be calculated using the GWP for CO_2, CH_4, and N_2O. The GWP value varies for emissions by specific time horizons. The most commonly used time horizons for GWP are 20, 100, and 500 years. The 20-year time horizon is useful for assessing the impact of GHGs that disappear from the atmosphere relatively quickly, causing strong warming in the short term. An example of a rapidly disappearing GHG is CH_4 (United, 2004). The time horizon of 100 years is the most common, and is often used in international climate agreements such as the Kyoto Protocol and the Paris Climate Agreement (Nations, 1998) (Nations, 2024). The last time horizon, of 500 years, is the least common, but useful for evaluating the long-term

effects of greenhouse gases that remain longer in the atmosphere. Examples of GHGs remaining in the atmosphere for a long time are tetrafluoromethane (CF4) and SF_6 (United, 2004).

2.4.2. Approaches for quantifying greenhouse gas emissions

In this subsection, approaches existing in the literature for quantifying GHG emissions during OWF decommissioning will be provided. This answers research question 2a. Quantifying GHG emissions is key for understanding environmental impacts and formulating strategies regarding climate action. Several methodologies have been developed and each of them is adapted to specific types of emissions and data. In this section several prominent methodologies will be described. The approaches that will be discussed in detail are the continuous emission measurement (CEM), GHG inventory approach, process-based model and the life cycle assessment (LCA). For each of these approaches, the working principle, mathematical principle, application, limitation, scope and reference studies will be described.

The first approach to be discussed is CEM, which provides real-time monitoring of gas emissions directly from the emission source. The mathematical principle of this method relies on the direct measurement of mass emissions rates (S. Lee et al., 2014). For real-time monitoring, the concentrations and flow rate of gas emissions are measured continuously by CEM.

First, the volumetric flow rate is measured:

$$Q = \frac{\dot{m}}{\rho} \tag{2.1}$$

where Q is the volumetric flow rate, $\dot{m}$ is the mass flow rate, and ρ is the density of the gas.

Next, the emission rate at any given time is determined using:

$$E(t) = C(t) \times Q(t) \tag{2.2}$$

where $E(t)$ is the emission rate at time t, $C(t)$ is the concentration of the pollutant, and $Q(t)$ is the volumetric flow rate of the gas stream.
Finally, to obtain the total emissions over a period T, the emission rate is integrated over time:

$$E_{total} = \int_0^T E(t)\, dt \tag{2.3}$$

where E_{total} is the total emissions over the time period T.

CEM only measures scope 1 emissions, since the emissions are directly measured from the emission source. CEM systems are extensively applied in industries where continuous monitoring is crucial, such as power plants and manufacturing facilities. Limitations of CEM systems include their high costs, and they may not effectively monitor intermittent or diffuse emission sources (Gillenwater, 2005).

The second approach outlined is the GHG inventory methodology, which involves compiling an inventory of GHG sources over time to track emissions. The method can be divided into activity-based and emission factor-based approaches (S. Lee et al., 2014). The mathematical principle is a product of the activity data and emission factors. This calculation is done following Intergovernmental Panel on Climate Change (IPCC) guidelines.

First, the total emissions for an activity-based approach are calculated:

$$E = \sum_{i=1}^{n} (AD_i \times EF_i) \tag{2.4}$$

where E is the total emissions, AD_i is the activity data for activity i, and EF_i is the emission factor for activity i.

Similarly, for an emission-based approach:

$$E = \sum_{i=1}^{n} (FC_i \times EF_i) \tag{2.5}$$

where E is the total emissions, FC_i is the fuel consumption for source i, and EF_i is the emission factor per unit of fuel consumed.

Finally, the total emissions from all sources are aggregated:

$$E_{total} = \sum_{i=1}^{n} E_i \tag{2.6}$$

where E_{total} is the total emissions from all sources, and E_i is the emissions from source i.

Emissions estimated using this method are classified into tiers, which reflect the methodological complexity. There are three different tiers:

- **Tier 1**: The basic method, using generally available national or international statistics and standard emission factors.
- **Tier 2**: Medium complexity, combining country-specific activity data and emission factors with IPCC standard values.
- **Tier 3**: The highest complexity, using advanced modelling techniques and country-specific activity data, including extensive monitoring (Climate Change Committee, 2017).

GHG inventory can cover emissions in scope 1, 2, and 3, depending on the breadth of the inventory (Mohareb et al., 2011). The methodology is applied by governments and environmental organisations for national and corporate emission reporting. A limitation of this approach is that it heavily depends on the accuracy of emissions factors and activity data (Sówka et al., 2017).

The third approach described is a process-based model, which simulates the physical and chemical processes that result in GHG emissions. The mathematical principle uses differential equations to capture the dynamics of the generation and losses of emissions (Zhang et al., 2017). This approach focuses on scope 1 emissions.

First, the total emissions are calculated based on process parameters and emission factors:

$$E = \sum_{j=1}^{m} (P_j \times EF_j) \tag{2.7}$$

where E is the total emissions, P_j is the process parameter (e.g., energy use, material flow) for process j, and EF_j is the emission factor for process j.

Optimisation can be achieved by minimising emissions subject to input-output balance constraints:

$$\text{Minimise } E \quad \text{subject to: } \sum \text{Inputs} = \sum \text{Outputs} \tag{2.8}$$

Process-based models are particularly valuable in academic research for studying ecosystem interactions and industrial processes. A limitation of this approach is the complexity and data intensity of these models, which in turn limits their use to only well-sourced projects.

The final approach discussed is the LCA method, which assesses the environmental impacts of a product or service throughout its entire life cycle. The mathematical principle of this method calculates this impact by taking the product of the quantity of emissions and the impact factor (Kramel et al., 2021). This approach covers emissions in scope 1, 2, and 3, as it assesses the impact throughout the entire life cycle of a product.

First, life cycle emissions are calculated as follows:

$$E = \sum_{k=1}^{p} (L_k \times EF_k) \tag{2.9}$$

where E is the life cycle emissions, L_k is the life cycle inventory data for process k, and EF_k is the emission factor for process k.

An approach within LCA is the Input-Output Analysis (IOA). The IOA method connects economic activities with their associated emissions intensities of goods and services. The mathematical principle of IOA is the product of economic activity and emission intensity (Kumar et al., 2016).

Additionally, Input-Output Analysis (IOA) within LCA connects economic activities with their associated emissions:

$$I = \sum_{l=1}^{q} (E_l \times CF_l) \tag{2.10}$$

where I is the impact indicator (e.g., GHG emissions), E_l is the inventory data for impact category l, and CF_l is the characterization factor for impact category l.

LCA models are widely used in product development, policy-making, and sustainability reporting across various industries. A limitation of LCA in general is the comprehensive data collection, which is resource-intensive (Mello & Robaina, 2020).

2.4.3. Multi-criteria decision analysis

In this subsection, the evaluation of the approaches outlined in subsection 2.4.2 will be conducted using a MCDA. This analysis addresses research questions 2b and 2c, ultimately identifying the most suitable method for quantifying GHG emissions during the decommissioning of OWF. First, the type of MCDA employed in this study will be explained. Then, the decision criteria will be presented and explained, and the derivation of the weights for each criterion will be described. Subsequently, the points of fulfilment will be introduced and the allocation of points to each method across all decision criteria will be detailed. Finally, the Weighted Sum Model (WSM) will be applied to calculate and determine the most appropriate method.

MCDA is a tool that supports multi-objective decision making. It is a structured and systematic way of evaluating and comparing certain options based on multiple criteria and objectives (Team, 2024). There exist about 56 different MCDA methods and combinations of these (Wątróbski et al., 2019). There are a few methods commonly used in MCDA to support decisions made during a process. The first method is the weighted sum model (WSM). In this method, each criterion is assigned a weight based on subjective assessment. A weighted sum is then calculated for each alternative. The second method is the analytic hierarchical process (AHP). This method decomposes complex decisions into a hierarchical structure of criteria and sub-criteria. A pairwise comparison matrix is used to assign a weight to each criterion. It is a structured technique for organising and analysing complex decisions (Eckardt, 2022). In this study, it was decided to use a combination of these two commonly used methods of MCDA. This hybrid approach will start by assigning weights to decision criteria by using the pairwise comparison matrix of the AHP method. Next, WSM will be used to evaluate the alternatives based on points distributed and the weights of the criteria.

The four most relevant decision criteria for an approach to quantify direct GHG emissions during the offshore transportation and operations of OWF decommissioning have been established and are described here. The first decision criterion assesses the accuracy and precision of each approach. The focus point of the criterion is how precisely the quantification of scope 1, direct, GHG emissions from the relevant sources, such as transportation and equipment operations, are measurable. It includes sensitivity to direct emissions and margin of error in the assessment. Margin of error means how close the estimated direct emissions are to the actual direct emissions. The second decision criterion assesses the computational time of each approach. The focus of the criterion is how fast the calculations

and simulations are performed. It incorporates resource utilisation and efficiency into the assessment. The third decision criterion assesses the flexibility and adaptability of each approach. The focus point of the criterion is the ability of the approach to adapt for varying scenarios and project specifications. It incorporates versatility and scalability into the assessment. The fourth decision criterion assesses data size, type and availability for each approach. The focus of the criterion is quantity and quality required. It includes data requirements and integrity in the assessment.

The pairwise comparison matrix from the AHP method is thus applied to determine weights of the decision criteria mentioned above. In such a matrix, all pairwise comparisons between all pairs of criteria are performed. If one criterion seems more important than the other, for the specific situation, then the more important criterion receives 2 points and the less important criterion receives 0 points. When both criteria seem equally important, they each receive 1 point (Eckardt, 2022). The pairwise comparison matrix is given in table 2.3 below.

Table 2.3: Pairwise comparison of the decision criteria

	Acc. & Prec.	**Comp. Time**	**Meth. Robustn.**	**Data Req. & Avail.**
Accuracy & Precision	1	2	1	1
Computational Time	0	1	2	1
Methodology Robustness	1	0	1	1
Data Requirements & Availability	1	1	1	1

Using this table, the weights can be calculated for each criteria. This is done by first adding up all the values in the columns. Then dividing each cell in the corresponding column by that sum. The next step is to average the values in each row. If the sum of these averages equals 1, then these are the weights for the criteria. If the sum of these averages does not equal 1, then each average will have to be normalised first. Figure 2.19 presents the rounded weights for each criterion, calculated using the numbers from the table.

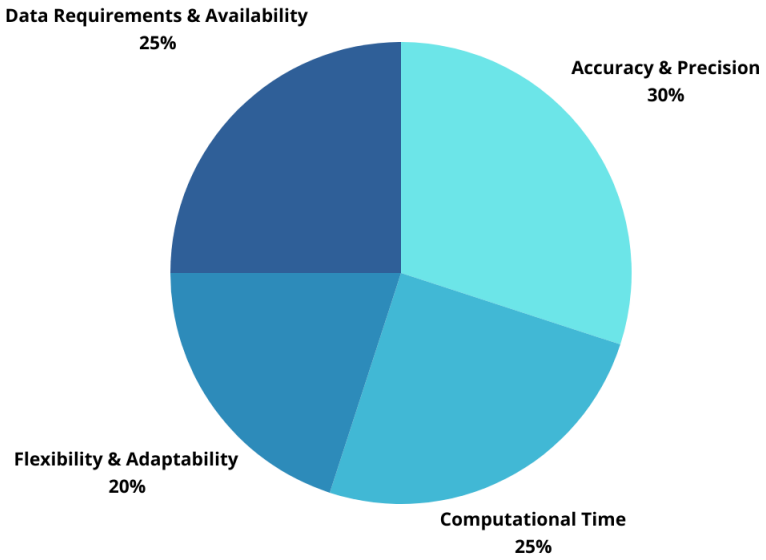

Figure 2.19: By AHP obtained weights for decision criteria

In order to evaluate the approaches more objectively on each decision criterion, a table with points of fulfilment is provided. It describes with explanation when for each decision criterion 1, 4, 7 and 10 points may be distributed to an approach. Figure 2.20 shows the prepared table. In addition to this points of fulfilment table, a no go constraint is established. This no go constraint implies that if an approach is

assigned 1 point on more than one decision criterion, it cannot be used even if the approach ends up as the most suitable one.

		Decision Critera			
		Accuracy & Precision	***Computational Time***	***Flexibility & Adaptability***	***Data Requirements & Availability***
Points	**1** ***(not fulfilled)***	**>10% error** Overlooks significant direct emissions	**Extremely slow** Limits daily analyses	**Rigid** One project type	**>80% data hard to obtain** Limits applicability
	4 ***(satisfactory)***	**5-10% error** Misses minor sources, captures most	**Slow** Supports one analysis per day	**Some but limited** Similar types of projects with little variability	**50-80% data hard to obtain** Requires effort
	7 ***(good)***	**2-5% error** Identifies nearly all sources	**Moderately fast** Enables several runs per day	**Fairly** Broad range of project	**20-50% data hard to obtain** Well-supported
	10 ***(excellent)***	**<2% error** Exceptionally precise	**Very fast** Support rapid iterations	**Highly** Universal appllicability	**<20% data hard to obtain** High data intigrity

Figure 2.20: Points of fulfilment with explanation for each decision criteria

Using the table with points of fulfilment, the points were assigned to the approaches for each criterion. How these points were distributed is shown in table 2.4. An explanation will be provided regarding the amount of points assigned to each requirement for all four approaches. Starting with CEM, which provides direct measurements of emissions. This ensures high accuracy and precision. However, CEM requires continuous monitoring and data analysis, which can be time-consuming. Although CEM is accurate, it can be vulnerable to technical failures and require regular calibration. In addition, CEM requires extensive and continuous data acquisition, which can be challenging in remote locations (S. Lee et al., 2014). Second, an explanation for the points distributed to the GHG inventory method is given. GHG inventories use detailed data, but can have variability in emission factors, which can affect accuracy somewhat. The computational time is generally short because they use existing data and emission factors. These methods are robust, but accuracy depends greatly on the emission factors and data sources used. GHG inventory methods use existing data, which increases availability and ease of use (Sówka et al., 2017). Subsequently, an explanation for the points distributed to the process-based method is provided. This approach relies on estimates and assumptions, which can lead to inaccuracies. Moreover, it can be very complex and time-consuming because of the need for detailed process modelling. However because of this, process-based methods are very robust because it involves detailed process analysis. Simultaneously, this is often accompanied by difficult to obtain process data (Zhang et al., 2017). Finally, an explanation of the points distributed to LCA is outlined. Finally, an explanation of the points distributed to LCA is outlined. This method provides a detailed and comprehensive overview, but its accuracy is highly dependent on the availability and quality of input data. LCA is less time-consuming in terms of computational requirements compared to CEM and process-based methods, due to its systematic approach and mathematical robustness. However, obtaining complete and high-quality datasets remains a significant challenge, as data can be difficult to acquire or incomplete (Mello & Robaina, 2020).

As explained why certain amounts of points were assigned for each of the approaches, conclusions will be drawn from this allocation. First, the applicability of the no-go constraint will be considered. As visible in table 2.4, the process-based method received 1 point for the requirement data requirements and availability. Therefore this method will immediately be discarded based on the no go constraint. For the other three approaches, the assigned points for each decision criterion will be multiplied by their respective weights. Then, for each method, all these values of the decision criteria are summed. The

result of these calculations are shown in table 2.4. This table shows that the GHG inventory method clearly scores the best and, as a result, has been selected as the method for quantifying direct GHG emissions for OWF decommissioning.

Table 2.4: Distribution of points to approaches for each decision criteria

	CEM	**Inventory**	**Process-based**	**LCA**
Accuracy & Precision	10	7	4	7
Computational Time	4	10	1	7
Methodology Robustness	4	7	10	7
Data Req. & Avail.	4	7	1	4
Result	**5.8**	**7.8**	**-**	**6.3**

3

Modelling greenhouse gas emissions

This chapter presents the development of the model designed to quantify direct GHG emissions from offshore activities involved in OWF decommissioning, addressing the third research question. First, section 3.1 introduces the deterministic model, describing its structure and key principles. Subsequently, section 3.2 provides a detailed description of the mathematical formulation of the model, starting with the indices of the system, followed by an overview of the model inputs and outputs, and ultimately the functional relationships required between them. Finally, section 3.3 assesses the uncertainty of the model.

3.1. Model design

This section presents the design of the model used to quantify direct GHG emissions from OWF decommissioning. The objective of this section is to provide a clear explanation of the design choices and the key parameters of the model. First, an introduction to the chosen methodology and its application will be provided. This will be followed by a comprehensive overview of the model, including a detailed description of its inputs and outputs. Subsequently, all intermediate steps within the model will be explained. For each of the relevant parameters, tables will be presented, listing their values. Finally, the approach for the sensitivity analysis of the designed model will be described.

First, an introduction to the chosen methodology and its application will be provided. The focus of this research is on quantifying direct GHG emissions from OWF decommissioning. The chosen methodology for quantifying these emissions is based on activity-based (equation 2.4) and emission factor-based (equation 2.5) approaches, following the guidelines set by the IPCC (Climate Change Committee, 2017). The equations combine the activity data, such as fuel consumption during decommissioning activities, with specific emission factors to estimate the total emissions. This approach allows for a detailed breakdown of emissions across the different stages of the decommissioning process. The different stages of decommissioning consist of various processes, contributing to the total direct emissions. An overview of these stages is provided in figures 2.8 to 2.17. The total direct emission can be determined by summing the emissions, as represented by equation 2.6. This equation can be further specified for OWF decommissioning stages as follows:

$$E_{total} = E_{pre} + E_P + E_{WT} + E_F + E_{OSS} + E_{MM} + E_C + E_{SP} + E_{post} \tag{3.1}$$

where E_{total} represents the total emission amount, while E_{pre}, E_P, E_{WT}, E_F, E_{OSS}, E_{MM}, E_C, E_{SP} and E_{post} correspond to the emissions produced during the survey in pre-decommissioning, preparations, WT removal, foundation removal, OSS removal, MM removal, cable removal, SP removal and the post-decommissioning survey, respectively.

Additionally, for all stages the emissions arise primarily from fuel consumption and can be further divided into equipment operations and transport-related emissions, as described by equation 3.2.

$$E_i = E_i^0 + E_i^{tr} \tag{3.2}$$

where E^0 represents the amount emissions produced by equipment operations for removal, E^{tr} the amount of emissions caused by transport of dismantled components and therefore E the total amount of emissions from these two processes, all for stage i. While these processes account for the majority of emissions, smaller contributions from auxiliary activities are not fully captured in this equation, indicating that the overall emission profile might include additional minor sources.

Second, the comprehensive overview of the model is outlined. Figure 3.1 provides an overview of the input and output of the model. The inputs are categorised into variable and fixed input. The variable inputs represent case-specific information, while the fixed inputs are constants based on known data.

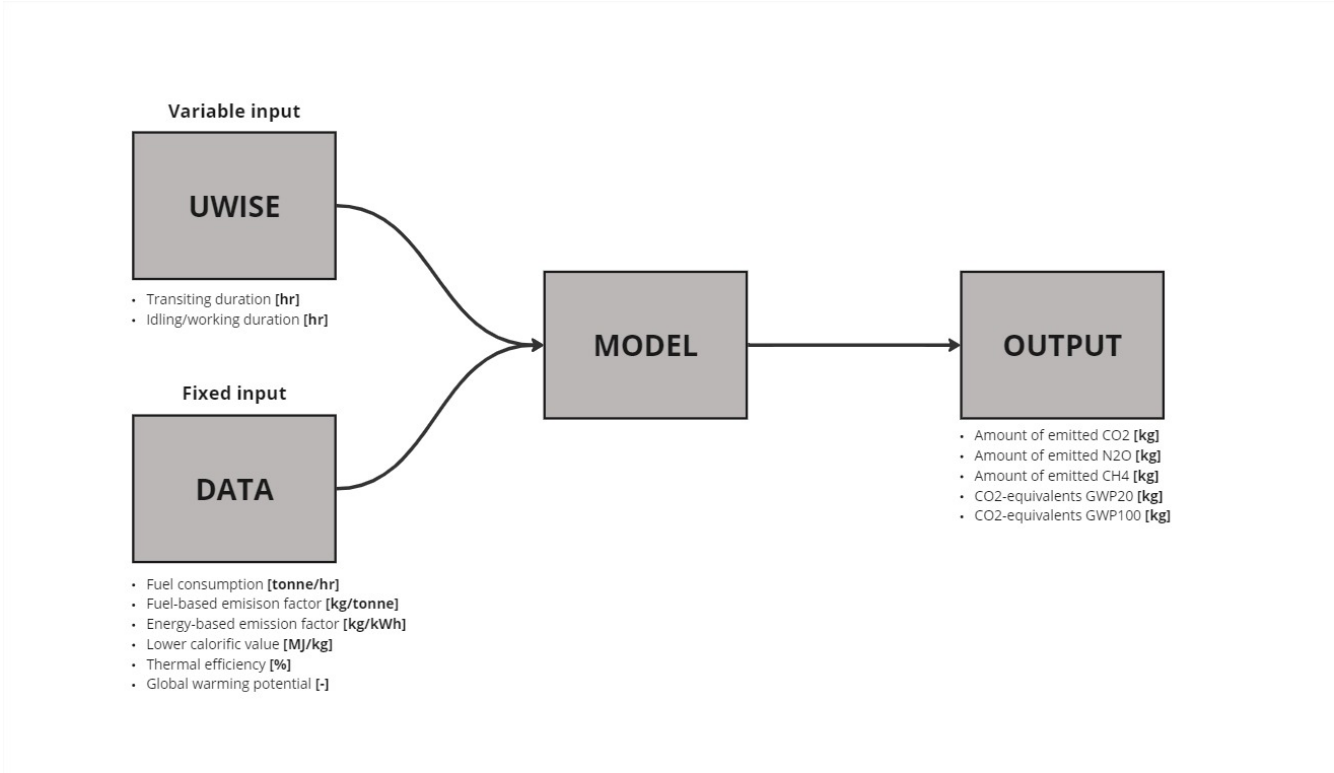

Figure 3.1: Input and output of the model

The model processes both variable and fixed inputs to quantify the GHG emissions associated with OWF decommissioning activities. The **UWiSE** module provides the variable, case-dependent input data, while the **data** module contains the fixed input parameters required for the calculations. The variable inputs generated in UWiSE simulations include key durations for each vessel. Specifically, the relevant durations for this research are the total transit, immobile at sea, and total transfer durations. These three durations are converted into two key operational states: transiting (state 1) corresponds to the total transit duration, while idling/operating (state 2) combines the immobile at sea and total transfer durations. State 1, representing transiting durations, is directly associated with transport-related (E^{tr}) emissions in equation 3.2. State 2, representing idling/operating durations, captures both emissions from vessels are waiting at sea (idling) and performing operations (operating). The emissions generated during operating activities are classified as equipment-related emissions (E^0), as outlined in equation 3.2. By categorising the vessel durations into these two states, the GHG inventory tool ensures a clear allocation of emissions based on the specific operational activities being carried out. Conversely, fixed input parameters, including fuel consumption, emission factors, calorific value, thermal efficiency and GWP, remain unchanged for all decommissioning cases. The **model** module integrates these inputs to compute the total GHG emissions for each vessel and operation. Finally, the **output** module generates the model results, including the quantities of CO_2, CH_4, and N_2O emissions, as well as their CO_2-equivalent values based on 20 and 100 year time horizons.

The interaction between these modules is deterministic, ensuring that the model consistently generates the same outputs for a given set of inputs. The **UWiSE** module supplies the **model** module with case-dependent operational data, specifically the durations of the utilised vessels in state 1 and 2, which directly influence fuel consumption and emissions. These values differ for every case, as OWF decommissioning is unique. A more detailed description on the UWiSE Decommission tool is provided in section 2.3. Simultaneously, the **data** module communicates fixed input, including fuel consumption, emission factors, calorific value, thermal efficiency and GWP, to the **model** module. The calculated emissions are subsequently transferred to the **output** module, where they are presented.

Subsequently, all intermediate steps between the input and output of the model will be described in detail. As already stated in subsection 2.4.1, the focus is on emission types CO_2, CH_4 and N_2O. This is because these are the three GHGs most extensively emitted from fuel burning processes in vessels at sea during OWF decommissioning. The aim of the model is to quantify the amount of each of these GHGs released by each vessel utilised in OWF decommissioning.
IMO indicated in Faber et al. (2021) that calculation of the amount of emissions is based on either fuel or energy, depending on the type of pollutant.

First, the fuel-based emission types will be considered. CO_2, SO_x and BC for marine diesel engines are pollutants calculated using the fuel consumption and fuel-based emission factors. Only CO_2 is considered, as this is a direct emission. Equation 3.3 shows this fuel-based calculation for these specific pollutants.

$$E = EF_f \times FC \tag{3.3}$$

where E is the amount of emissions [kg], EF_f reflects the fuel-based emission factor [kg/tonne] and FC denotes the fuel consumed [tonne].

The fuel-based emission factors for CO_2 are provided in table 3.1.

Table 3.1: Fuel-based emission factors (EF_f) for CO_2 for different fuels, data retrieved from (Faber et al., 2021)

Fuel type	EF_f [kg/tonne]
MDO/MGO	3206
HFO	3114
LNG	2750

The total fuel consumed (FC) by a vessel is calculated by multiplying the vessel duration in both operational states by the corresponding fuel consumption rates. The fuel consumed in state 1 and 2 is then added to the total fuel consumed by the vessel. This calculation is reflected in the following equation:

$$FC = (t_{transit} \times FC_{transit}) + (t_{idle/operate} \times FC_{idle/operate}) \tag{3.4}$$

where FC is de fuel consumed [tonne], $t_{transit}$ and $t_{idle/operate}$ reflect the durations in transiting and idling/operating state [hr], and $FC_{transit}$ and $FC_{idle/operate}$ denote the fuel consumption rates in transiting and idling/operating state [tonne/hr].

The vessel durations, $t_{transit}$ and $t_{idle/operate}$, are case-dependent and provided by UWiSE Decommission simulations. In subsection 2.2.3, all possible vessels utilised during OWF decommissioning are listed. The fuel consumption rates in state 1 and 2 are provided in table 3.2 for all vessels with own propulsion systems. It is acknowledged that different operations during decommissioning likely have varying fuel consumption rates. However, due to insufficient data on fuel consumption across these operations, the model has been simplified to group all these operational activities under state 2 (idling/operating). Additionally, the fuel consumption rates are assumed to remain constant, regardless of whether the vessel is loaded with OWF components. While it is recognised that loaded vessels generally consume more fuel, this simplification was necessary due to the lack of specific data on vessel durations in both loaded and unloaded conditions from UWiSE.

Furthermore, detailed fuel consumption rates for vessels during both loaded and unloaded transit are unavailable. These assumptions allow the analysis to continue despite the limited availability of operational and fuel consumption data for vessels.

Table 3.2: Vessels with their respective fuel type, engine type in state 1 and fuel consumption rate when transiting and idling/operating

Vessel type	Fuel	Engine (k1)	$FC_{transit}$ [tonne/hr]	$FC_{idle/operate}$ [tonne/hr]	Data sheet
Anchor handling tug supply	MDO/MGO	MS	0.479	0.250	(Vroon, 2022)
Cable laying vessel	MDO/MGO	SS	1.667	0.750	(Submarine, 1999)
Crane vessel	HFO	SS	1.425	0.673	(LTD, 1980)
CTV - catamaran	MDO/MGO	HS	0.327	0.111	(Gray, 2021)
CTV - monohull	MDO/MGO	HS	0.598	0.257	(VLmaritime, 2017)
CTV - AHTS	MDO/MGO	HS	0.598	0.257	(VLmaritime, 2017)
Deck carrier	HFO	MS	0.515	0.158	(Licorn, 2007)
Dredger	MDO/MGO	MS	0.269	0.100	(IHC, 2023)
Heavy lift vessel	HFO	SS	1.830	0.583	(Windcarrier, 2021)
JUV - medium	HFO	MS	1.464	0.466	(Windcarrier, 2021)
JUV - Large	HFO	SS	1.830	0.583	(Windcarrier, 2021)
Multi-purpose vessel	MDO/MGO	MS	0.557	0.354	(Yard, 2015)
Offshore support vessel	MDO/MGO	MS	0.457	0.333	(Fujian, 2017)
Rock dumping vessel	HFO	MS	0.269	0.100	(IHC, 2023)
Semi-submersible crane vessel	HFO	SS	1.830	0.583	(Windcarrier, 2021)
Service operation vessel	MDO/MGO	MS	0.850	0.102	(Gray, 2021)
Survey vessel	MDO/MGO	MS	0.379	0.106	(ALPHAMARINE, 2021)
TB - lead	MDO/MGO	HS	0.086	0.016	(INC., 2011)
TB - assist	MDO/MGO	HS	0.086	0.016	(INC., 2011)
Walk-to-work-vessel	MDO/MGO	MS	0.221	0.043	(Floatels, 2007)

Second, the energy-based emission types will be considered. NO_x, CH_4, CO, N_2O, PM and NMVOC are pollutants that are calculated using the effective engine energy and an energy-based emission factor. Only CH_4 and N_2O are considered, as these are direct emissions. Equation 3.5 shows this energy-based calculation for these specific pollutants.

$$E = EF_e \times W \tag{3.5}$$

where E is the amount of emissions [kg], EF_e denotes the energy-based emission factor [kg/kWh] and W refers to the effective energy of an engine [kWh].

The energy-based emission factor, EF_e, for both CH_4 and N_2O are provided in table 3.3 and table 3.4, respectively.

Table 3.3: Energy-based emission factors (EF_e) for CH_4 for different engine and fuel types, data retrieved from (Faber et al., 2021)

Engine type	Fuel type	EF_e x10^{-3} [kg/kWh]
SS	MDO/MGO	0.010
	HFO	0.010
	LNG	2.5
MS	MDO/MGO	0.010
	HFO	0.010
	LNG	5.5
HS	MDO/MGO	0.010
	HFO	0.010
	LNG	-
Auxiliary	MDO/MGO	0.010
	HFO	0.010
	LNG	5.5

Table 3.4: Energy-based emission factors (EF_e) for N_2O for different engine and fuel types, data retrieved from (Faber et al., 2021)

Engine type	Fuel type	EF_e x10^{-3} [kg/kWh]
SS	MDO/MGO	0.030
	HFO	0.031
	LNG	0.020
MS	MDO/MGO	0.030
	HFO	0.034
	LNG	0.020
HS	MDO/MGO	0.034
	HFO	0.030
	LNG	-
Auxiliary	MDO/MGO	0.036
	HFO	0.040
	LNG	0.020

The effective energy W of an engine depends on the fuel consumption of the vessel, calorific value of the consumed fuel and thermal efficiency of the engine. Equation 3.6 illustrates how these factors contribute to the effective energy output of an engine:

$$W = FC \times CV \times TE \times 277.8 \tag{3.6}$$

where W is the effective engine energy [kWh], FC is the fuel consumed [tonne], CV refers to the calorific value [MJ/kg] and TE denotes the thermal efficiency [%].

This equation is based on the principle of the first law of thermodynamics. This principle states that energy cannot be created or destroyed, but can only be converted from one form to another. In this context, the energy from the fuel is converted into the effective energy of the engine by factoring in its thermal efficiency and a conversion constant (Libretexts, 2024).
To start, the total fuel consumed (FC) by a vessel is determined using equation 3.4, by multiplying the vessel's operating durations in both operational states by the corresponding fuel consumption rates The vessel durations are obtained from UWiSE simulations, while the fuel consumption rates are provided in table 3.2.

For the calorific value, there are two options: the lower calorific value (LCV) and the higher calorific value (HCV). Either value can be used accurately, provided the corresponding thermal efficiency is applied consistently throughout the analysis. The distinction between LCV and HCV concerns the treatment of water vapor in the combustion products. LCV represents the energy content of a fuel when the water vapor remains in a gaseous state, excluding the latent heat from condensation. In contrast, HCV includes the energy from the condensation of water vapor, providing a measure of the total energy released during combustion (Garg et al., 2006). In engine applications, LCV is more commonly used, and the same applies thermal efficiencies of the vessel engines in this study are calculated accordingly (Energy, 2020). Therefore, this research has consistently employed the LCV of fuels in the calculation of the effective engine energy. The LCV values, along with other relevant fuel properties, are detailed in table 3.5.
Finally, the thermal efficiencies of the engines considered in this study are provided in table 3.6. The type of engine plays a critical role in fuel consumption. In state 1, corresponding to transiting mode, vessels use their main engine, which can range from slow-speed (SS), medium-speed (MS), to high-speed (HS) engines, as detailed in table 3.2. SS engines are typically two-stroke with speeds up to 300 RPM, while MS engines operate between 300 and 900 RPM, and HS engines function at speeds above 900 RPM (Faber et al., 2021). In state 2, which corresponds to idling/operating mode, vessels rely on auxiliary engines (Ahmed, 2023). The thermal efficiency of a vessel's engine is assumed to remain constant throughout its operational lifetime, regardless of engine age. Although it is widely recognised that thermal efficiency tends to degrade over time, this assumption was necessary due to the unavailability of specific data regarding engine age in the case studies. Moreover, the rate at which thermal efficiency declines varies significantly depending on engine type and operational conditions, which further complicates its inclusion in the analysis. This simplification ensures consistency across the study despite the lack of detailed engine performance data over time.

Table 3.5: Characteristics for the fuel types considered, data retrieved from (van Lieshout et al., 2020)

Characteristics	**MDO/MGO**	**HFO**	**LNG**
Chemical structure	$C_{12}H_{26}$-$C_{14}H_{30}$	$C_{20}H_{42}$-$C_{50}H_{120}$	CH_4
Density [kg/m^3]	850	900-1000	450
Boiling point [$\circ$C]	180-360	121-600	-161
Lower heating value [MJ/kg]	42.6	40-42	48-50

Table 3.6: Thermal efficiency for the main engine types, data retrieved from (Tatsuo Takaishi & Sakaguchi, 2008) and (Kyrtatos et al., 2016)

Engine type	**Thermal efficiency [%]**
SS	45-55
MS	40-50
HS	35-45
Auxiliary	30-40

When the amount of CO_2, CH_4 and N_2O emitted is determined, the CO_2-equivalents can be calculated. The amount of CO_2-equivalents can be calculated using the GWP for CO_2, CH_4, and N_2O (IPCC, 2021). The general equation is as follows:

$$CO_2\text{-equivalents} = CO_2 + (GWP_{CH_4} \times CH_4) + (GWP_{N_2O} \times N_2O) \tag{3.7}$$

where CO_2, CH_4, and N_2O represent the amount of carbon dioxide, methane, and nitrous oxide emitted [kg], respectively, and GWP_{CH_4} and GWP_{N_2O} are the GWP factors for methane and nitrous oxide [dimensionless], as provided by the IPCC.

The selection of the time horizon affects the amount of CO_2-equivalents. This in turn determines how a project's emissions are assessed against climate goals. The selection of the time horizon must be aligned with the type of stakeholders to ensure that the approach is consistent. Therefore, an overview of potential stakeholders for the model that is developed. Figure 3.2 provides this overview for the most common time horizons. Specific organisations and companies are given for each category. For the GWP20 time horizon, environmental organisations such as Greenpeace and the World Wildlife Fund are highlighted. In the case of GWP100, international agreements like the UNFCCC, alongside companies such as Ørsted, are noted. For the GWP500 horizon, long-term research institutions, including NASA, and policy makers like the European Commission are emphasised.

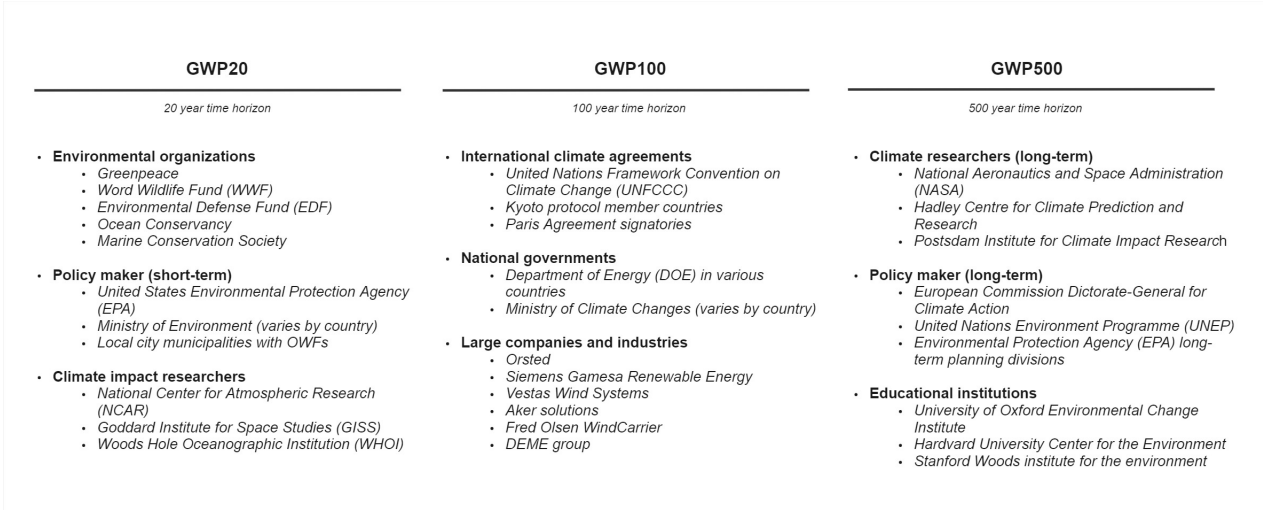

Figure 3.2: Most common time horizons for GWP with respective stakeholders

Subsequently, figure 3.3 provides an overview of the stakeholder categories for the model being developed.

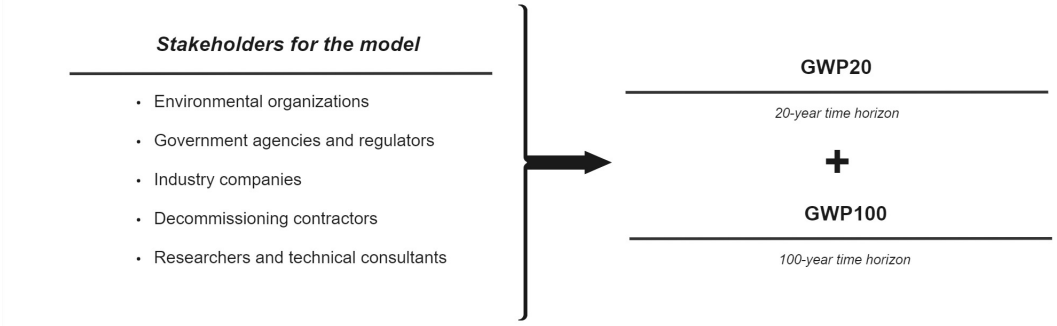

Figure 3.3: Specific stakeholders for the GHG emission of OWF decommissioning assessment model

Since the model will quantify direct GHG emissions during offshore OWF decommissioning, stakeholders will include environmental organisations, government agencies and regulators, industry companies, decommissioning contractors and research consultants. The time horizons relevant for the model are determined using the stakeholder categories established for the model, and the overview of stakeholder for each time horizon. As the devised stakeholders for the model are all covered in the time horizons of 20 and 100 years, both will be included for the calculation of CO_2-equivalents. Together, both time horizons will provide a complete image of both the short-term and long-term impacts of GHGs. The 20-year time horizon will provide a more accurate picture of the impact of CH_4 compared to other time horizons, which is essential for policy decisions aimed at quick results in climate control. Besides, the 100-year time horizon will provide a useful benchmark for projects focused on long-term sustainability goals and compliance with international standards.

The IPCC has published several assessment reports (ARs), each providing updated guidelines for GWP values (Manageruser, 2023). Table 3.7 presents the GWP values from the most recent report, AR6, for the time horizons relevant to this research. While AR6 reports these values as ranges, this model adopts a deterministic approach, and therefore the average values of these ranges are used.

Table 3.7: Average GWP values for type horizon of 20-years, and 100-years, data retrieved from (IPCC, 2021)

Emission type	GWP20	GWP100
CO_2	1	1
CH_4	84	29.8
N_2O	273	273

In conclusion, this model quantifies the offshore direct emissions of CO_2, CH_4, N_2O, and CO_2-equivalents over 20- and 100-year time horizons, for OWF decommissioning. Given the deterministic model input, the output remains consistent and uniform across all simulations, ensuring reliable results for each case study. Subsequently, it is important to perform a deterministic sensitivity analysis (DSA) to evaluate how sensitive the model results are to changes in input parameters. Several methods can be employed for such a DSA. One widely used approach is local sensitivity analysis, where small changes are applied to input parameters to measure their local effect on the output. Another common DSA technique is the one-at-a-time (OAT) approach, which systematically varies one input parameter while keeping all others constant. This allows for a clear assessment of how individual changes impact the overall results (Hamby & Society, 1994). A third method is gradient-based sensitivity analysis, which computes the gradient of the output with respect to input parameters, providing insight into which parameters exert the most influence on the model's outcome. The OAT approach is selected to perform the DSA due to its simplicity. The main objective is to identify how individual parameters affect the outcomes and discover general trends.

3.2. Mathematical formulation of the model

This section presents the mathematical formulations for the model. This mathematical framework is based on the model design described in section 3.1. First, subsection 3.2.1 introduces the notations for the indices, followed by model input in subsection 3.2.2 and model output in subsection 3.2.3. Finally, in subsection 3.2.4, defines the support and output functions utilised in the model.

3.2.1. Indexing

This subsection provides the indices utilised in the model. These indices facilitate the systematic representation of the parameters and variables across different components of the model.

The following indices are utilised in the model for the parameters and variables:

j : Index for type of vessel $(1 \leq j \leq 20)$

1. *Anchor handling tug supply (AHTS)*
2. *Cable laying vessel (CLV)*
3. *Crane vessel*
4. *Crew transfer vessel (CTV) – catamaran*
5. *Crew transfer vessel (CTV) – monohull (also site inspections)*
6. *Crew transfer vessel (CTV) – small waterplane area twin hull*
7. *Deck carrier*
8. *Dredger*
9. *Heavy lift vessel (HVL)*
10. *Jack-up vessel (JUV) – medium*
11. *Jack-up vessel (JUV) – large*
12. *Multicat (multi-purpose vessel)*
13. *Offshore support vessel (OSV)*
14. *Rock dumping vessel (ROV)*
15. *Semi-submersible crane vessel (SSCV)*
16. *Service operation vessel (SOV)*
17. *Survey vessel (SV)*
18. *Tug boat (TB) – lead*
19. *Tug boat (TB) - assist*
20. *Walk to work vessel (W2WV)*

k : Index for certain state vessel j is in $(1 \leq k \leq 2)$

1. *Transiting*
2. *Idling / operating*

l : Index for type of GHG emissions $(1 \leq l \leq 3)$

1. *CO_2*
2. *CH_4*
3. *N_2O*

m : Index for type of time horizon of GWP $(1 \leq m \leq 2)$

1. *GWP_{20}*
2. *GWP_{100}*

n : Index for type of fuel used in vessels $(1 \leq n \leq 3)$

1. *MDO/MGO*
2. *HFO*
3. *LNG*

o : Index for type of engine in the vessel $(1 \leq o \leq 4)$

1. *Slow speed (SS) engine*
2. *Medium speed (MS) engine*
3. *High speed (HS) engine*
4. *Auxiliary engine*

3.2.2. Model input

This subsection provides an overview of the model input. First, the parameters are outlined, followed by the presentation of the variables.

The following parameters are utilised in the model:

FC : Fuel consumption for vessel j in state k **[tonne/hr]**
EF_f : Fuel-based emission factor for CO_2 for fuel type n **[kg/tonne]**
EF_e : Energy-based emission factor for emission type l between $(2 \leq l \leq 3)$ for fuel type n, considering engine type o **[kg/kWh]**
GWP : Global warming potential for emission type l and time horizon m **[-]**
LCV : Lower calorific value for fuel type n **[MJ/kg]**
η : Thermal efficiency for engine type o **[kg/MJ]**

The following variables are utilised in the model:

$T_{transit}$: Total transit duration for vessel j **[hr]**
T_{idle} : Total idling / operating duration for vessel j **[hr]**

3.2.3. Model output

This subsection presents an overview of the model output. First, the outputs per vessel are detailed, followed by the aggregated outputs.

The following outputs are calculated for each vessel:

CO_{2j} : Amount of CO_2 emitted by vessel j **[kg]**
N_2O_j : Amount of N_2O emitted by vessel j **[kg]**
CH_{4j} : Amount of CH_4 emitted by vessel j **[kg]**
$CO_2 - eq_j$: Amount of CO_2-equivalent emissions by vessel j with GWP time horizon m **[kg]**

The outputs from all individual vessels are aggregated, and the following represent the final outputs:

U_{CO_2} : Total amount of CO_2 emissions from all vessels **[kg]**
U_{N_2O} : Total amount of N_2O emissions from all vessels **[kg]**
U_{CH_4} : Total amount of CH_4 emissions from all vessels **[kg]**
U_{CO_2-eq} : Total amount of CO_2-equivalent emissions from all vessels with GWP time horizon m **[kg]**

3.2.4. Functional relationships

This section describes the functional relationships utilised in the model. It begins with the support functions, followed by the output functions.

The following support functions are utilised to compute the outputs for each vessel:

The fuel consumption per vessel and state is determined by:

$$FC_{tot,j,k} = FC_{j,k} \times T_{j,k} \tag{3.8}$$

The total fuel consumption per vessel is determined by:

$$FC_{tot,j} = \sum_{k=1}^{2} FC_{tot,j,k} \tag{3.9}$$

The effective engine energy per vessel and state is determined by:

$$W_{j,k,o,n} = FC_{tot,j,k} \times LCV_n \times \eta_o \times 277.8 \tag{3.10}$$

The CO_2 emissions per vessel are determined by:

$$CO_{2j} = FC_{tot,j} \times EF_{CO_2,n} \tag{3.11}$$

The CH_4 emissions per vessel and state are determined by:

$$CH_{4j,k} = W_{j,k,o,n} \times EF_{CH_4,k,o,n} \tag{3.12}$$

The total CH_4 emissions per vessel are determined by:

$$CH_{4j} = \sum_{k=1}^{2} CH_{4j,k} \tag{3.13}$$

The N_2O emissions per vessel and state are determined by:

$$N_2O_{j,k} = W_{j,k,o,n} \times EF_{N_2O,k,o,n} \tag{3.14}$$

The total N_2O emissions per vessel are determined by:

$$N_2O_j = \sum_{k=1}^{2} N_2O_{j,k} \tag{3.15}$$

The CO_2-equivalent emissions per vessel are determined by:

$$CO_2 - eq_{j,m} = CO2_j + (N_2O_j \times GWP_{N_2O,m}) + (CH_{4j} \times GWP_{CH_4,m}) \tag{3.16}$$

The following output functions are utilised to compute the final outputs:

The total amount of CO_2 emissions is determined by:

$$U_{CO_2} = \sum_{j=1}^{20} CO_{2j} \tag{3.17}$$

The total amount of CH_4 emissions is determined by:

$$U_{CH_4} = \sum_{j=1}^{20} CH_{4j} \tag{3.18}$$

The total amount of N_2O emissions is determined by:

$$U_{N_2O} = \sum_{j=1}^{20} N_2O_j \tag{3.19}$$

The total amount of CO_2-equivalent emissions is determined by:

$$U_{CO_2-eq_m} = \sum_{j=1}^{20} CO_2eq_{j,m} \tag{3.20}$$

3.3. Model uncertainty

In this section, the uncertainty in the model will be assessed. First, the importance of uncertainty propagation will be explained. Subsequently, the probability distributions of the input parameters will be specified. The specified distributions will be described using literature. Based on this, each of the uncertain parameters will be described in more probabilistic detail. Finally, the sensitivity analyses available for uncertainty propagation will be described, indicating which one is most appropriate for this type of model.

First, the importance of uncertainty propagation will be explained. The goal of uncertainty analysis is to quantify the probability of specific output values (Kleijnen et al., 1994). The uncertainty analysis is conducted in several steps. The first step is deriving distribution functions for the different inputs. In the second step, a pseudo-random number generator is used to sample input values within the ranges defined by the distribution. This process is typically carried out using the Monte Carlo method, where the model runs for every sampled set of inputs. The result is a set of output data, to which a distribution can be assigned. This allows the probabilities of the output values to be quantified, thus achieving the goal of the uncertainty analysis (Daniel P. Loucks, 2016).

The first step of uncertainty analysis will be performed. This is as just described, assigning specific distributions to input parameters. This will generate uncertainty propagation. As clearly described in section 3.2, there are both variable and fixed inputs to the model. In order to establish an uncertainty model, all fixed parameters will be assigned distributions. The fixed parameters as visible in subsection 3.2.2 are the fuel consumption, fuel-based emission factor, energy-based emission factors, LCV, thermal efficiency and global warming potentials. In deriving the appropriate distribution for the fixed parameters just named, sample data can be used. In that case, the characteristic variation and uncertainty of the data is investigated. If sample data is not available, a distribution can also be derived from literature (Kleijnen et al., 1994).

All fixed input parameters will now be assigned a distribution, either based on literature or sample data. To begin with the fuel consumption per hour, which varies substantially depending on conditions such as load and efficiency. Based on the article Davie et al. (2014) and the fact that fuel consumption per hour varies a lot, a lognormal distribution is prescribed for this input parameter. The second input parameter for which a distribution will be established is the fuel-based emission factor for CO_2. Fuel-based emission factors are often determined by relatively stable, controlled processes and have a symmetrical distribution around an average value (T. Lee & Frey, 2012). Therefore, a normal distribution is prescribed for this input parameter. The subsequent parameters for which a distribution is prescribed are the energy-based emission factors for CH_4 and N_2O. These show energy-based emission factors show more variation than the fuel-based emission factors (Brandt et al., 2016) (Levy et al., 2017). Based on this, lognormal distributions are prescribed for both parameters. Subsequently, the LCV parameter, which is relatively stable and has a symmetric distribution around a mean value, is introduced (van Lieshout et al., 2020). Hence, this parameter fits the normal distribution. Thermal efficiency also fits a normal distribution since it is measured in controlled environments, resulting in a central value and symmetric variations (Dernotte et al., 2015). The last fixed input parameter is the GWP for the emission types CO_2, CH_4 and N_2O. These are determined by scientific studies, which assume a mean value with a standard deviation (IPCC, 2021). Therefore, a normal distribution is also appropriate for this input parameter.

The first step of uncertainty analysis has just been initiated. Namely, assigning a type of distribution to the various fixed input parameters of the model. Thereby it was apparent that all fixed input parameters of the model are described by either a normal or a lognormal distribution. In order to describe the parameters in more probabilistic detail, both of these distributions will be presented first. The normal distribution, also known as the Gaussian distribution, is characterised by the symmetric bell-shaped curve defined by the parameters mean (μ) and standard deviation (σ) (Chen, 2024). The distribution is mathematically described by the function:

$$f(x) = \frac{1}{\sigma\sqrt{2\pi}} e^{-\frac{1}{2}\left(\frac{x-\mu}{\sigma}\right)^2} \tag{3.21}$$

Here, μ indicates the mean of the data, while σ represents the standard deviation of the data. This distribution is fundamental in statistics because of the 68-95-99.7 empirical rule. This rule indicates that 68%, 95%, and 99.7% of the data fall within one, two, and three standard deviations of the mean, respectively. The lognormal distribution describes a parameter whose logarithm is normally distributed. This means that if a parameter X is lognormally distributed, then Y = ln(X) is normally distributed. This distribution is often used for data that are not negative and exhibit exponential growth (Pavlovic, 2024). The distribution is mathematically described by the function:

$$f(x) = \frac{1}{x\sigma\sqrt{2\pi}} e^{-\frac{1}{2}\left(\frac{\ln(x)-\mu}{\sigma}\right)^2} \tag{3.22}$$

Here, μ is the location parameter and σ is the scale parameter, which describe the mean and standard deviation of the logarithmic values of the data, respectively.

Based on the description of the two distributions, the uncertainties of the input parameters will now be presented in more detail. First, the normally distributed input parameters will be described in more detail. Starting with the fuel-based emission factor for CO_2. The deterministic values of this input parameter can be found in section 3.1 in table 3.1. As visible, these values were taken from article Faber et al. (2021) and were provided as a specific value. Since the nature of the fuel-based emission factor is relatively stable, a standard deviation of 1% was chosen. The probabilistic values for the fuel-based emission factor for CO_2 are provided in table 3.8.

Table 3.8: Probabilistic values of CO_2 fuel-based emission factors EF_f for different fuels, data retrieved from (Faber et al., 2021)

Fuel type	μ	σ
MDO/MGO	3206	32.06
HFO	3114	31.14
LNG	2750	27.50

The second and third normally distributed input parameters are the LCV and thermal efficiency. The deterministic values for both parameters can be found in section 3.1 in tables 3.5 and 3.6, respectively. As visible, both the LCV and thermal efficiency were provided in ranges. As indicated in the description of the normal distribution, the empirical rule can be used to determine the standard deviation if the input is given in a range. The 95% rule was selected, given the nature of the LCV of fuels and thermal efficiency of engines. In addition, this particular rule is common and reflects a realistic spread. The probabilistic values for LCV and thermal efficiency are summarized in tables 3.9 and 3.10, respectively.

Table 3.9: Probabilistic values of lower calorific value for different fuel types, data retrieved from (van Lieshout et al., 2020)

Fuel type	μ	σ
MDO/MGO	42.6	0.426
HFO	41.0	0.5
LNG	49.0	0.5

Table 3.10: Probabilistic values of thermal efficiency for the main engine types, data retrieved from (Tatsuo Takaishi & Sakaguchi, 2008) and (Kyrtatos et al., 2016)

Engine type	μ	σ
Slow speed (SS)	50	2.5
Medium speed (MS)	45	2.5
High speed (HS)	40	2.5
Auxiliary engine	35	2.5

The last normally distributed parameter is the GWP. The deterministic values of this input parameter can be found in section 3.1 in table 3.7. These values were obtained from article IPCC (2021) and provided in a range. For CO_2, a very small percentage of uncertainty was selected (0.1%), as its GWP remains effectively constant by definition. However, for CH_4 and N_2O, the 95% empirical rule was applied due to the inherent variability in the GWP of these gases. The corresponding probabilistic values for the GWP across different time horizons are presented in table 3.11.

Table 3.11: Probabilistic values of GWP for different gases with different time horizons, data retrieved from (IPCC, 2021)

	GWP20		**GWP100**	
	μ	σ	μ	σ
CO_2	1.0	0.001	1.0	0.001
CH_4	84.0	12.15	29.8	5.5
N_2O	273	59	273	65

Second, the lognormally distributed input parameters will be described in more detail. Starting with the energy-based emission factors for both CH_4 and N_2O. The deterministic values for both parameters can be found in section 3.1 in tables 3.3 and 3.4, respectively. As visible, both values were taken from article Faber et al. (2021) and were provided as a specific value. Due to the increased uncertainty and variability associated with energy-based emission factors compared to fuel-based factors, a scale parameter of 5% was applied to both CH_4 and N_2O. The probabilistic values for the energy-based emission factors for are provided in tables 3.12 and 3.13.

Table 3.12: Probabilistic values of CH_4 energy-based emission factors EF_e for different engine and fuel types, data retrieved from (Faber et al., 2021)

Engine Type	**Fuel Type**	μ	σ
SS	MDO/MGO	-11.5129	0.05
	HFO	-11.5129	0.05
	LNG	0.9163	0.05
MS	MDO/MGO	-11.5129	0.05
	HFO	-11.5129	0.05
	LNG	1.7047	0.05
HS	MDO/MGO	-11.5129	0.05
	HFO	-11.5129	0.05
	LNG	0	0.05
Auxiliary	MDO/MGO	-11.5129	0.05
	HFO	-11.5129	0.05
	LNG	1.7047	0.05

Table 3.13: Probabilistic values of N_2O energy-based emission factors EF_e for different engine and fuel types, data retrieved from (Faber et al., 2021)

Engine Type	Fuel Type	μ	σ
SS	MDO/MGO	-10.4146	0.05
	HFO	-10.3756	0.05
	LNG	-10.8198	0.05
MS	MDO/MGO	-10.4146	0.05
	HFO	-10.2892	0.05
	LNG	-10.8198	0.05
HS	MDO/MGO	-10.2892	0.05
	HFO	-10.4146	0.05
	LNG	0	0.05
Auxiliary	MDO/MGO	-10.2239	0.05
	HFO	-10.1266	0.05
	LNG	-10.8198	0.05

The last lognormally distributed parameter is fuel consumption. The deterministic values of this input parameter can be found in section 3.1 in table 3.2. As visible, these values were from different data sheets and given in a specific value. The fuel consumption can have a wide spread due to the variability in operational conditions, therefore a scale parameter of 10% was selected. The probabilistic values for the fuel consumption rates are provided in table 3.14.

Table 3.14: Probabilistic values of fuel consumption rates of all vessels in states 1 and 2

Vessel	k1 μ	k1 σ	k2 μ	k2 σ
Anchor handling tug supply	-0.736	0.1	-1.386	0.1
Cable laying vessel	0.511	0.1	-0.287	0.1
Crane vessel	0.353	0.1	-1.148	0.1
CTV - catamaran	-1.211	0.1	-2.198	0.1
CTV - monohull	-0.514	0.1	-1.356	0.1
CTV - AHTS	-0.514	0.1	-1.356	0.1
Deck carrier	-0.665	0.1	-1.845	0.1
Dredger	-1.313	0.1	-2.303	0.1
Heavy lift vessel	0.604	0.1	-0.540	0.1
JUV - medium	0.381	0.1	-0.766	0.1
JUV - Large	0.604	0.1	-0.540	0.1
Multi-purpose vessel	-0.586	0.1	-1.038	0.1
Offshore support vessel	-0.783	0.1	-1.099	0.1
Rock dumping vessel	-1.313	0.1	-2.303	0.1
Semi-submersible crane vessel	0.604	0.1	-0.540	0.1
Service operation vessel	-0.163	0.1	-2.283	0.1
Survey vessel	-0.970	0.1	-2.239	0.1
TB - lead	-2.453	0.1	-4.140	0.1
TB - assist	-2.453	0.1	-4.140	0.1
Walk-to-work-vessel	-1.510	0.1	-3.147	0.1

The uncertainty propagation is represented with distributions for each input parameter. Subsequently, it is essential to perform sensitivity analysis to understand how variations in input parameters affect the output. Sensitivity analysis helps identify which parameters significantly affect the model output and to what extent (Daniel P. Loucks, 2016). For a probabilistic model, global sensitivity analysis (GSA) is more appropriate than DSA. GSA considers varying more input parameters at the same time. This is crucial for probabilistic models where input parameters have distributions rather than fixed values. Several global sensitivity analysis methods are available, i.e. the Morris method, Borgonova indices, Sobol' indices, ANCOVA indices and the Kucherenko indices. All of these sensitivity analyses will be briefly described. To begin with the Morris method, which creates a grid of possible input values and perturbs them to measure the mean and standard deviation of output changes. It identifies both the importance and interaction of input variables. Second, the Borgonovo index, which measures the expected shift in the output distribution when an input variable is fixed at different values. This method is applicable without assumptions about the dependency structure of input variables. Third, the Sobol' indices, which decompose the variance of model output into contributions from individual input parameters and their interactions. The method is ideal for independent input variables. Fourth, the ANCOVA indices, which generalise the Sobol' indices for correlated inputs by decomposing the variance into contributions of independent variation and dependent interactions. Finally, the Kucherenko indices, which use the law of total variance to account for the effects of dependent inputs by estimating the variance contributions of subsets of inputs (Marelli et al., 2024). The Sobol method is selected for uncertainty analysis because it offers a comprehensive decomposition of the contributions to variance, including first-order effects of individual input parameters and higher-order effects resulting from their interactions. The Sobol analysis is particularly suitable for treating independent variables, making it a valuable tool for initial explorations.

4

Model verification

This chapter will conduct verification of the model described in chapter 3. The verification is divided into two parts. First, a consistency check is performed in section 4.1. Subsequently, a benchmark analysis is conducted in section 4.2. Based on both verification components, the usability of the tool is considered in section 4.3

4.1. Consistency check

This section will conduct the first verification of the model defined in chapter 3. This verification consist of a consistency check. First, verification in general will be explained and the different existing techniques will be introduced. Subsequently, specific techniques are selected and a verification scenario is defined. Finally, the results of the verification will be observed, from which conclusions will be drawn.

Verification refers to the process of ensuring that the conceptual model has been correctly translated into the simulation model, as depicted in figure 4.1. Essentially, verification involves checking whether the model operates as intended, which can be likened to 'debugging'. This step ensures the model's functionality aligns with its design objectives. Several techniques are available for verification, including one-step analysis, continuity, degeneracy and consistency testing (The University of Edinburgh, 2003).

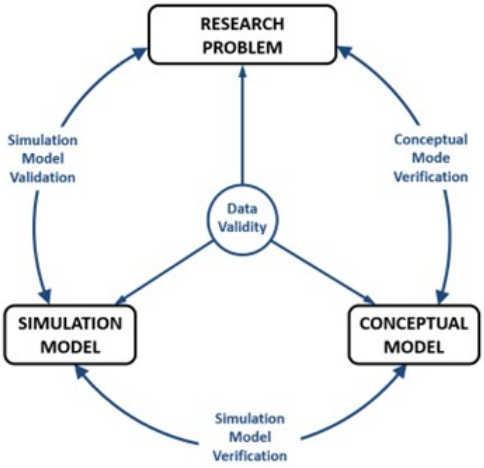

Figure 4.1: Model verification and validation architecture (Yin & McKay, 2018)

For this research, verification is divided into two methods: one-step analysis and degeneracy testing. One-step analysis involves a step-by-step walk through of the conceptual model, with manual verification of calculations at each stage. Therefore, it forms the foundation of the verification process. To complement this, degeneracy testing, also known as extreme value theory (EVT), is employed. This method tests the model's response to extreme input values, to ensure that the model processes them correctly. This approach was chosen to uncover potential errors that might not be apparent under standard conditions, thereby enhancing the model's robustness and reliability under atypical scenarios (Casati, 2013).

The verification scenarios for both one-step analysis and degeneracy testing are designed to be as simple as possible to ensure that the simulation model correctly implements the conceptual model. For this verification, a single vessel type, specifically a WTIV, is employed to perform both transport and decommissioning operations. As part of EVT, extreme (i.e., minimum and maximum) values are introduced into the model. As discussed in subsection 3.2.2, the two key variables are the transiting and idling/operating durations of vessels. Table 4.1 presents the input values for the WTIV used for the EVT verification. These input durations are not derived from UWiSE simulations and therefore do not reflect realistic decommissioning durations. This because the objective is to ensure that lower input values produce proportionally lower outputs, and higher input value result in correspondingly higher outputs. Although this verification focuses on a single vessel type (WTIV), the array-based nature of the calculations ensures that the model is applicable to other vessel types. Therefore, the simplicity of the chosen scenario does not compromise the thoroughness of the verification process.

Table 4.1: Minimum and maximum input values of WTIV for verification

	Minimum	**Maximum**
$T_{transit}$ [hr]	1	1000
$T_{idle/operate}$ [hr]	35	35000

By inserting the values from table 4.1 into the conceptual model, the corresponding output values are generated, as shown in table 4.2. First, the one-step analysis was conducted for both the minimum and maximum input values. This process involved manually calculating each step, using both the support and output functions from subsection 3.2.4. The results were exactly the same as the values in table 4.2. Therefore, the model's accuracy is confirmed with the one-step analysis.

Table 4.2: Minimum and maximum output values of WTIV for verification

	Minimum	**Maximum**
CO_2 emissions [kg]	69,240	69,239,790
CH_4 emissions [kg]	0.92	917.65
N_2O emissions [kg]	3.58	3,576.80
CO_2-eq. (20 years) [kg]	70,293	70,293,337
CO_2-eq. (100 years) [kg]	70,243	70,243,601

The outputs presented in table 4.2 demonstrate that the minimum values are consistently lower by an order of magnitude (10^3) compared to the maximum values. This is an expected output, given that the input values also differ by this factor. These results confirm that the model performs well under extreme conditions, demonstrating its robustness. Consequently, the model passes the degeneracy tests successfully.

4.2. Benchmark analysis

This section will conduct the second verification of the methodology described in chapter 3. This verification consists of a benchmark with an existing tool. The benchmark will be described using several subsections. First, in subsection 4.2.1 benchmarking methodology will be introduced. In addition, the aim of this particular benchmark and the tool used for it will be presented. Subsequently, in subsection 4.2.2, the benchmark scenario will be defined. Finally, subsection 4.2.3 will present the results of the benchmark.

4.2.1. Introduction to benchmarking

This subsection introduces benchmark analysis. First, benchmarking methodology will be described in general. Subsequently, benchmarking for this particular study will be considered. Finally, the tool used to benchmark will be illustrated.

In section 4.1, the one-step analysis and degeneracy tests were performed as initial verification. However, these tests alone are insufficient to establish the accuracy and reliability of the conceptual model. Therefore, this section introduces benchmarking as the second part of the verification. Benchmarking was chosen because there is no real-world data available on GHG emissions from OWF decommissioning. This implies that there is no opportunity for validation of the methodology. In such cases, benchmarking serves as a substitute for validation. It is a systematic process to compare the model's performance against industry standards, identifying best practices and improving performance (Ahmad et al., 2021). The objective of this benchmark is to verify the GHG inventory model, which focuses exclusively on direct (scope 1) emissions from offshore activities during OWF decommissioning. This benchmark evaluates CO_2, CH_4, N_2O, and their CO_2-equivalents over 20- and 100-year time horizons.

The results of the GHG inventory model are compared to those generated by an existing tool, the Activity Browser. The Activity Browser is an open-source software that builds on the Brightway framework, which provides a robust platform for advanced LCA (Brightway, 2024). Brightway serves as the underlying computational framework, while the Activity Browser acts as the GUI that simplifies common LCA tasks, such as managing projects, life cycle inventories, and analysing LCA results. The Activity Browser allows users to perform advanced scenario modelling, sensitivity analysis, and result visualisation, supporting both standard and non-standard LCA tasks (Steubing et al., 2020). The Brightway framework, as an open-source Python-based LCA tool, provides core functions to compute life cycle impacts using datasets such as those from the ecoinvent database (Database, 2024). The ecoinvent database supplies necessary input data for estimating emissions from OWF decommissioning, following the methodology outlined in (IMO, 2015). This is the preparatory study for Faber et al. (2021), and therefore uses the same methodology for calculating emission as described in chapter 3. The ecoinvent database for offshore transport is limited to data of a single fuel type (HFO) and two vessel types: container ships and ferries. Additionally, it provides generalised average values for fuel consumption, combining operational states like idling and transiting.

It is essential to clarify how the Activity Browser, Brightway framework, and ecoinvent database interact. The Activity Browser processes the data using Brightway's LCA framework, which performs the LCA calculations based on input parameters such as fuel consumption, operational states, and emission factors. The data from the ecoinvent database feeds into Brightway, providing generalised fuel consumption and emission factors based on weighted averages of different vessel sizes and operational modes. Figure 4.2 illustrates the data flow between the ecoinvent, Brightway and Activity Browser.

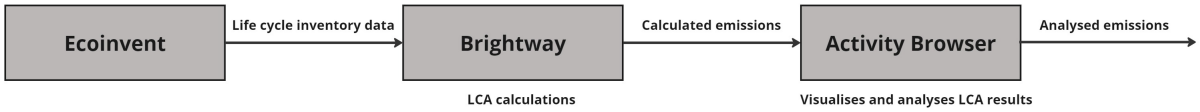

Figure 4.2: Data flow between ecoinvent, Brightway and Activity Browser, data retrieved from (Steubing et al., 2020)

This data flow starts with the ecoinvent database, is processed through Brightway, and is visualised and further analysed in the Activity Browser. This hierarchy ensures that the LCA calculations capture both direct emissions (scope 1) and indirect life cycle emissions (scopes 2 and 3), which are calculated separately. However, as this research focuses exclusively on direct emissions from offshore activities, only scope 1 emissions are considered relevant for this benchmark.

In summary, the Activity Browser, powered by the Brightway framework, plays a central role in the benchmark analysis by providing an LCA platform capable of handling advanced scenario modelling and emissions calculations. Since the Activity Browser calculates emissions using parameters in different units, additional processing steps are required to align its outputs with those of the GHG inventory model. The LCA tool calculates emissions in kilograms per tonne burned fuel , while the GHG inventory tool calculates emissions directly in kilograms.

To ensure clarity, the **LCA tool** will henceforth refer to the Activity Browser and the **framework** will refer to Brightway.

4.2.2. Description of benchmark scenario

This subsection describes the benchmark scenario to compare the GHG inventory model with an existing LCA tool. First, the scenario is introduced, followed by the presentation of the relevant input data to conduct the benchmark with the GHG inventory tool. Finally, the input data required for the LCA tool to perform the benchmark is provided.

As outlined in subsection 4.2.1, the objective of this benchmark is to verify the developed GHG inventory model, by comparing its results with those of an existing LCA tool. Both tools operate using different units for input and output data. The LCA tool calculates emissions in kilograms per tonne burned fuel, while the GHG inventory tool calculates emissions in kilograms. To enable a direct comparison of their outputs, a benchmark scenario was developed that evaluates the emissions produced per tonne of fuel consumed. For constructing this benchmark scenario, it is important to consider the necessary inputs for both tools to generate comparable results.

The first step involves defining the case-dependent inputs for the GHG inventory tool, which are the transiting and idling/operating durations of the vessels involved. Since the benchmark requires a total fuel consumption of 1 tonne, the operational durations will need to be adjusted accordingly. The OWF Lincs Limited decommissioning is used as a reference case study to determine the operational durations of the vessels. Lincs Limited, situated 8 kilometres off the coast of Skegness in United Kingdom, consists of 75 wind turbines. This offshore wind farm was commissioned in 2013 after its construction between 2010 and 2012. The UWISE Decommission tool simulated the transiting and idling/operating durations for the vessels involved in the decommissioning of the WT topsides, focusing specifically on the blades, nacelle, and tower. The decommissioning process employed the feeder concept, utilising one WTIV and two barges, supported by two tug boats (TBs). However, for simplification of the benchmark scenario, only the WTIV and one TB are considered. Further details regarding the specifications of OWF Lincs Limited and the decommissioning process are provided in chapter 5. Table 4.3 presents the average operational durations for the WTIV and TB from the UWISE simulations, alongside the total fuel consumed.

The total fuel consumed was calculated by multiplying the respective durations by the fuel consumption rates provided in section 3.1 in table 3.2. Specifically, the fuel consumption rate for the WTIV corresponds to that of a large JUV, while the leading TB has been selected for the TB.

Table 4.3: Durations for vessels in OWF Lincs limited for conducting the WT topsides decommissioning, data retrieved from UWiSE

Vessel type	T_{transit} [hr]	$T_{\text{idle/operate}}$ [hr]	Fuel consumed [t]
WTIV	8.39	2253.62	1329.21
TB1	61.16	1167.25	23.94

To determine the durations for the benchmark scenario, the average durations were proportionally scaled to ensure that the total fuel consumption equals exactly 1 tonne. These scaled durations, as shown in table 4.4, provide the relevant input data for the GHG inventory tool. Additionally, as noted in subsection 4.2.1, the LCA tool operates using the ecoinvent database, which assumes that all vessels utilise HFO. To ensure consistency, the GHG inventory tool also assumes HFO as the fuel type for both the WTIV and TB, despite literature indicating that MDO/MGO is more commonly used for TBs. This affects the emissions by the LCV of the fuels, which plays a role in the emission calculations, as outlined in section 3.1.

Table 4.4: Relevant input data for GHG inventory tool to perform benchmark

Vessel type	Fuel type	T_{transit} [hr]	$T_{\text{idle/operate}}$ [hr]
WTIV	HFO	0.0063	1.70
TB	HFO	2.55	48.76

The second step involves defining the inputs for the LCA tool, which employs a different approach. This tool utilises the ecoinvent database and performs calculations within the framework. The primary input consists of selecting the appropriate vessel categories for the decommissioning process. The vessels were categorised based on an their dead weight tonnage and data from the ecoinvent database (Database, 2024). For this benchmark, the WTIV and TB were classified as container ships and ferries, respectively. Table 4.5 presents this relevant input data for the LCA tool to perform the benchmark. Selecting a vessel type automatically integrates all necessary data, as provided by the ecoinvent database. This necessary data includes the utilised fuel type and fuel consumption. Fuel consumption is expressed in kilograms per tonne-kilometre [kg/tkm], representing the fuel required to transport one metric tonne of freight over one kilometre. This streamlined approach ensures that emissions for each vessel category are calculated directly by the framework of the LCA tool using predefined parameters from the ecoinvent database.

Table 4.5: Relevant input data for LCA tool to perform benchmark, data retrieved from (Database, 2024)

Vessel category
Transport, freight, sea, container ship
Transport, freight, sea, ferry

In conclusion, the GHG inventory tool is based on operational durations for each vessel, while the LCA tool uses vessel categories. By applying a scenario that calculates emissions per tonne of fuel consumed, the comparison between the two tools outputs is direct, thereby ensuring transparency and accuracy in the benchmark analysis.

4.2.3. Benchmark results

This subsection presents the results of the benchmark. First, the approach for evaluating the benchmark will be described. Subsequently, the results of both tools will be provided and analysed. Finally, conclusions will be drawn from the benchmark results.

The benchmark was conducted using the scenario described in subsection 4.2.2. This scenario was designed to calculate the emissions per tonne of fuel burned using both the GHG inventory and LCA tools. For the GHG inventory tool, the WTIV and TB vessels were specified for this scenario, with the relevant input data provided in table 4.4. In contrast, the LCA tool uses vessel categories, specifically a container ship and a ferry for this benchmark, with the relevant input data provided in table 4.5. Both tools calculated the emissions of CO_2, CH_4, N_2O and CO_2-equivalents over 20- and 100-year time horizons, per tonne of fuel burned. The GHG inventory tool calculated these emissions for the WTIV and TB, while the LCA tool calculated them for the container ship and ferry.

The LCA tool calculates both direct and indirect emissions per tonne of fuel burned. To highlight the differences between these types of emissions, the results are presented in table 4.6.

Table 4.6: Emissions calculated by LCA tool per tonne burned fuel

	Direct emissions [kg/t]		**Indirect emissions [kg/t]**	
	Container ship	**Ferry**	**Container ship**	**Ferry**
CO_2	3117.63	3118.57	3697.68	3673.28
CH_4	0.054	0.054	10.83	10.73
N_2O	0.16	0.16	0.17	0.17
CO_2-eq. (20 years)	3165.53	3166.49	4643.35	4610.15
CO_2-eq. (100 years)	3162.67	3163.63	4071.63	4043.75

The results show that direct CO_2 emissions are significant, but indirect emissions are even greater. For CH_4, direct emissions are negligible, while indirect emissions are much larger. This illustrates the substantial contribution of upstream processes to the emissions of both CO_2 and CH_4. In contrast, N_2O emissions remain low for both direct and indirect sources. Finally, across both time horizons for CO_2-equivalents, direct and indirect emissions exhibit similar behaviour to that of CO_2. In conclusion, although indirect emissions have a notable impact, they fall outside the scope of this study and are not included in the benchmark analysis.

This research focuses on direct emissions. Therefore, the calculated direct emissions per tonne of fuel burned is examined. The results of the GHG inventory tool for the WTIV and the LCA tool for the container ship are presented in table 4.7, while the corresponding results for the TB and the ferry are outlined in table 4.8. In addition to the calculated emissions, the tables also provide the differences between the results. These differences are determined using the following equation:

$$D = \frac{E_{\text{GHG}} - E_{\text{LCA}}}{E_{\text{LCA}}} \times 100\% \tag{4.1}$$

where E_{GHG} represents emissions [kg/t] calculated by the GHG inventory tool, E_{LCA} represents emissions [kg/t] calculated by the LCA tool and D represent the difference [%].

Table 4.7: Output data for WTIV from GHG inventory and for container ship from LCA tool

	E_{GHG} [kg/t]	**E_{LCA} [kg/t]**	**D [%]**
CO_2	3,122.19	3,117.63	0.15
CH_4	0.040	0.054	-25.80
N_2O	0.16	0.16	0.61
CO_2-eq. (20 years)	3,169.26	3,165.53	0.11
CO_2-eq. (100 years)	3,167.08	3,162.67	0.14

Table 4.8: Output data for TB from GHG inventory and for ferry from LCA tool

	E_{GHG} [kg/t]	E_{LCA} [kg/t]	D [%]
CO_2	3,112.32	3,118.57	-0.20
CH_4	0.041	0.054	-24.40
N_2O	0.15	0.16	-2.98
CO_2-eq. (20 years)	3,157.91	3,166.49	-0.27
CO_2-eq. (100 years)	3,155.69	3,163.63	-0.25

As shown in table 4.7, the difference in CO_2 emissions between the GHG inventory tool and the LCA tool for the WTIV and container ship is minimal, with a variance of just 0.15%. Similarly, N_2O emissions exhibit a negligible difference of 0.61%. However, CH_4 emissions show a more substantial variation, with a difference of approximately -25.8%. Despite this, the CO_2-equivalent values for both the 20- and 100-year time horizons remain consistent, with differences below 0.3%. In table 4.8, similar trends are observed for the TB and ferry, with minimal differences in CO_2, N_2O, and CO_2-equivalents. A similar discrepancy is observed for CH_4, with a difference of -24.4%.

The larger variation in CH_4 can be attributed to the sensitivity of these emissions to factors such as engine efficiency, operational conditions, and combustion technology, which may be handled differently by the two tools. However, given the small quantities of CH_4 emitted, the overall impact of this variation is minimal. Consequently, the variations in CH_4 emissions have a negligible effect on the overall GHG emissions assessment.

Based on the results of this benchmark, it can be concluded that the GHG inventory tool functions as intended and that the methodology has been implemented correctly. The similarities between the results of the two tools can be attributed to the use of common references and methodologies (Faber et al., 2021) (IPCC, 2021). However, these similarities do not eliminate the need for further research. Although the LCA tool performs adequately, this research remains necessary due to the limited database of the tool to specific vessel-related data. The framework was designed for a wide range of LCA applications for both direct and indirect emissions, which requires extensive datasets. Its limitations are evident, as it only considers two vessel and one fuel type. Additionally, the framework defines just one operational state for vessels. In contrast, the GHG inventory tool offers greater flexibility, enabling more accurate calculation of emissions for specific scenarios. This precision is crucial for conducting detailed and relevant emissions analyses.

4.3. Conclusion

This section provides a conclusion regarding the verification of the model. First, the conclusions drawn from the consistency check in section 4.1 will be discussed, followed by the conclusions from the benchmark analysis in section 4.2. Based on these individual conclusions, an overall assessment of the model's accuracy and reliability will be made.

Section 4.1 focused on verifying the model's internal consistency through one-step analysis and degeneracy testing. These tests confirmed that the model consistently produces accurate outputs under both standard and extreme input conditions. In section 4.2, the results from the GHG inventory tool were benchmarked against an existing LCA tool, using scenario that evaluates the emissions produced per tonne of fuel consumed. This comparison revealed that the GHG inventory tool delivers comparable results, further validating the accuracy and robustness of the model.

By combining the consistency check and the benchmark analysis, the model has been demonstrated to function correctly across a variety of conditions. The consistency check verified the correct implementation of the conceptual model into the simulation model, while the benchmark results confirmed that the tool is aligned with industry standards. Consequently, the model can be considered fully verified, providing reliable results under a range of scenarios, from standard operations to extreme conditions.

5

Case study

This chapter presents the case study, which is employed to evaluate the performance of the developed model. The results of the case study offer preliminary insights into GHG emission reduction strategies for future offshore wind farm decommissioning projects, thereby addressing the fourth research question. First, section 5.1 presents information on OWF Lincs Limited, detailing its components and the defined decommissioning scope. Subsequently, section 5.2 outlines the baseline emissions analyses, encompassing both vessel-related emissions, their associated uncertainties and activity-related emissions. In section 5.3 different decommissioning scenarios are analysed, with the focus on the influence of weather conditions, campaign start dates, and transport strategies. Finally, section 5.4 presents the sensitivity analyses, including both one-at-a-time (OAT) and global sensitivity approaches (GSA), to evaluate the impact of varying parameters.

5.1. Offshore wind farm Lincs Limited

This section provides specifications on the OWF utilised as a case study, namely Lincs Limited. The case study serves to evaluate the developed model. First, detailed information on the OWF and its components will be provided. Subsequently, the decommissioning scope as defined in the DP will be outlined, followed by a description of the defined scope of this specific case study. Finally, the process for obtaining case-specific input parameters for the model will be explained.

As stated, the case study is conducted using the OWF called Lincs Limited. This OWF was built during the period from 2010 to 2012, and officially commissioned in 2013. The OWF consists of 75 WTs located 8km from the coast at Skegness, Lincolnshire, UK (Jalili et al., 2022). Table 5.1 shows further specifications on the components of the OWF. As shown in the table, the OWF also contains an OSS, a MM, IAC and EC. The location of the OWF is illustrated in figure 5.1.

Table 5.1: Specification of OWF Lincs Limited (Jalili et al., 2022)

Specifications	Description
Site area	35 km^2
Distance to shore	8 km off the coast at Skegness, Lincolnshire, UK
Water depth	8 to 18 m
No. of WTs	75
WT type	Siemens Wind Power SWT-3.6
No. of OSS	1
No. of MM	1
Inter-array cables	33 kV cables with 85 km length
Export cable	132 kV cables with 48 km length

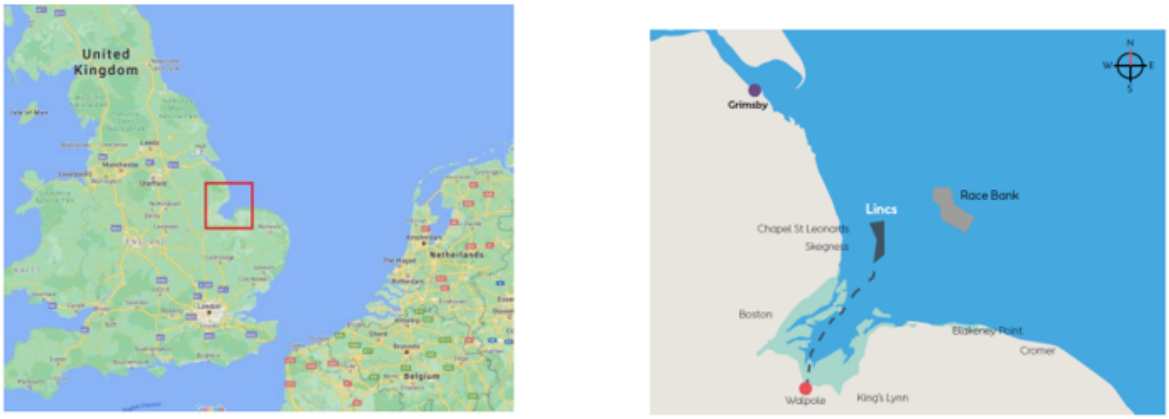

(a) Regional location (Google maps)

(b) Site layout

Figure 5.1: The location of OWF Lincs Limited (Jalili et al., 2022)

The offshore wind turbines have a monopile foundation, and the OSS and MM a jacket foundation. Further specifications for these foundations are shown table 5.2.

Table 5.2: Specifications of the foundations in OWF Lincs Limited (Jalili et al., 2022)

Foundation type	Description	Specifications
Monopiles	Outer shaft diameter	4.7 m - 5 m
	Shaft wall thickness	0.06 m – 0.1 m
	Overall length	36 m – 45 m
	Sea bed penetration	27 m – 38 m
	Monopile Mass	325-800 tons
	Steel	300-700 tons
	Concrete	25-100 tons for connecting the transition piece
Jacket	Size	20 m × 26 m × 30 m
	Piles	4 legs with 54” (1372 mm) diameter
	Sea bed penetration	26 m
	Jacket mass	750-1000 tons
	Total pile mass	580 tons

The decommissioning scope for the OWF Lincs Limited, as outlined in Jalili et al. (2022), is an adapted version of the original DP for Lincs Limited. This DP assumed a design life of 20 years, after which decommissioning would commence. As detailed in subsection 2.2.2, decommissioning involves several stages. The adapted DP in Jalili et al. (2022) provides more details on the removal processes for the WT topside, substructure, OSS, MM, IAC, EC, and SPL. According to the paper, the WT topside will be completely removed, using the reverse installation method. The part-by-part installation approach, commonly employed in the offshore wind industry, has been adopted in this decommissioning process based on the operational considerations discussed in this study, as indicated in section 2.1.2. Hence, the topside removal of WT will include blade 1, blade 2, blade 3, nacelle and tower, in this order. The vessels utilised for WT topside decommissioning are a WTIV, two BVs and two TBs. These employ the feeder concept as a transport strategy. The specific operations and their sequence during offshore WT topside decommissioning are illustrated in figure 2.10. In this figure, the top flow chart reflects this specific decommissioning. In addition, it was indicated that the WT substructures, which include the transition piece and monopiles, will be partially removed. The substructure will be cut 1 meter below the seabed using internal cutting techniques. The vessels involved in this stage are an OSV, a ROV, a WTIV, a BV, and a TB, utilising the feeder concept for transport. The operations and sequence for the partial substructure removal are illustrated in figure 2.11, where the top flow chart reflects this specific removal type.

Regarding the OSS, Jalili et al. (2022) indicates that it will be fully removed, although no specific details on the decommissioning method are provided. In this study, the vessels required for this operation have been selected based on operational requirements. These include an ROV, WTIV, BV, and TB, with the feeder concept employed for transport. Figure 2.12 presents the flow of operations, with the lower chart representing the complete removal process. The decommissioning strategy and vessels used for the MM decommissioning, are identical to those of the OSS. The specific operations and sequence of this dismantling of the MM can be observed in the bottom flow chart of figure 2.13. Finally, it was indicated in both the original and adapted DP that the IAC, EC and SPL will be left in situ. The specific operations and their sequence for leaving the IAC, EC and SPL in situ are shown in the bottom flow charts of figures 2.14, 2.15 and 2.16, respectively.

This research aligns with the specific objectives of the EU EoLO HUBs project, which focuses on the decommissioning of wind turbine blades (Dighe et al., 2024). The project's emphasis on blade decommissioning is particularly relevant, as it addresses key sustainability challenges in the life cycle of offshore wind farms. Furthermore, UWiSE Decommission simulated durations for this scenario, which are essential inputs for the GHG inventory tool developed in this research. As a result, the decommissioning scope in this study has been simplified to focus solely on the removal of wind turbine topsides, including the blades, nacelle, and tower, while the WT substructures, OSS, MM, IAC, EC, and SP are excluded. The decommissioning of the WT topsides will follow the method, vessels, and transport strategy outlined in the adapted DP. As mentioned above, this involves dismantling using the part-by-part method with a WTIV, and transport supported by two barges and two TBs, utilising the feeder concept. Since two barges and two tugboats are employed, this transport strategy is also referred to as the double feeder approach. Additionally, an OSV can be deployed to assist with other decommissioning operations such as equipment handling, monitoring, and ensuring safe working conditions during the decommissioning process. OWF Lincs Limited consists of 75 wind turbines, as shown in table 5.1. The components of 8 wind turbines fit on one barge, meaning that after dismantling 8 turbines, one barge and TB return to shore to unload the components. For continuous decommissioning, a second barge and TB remain offshore to support the removal process. The total campaign duration depends on weather conditions, but according to Dighe et al. (2024), the average duration for this decommissioning scope of OWF Lincs Limited is estimated to be approximately 5 months.

The methodology used in the developed GHG inventory tool is described in chapter 3. The different parameters and variables required to perform the calculations are listed in subsection 3.2.2. Variables are values that are case-dependent, and comprise for this tool the transit and idling/operating durations of vessels. These variables are obtained using UWiSE, the tool described in section 2.3. UWiSE simulates all specific operations described for the decommissioning of WT topsides, visible in the flowchart of figure 2.10. The simulation incorporates weather data from 24 different years (1996-2017), allowing the assessment of both seasonal variations and differences between years. By applying general weather constraints, the results take weather-related delays into account.The assumed weather limits for the three vessels used in the decommissioning of WT topsides of OWF Lincs Limited are shown in table 5.3.

Table 5.3: Maximum operational conditions for vessels used in Lincs Limited decommissioning (Mancini et al., 2023)

Vessel type	Max wind speed (@ 10m) [m/s]	Max Hs [m]
WTIV	16	3
OSV	16	2.5
BV + TB	16	1.5

As already indicated in section 2.3, different outputs are generated by UWiSE, namely simulation log files, an excel summary output file and the interactive Gantt chart. For the purpose of the developed GHG tool, only the excel summary output file is of interest. In fact, this excel provides transit and idling/operating durations for the vessels. With this data, deterministic baseline emission, scenario, sensitivity and uncertainty analyses are conducted, which will be treated in the next sections.

5.2. Deterministic baseline emissions

This section provides the results of deterministic baseline emission analyses. These analyses were conducted with the developed GHG inventory tool for OWF Lincs Limited decommissioning. The deterministic baseline emissions of this OWF were analysed with two approaches. First, subsection 5.2.1 will present emissions per vessel type, followed by the emissions per activity in subsection 5.2.2.

5.2.1. Emissions per vessel type

This subsection provides the vessel-related emissions for the decommissioning of WT topsides of OWF Lincs Limited. First, the amount of emitted CO_2, CH_4 and N_2O will be presented and discussed. Subsequently, the amount of emitted CO_2-equivalents with time horizons of 20- and 100 years will be analysed. For both, conclusions are drawn from the results.

The emissions from the different vessels are calculated using the developed GHG inventory tool, which applies the deterministic methodology described in section 3.1. The variable inputs for the tool are the vessel durations for the decommissioning of the WT topsides of OWF Lincs Limited. These durations are simulated with UWiSE for the decommissioning in different years (1994-2017), from which an average duration is calculated based on 24 simulations. The summary output file provides these average vessel durations for the OSV, TBs, and WTIV. The UWiSE-calculated durations are then converted into two key operational states for the GHG inventory tool: transiting and idling/operating durations. The average durations for the TBs and WTIV are presented in table 5.4. Since the OSV was not deployed during the decommissioning process, it is excluded from further discussion in the results.

Table 5.4: Durations ($T_{transit}$) and ($T_{idle/operate}$) for vessels during OWF Lincs Limited's decommissioning

Vessel type	**avg**	
	T_{transit} [hr]	$T_{\text{idle/operate}}$ [hr]
TB1	61.16	1167.25
TB2	57.84	1023.30
WTIV	8.39	2253.62

With the provided durations in table 5.4, the amount of CO_2, CH_4, N_2O and CO_2-equivalents over the 20- and 100-year time horizons were calculated for the TBs and WTIV.

Figure 5.2 illustrates the amount of CO_2, CH_4, N_2O and CO_2-equivalents with 20-year and 100-year time horizons emitted by each vessel during decommissioning of WT topsides of OWF Lincs Limited. In this figure, CO_2 is depicted in blue, CH_4 in yellow, N_2 in green, while CO_2-equivalents are shown in grey for the 20-year horizon and in red for the 100-year horizon.

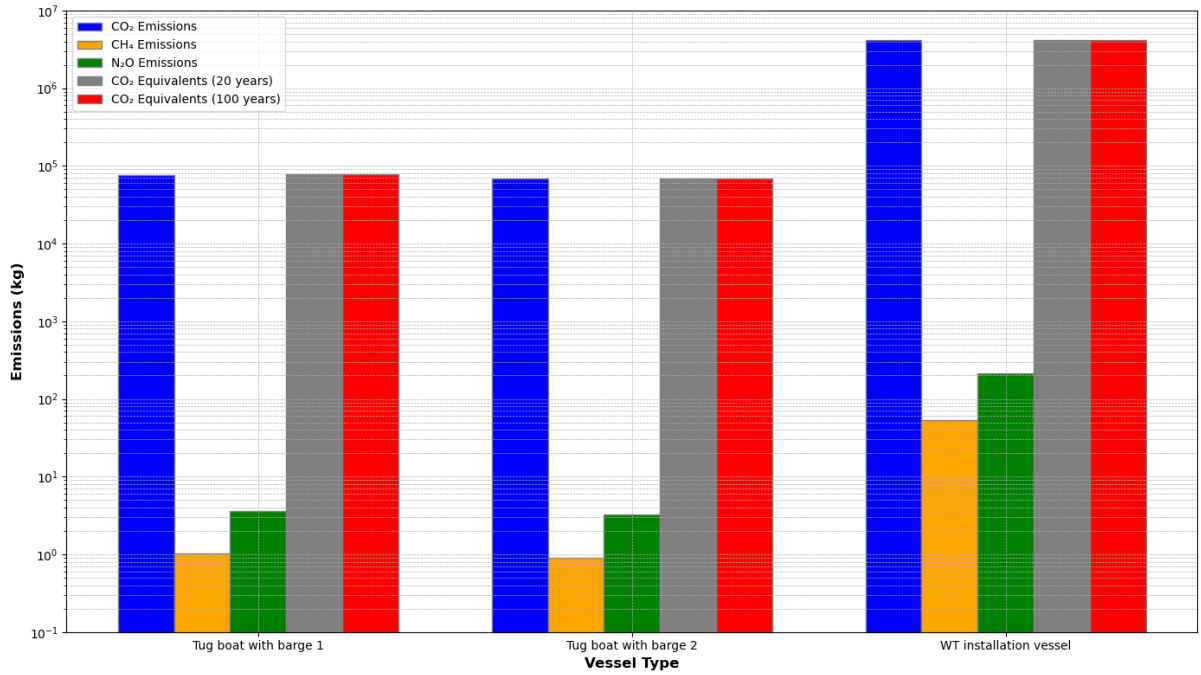

Figure 5.2: The amount of CO_2, CH_4, N_2O and CO_2-equivalents over 20- and 100-year time horizon released per vessel for the decommissioning of OWF Lincs

The figure shows that the WTIV emits approximately 10^2 as much as than TB1 and TB2 for all emission types. This result aligns with expectations, given the larger operational scope and energy demands of the WTIV. Across all vessels, CO_2 and its equivalents dominate the emissions profile, with values exceeding 10^6 kg, whereas CH_4 and N_2O emissions only slightly exceed 10^2 kg. This clearly demonstrates that CO_2 emissions are orders of magnitude higher than N_2O, and CH_2 emissions are negligible.

There is minimal difference in the CO_2-equivalent emissions between the 20-year and 100-year time horizons across all vessels. To clarify, figure 5.3 (a) and (b) shows the pie charts for the WTIV, showing CO_2-equivalent over 20-year and 100-year time horizons, respectively. The CO_2-equivalents of the TBs consist of almost exactly the same fractions. Therefore, the pie charts for these vessels are not provided. The fractions of CO_2, CH_4 and N_2O are illustrated in blue, yellow, and green, respectively, in both charts.

(a) Time horizon of 20 years

(b) Time horizon of 100 year

Figure 5.3: The pie charts with fractions CO_2, CH_4 and N_2O of CO_2-equivalents for WTIV during decommissioning of OWF Lincs Limited

Figure 5.3 shows that the fractions of the time horizons only differ by a maximum of 0.07%, and both

are mainly determined by the amount of CO_2. This indicates that the CO_2-equivalents over both time horizons are nearly identical due to the dominance of CO_2 emissions. This indicates that reducing CO_2 emissions is most effective strategy for reducing overall CO_2-equivalents. Although measures to reduce CH_4 and N_2O may contribute, their effect will be much smaller. Additionally, short- and long-term emission reduction strategies will produce similar results in terms of climate impact for the vessels studied, particularly the TB and WTIV.

To better understand the impact of different emission types on global warming, table 5.7 provides both the fractions of total emissions and CO_2-equivalents over a 20-year time horizon.

Table 5.5: Comparison of the fractions of CO_2, CH_4 and N_2O of the total emissions and CO_2-equivalents over a 20-year time horizon for the decommissioning of OWF Lincs Limited

	Total emissions [%]	**CO_2-equivalents GWP20 [%]**
CO_2	99.9	98.5
CH_4	0.001	0.1
N_2O	0.005	1.3

As visible in the table, CO_2 accounts for 99.9% of the total emissions, but its contribution slightly decreases to 98.5% in terms of CO_2-equivalents due to the influence of other GHG. While CH_4 represents only 0.001% of total emissions, its share rises to 0.1% in CO_2-equivalents due to its higher GWP over a 20-year horizon. Similarly, N_2O, which constitutes only 0.005% of emissions, contributes 1.3% to CO_2-equivalents due to its significantly higher GWP. This comparison highlights the disproportionately larger impact of CH_4 and N_2O on CO_2-equivalents compared to their total emissions, driven by their high GWP values. Nevertheless, CO_2 remains the dominant contributor to both total emissions and CO_2-equivalents over a 20-year time horizon. This pattern holds for the 100-year time horizon as well, as the fractions remain nearly identical across both time horizons.

From this point onward, only CO_2-equivalents with a 100-year GWP will be presented for results where the trends are consistent across all emission types. The choice to focus on CO_2-equivalents is driven by their ability to capture the impact of all greenhouse gases, providing a comprehensive representation of emissions. The choice between the 20- and 100-year time horizons is not significant, as the results are nearly identical. However, if a preference is required, the 100-year horizon is more suitable, as it aligns better with long-term climate policy, making it the preferred metric for stakeholders. Additionally, for cases where the same trends are observed across all vessels, only the results for the WTIV will be shown, as it is the primary contributor to emissions and thus the critical focus for reduction strategies.

5.2.2. Emissions per activity

This subsection provides the activity-related emissions associated with the decommissioning of WT topsides of OWF Lincs Limited. First, the methodology used to calculate these emissions is explained, followed by a discussion of the results. Finally, conclusions are drawn based on these results.

The deterministic model described in section 3.1 was used to calculate activity-related emissions. The detailed durations for WT topside removal activities were generated by UWiSE based on the 24 decommissioning years (1994-2017) along with a perfect weather scenario. In these simulations, transit durations between wind turbines are assumed due to the unspecified layout of the OWF. UWiSE simulated the total, core, and idle durations for each activity, as well as delays caused by permits, weather conditions, and resource availability. For emissions calculations, only the core duration is used, as it reflects the actual time spent on each activity. The core duration excludes idle periods and delays, ensuring a more accurate estimation of emissions by preventing overlaps between sequential activities. As a result, the core duration remains consistent across all activities in all 25 simulations, making additional simulations unnecessary. Therefore, only the perfect weather simulation was used. Table 5.6 outlines the offshore activities for the decommissioning of WT topsides of OWF Lincs Limited, including the vessel type, its operational state, and the core duration for each activity.

Table 5.6: Activity durations and corresponding vessel states during the decommissioning of OWF Lincs Limited

Activity	Vessel	State	Total core duration [hr]
Transit Tug + BV	TB	1	14.66
Transit JUB	WTIV	1	8.39
Positioning jack-up	WTIV	2	225.00
Jacking-up	WTIV	2	450.00
Remove blade (total)	WTIV	2	450.00
Remove nacelle	WTIV	2	187.50
Remove tower	WTIV	2	450.00
Jacking down	WTIV	2	75.00
Transit back	TB	1	22.61

With the provided in table 5.6, the amount of CO_2, CH_4, N_2O and CO_2-equivalents over 20- and 100-year time horizons were calculated for each activity.

Figure 5.4 illustrates the contribution of each activity to the total emissions during the decommissioning of WT topsides at OWF Lincs Limited, showing only the fractions of CO_2-equivalents with a 100-year time horizon. Since the focus is on the relative contributions of different activities to total emissions, the results are presented in a pie chart.

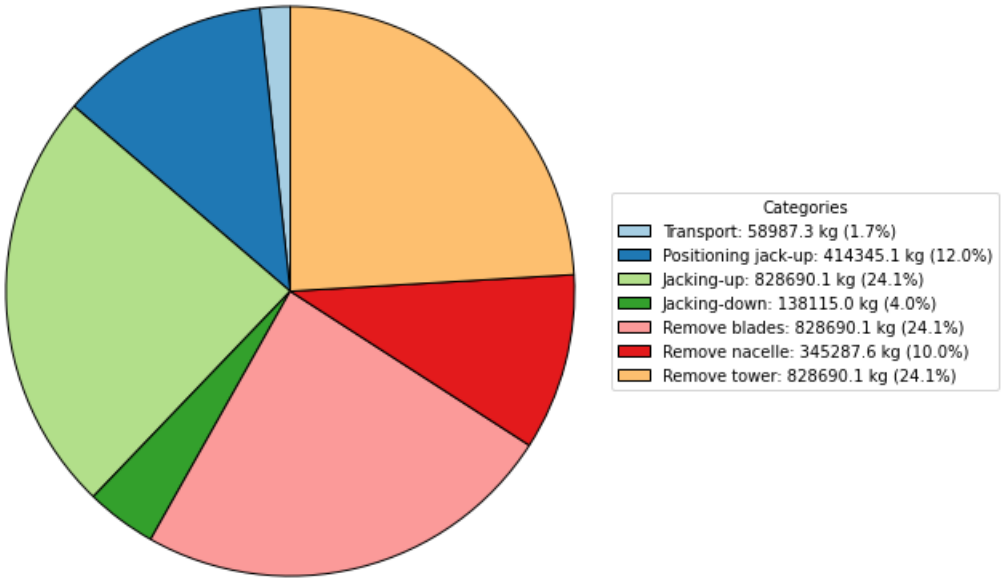

Figure 5.4: Pie chart with fractions of activities for CO_2-equivalent over 100-year time horizon released during decommissioning of OWF Lincs Limited

Figure 5.4 presents the breakdown of CO_2-equivalents over a 100-year time horizon for all decommissioning activities of WT topsides at OWF Lincs Limited, encompassing both transport and operational emissions. Transport emissions consist of activities such as 'transit tug and BV,' 'transit JUB,' and 'transit back of tug and BV,' all categorised under the transiting state. These transport emissions account for only 1.7% of the total emissions and are therefore grouped together under the 'Transport'. In contrast, operational emissions, which stem from activities such as 'positioning jack-up,' 'jacking up,' 'removing blades,' 'removing nacelle and tower,' and 'jacking down,' are classified under the idling/-operating states. These operational emissions account for the remaining 98.3% of the total and are shown separately to reflect their large contribution. The significant difference between transport and operational emissions is primarily attributed to the much longer durations of operational activities. As outlined in table 5.6, transit duration represents only 2.45% of the total core duration, while idling/operating durations account for 97.55%. Consequently, emissions are predominantly influenced by the duration of operational activities, which is further amplified by fuel consumption during these operations. The difference in durations is influenced by the decommissioning concept and batch size, as these factors can extend or reduce the overall durations.

Since all operational activities occur in the idling/operating state of the WTIV, fuel consumption remains constant across these activities. As a result, the distribution of emissions primarily reflects the duration of each activity. 'Jacking up,' 'removing blades,' and 'removing the tower' each contribute 24.1% to total emissions due to their longer durations, while 'positioning jack-up,' 'removing the nacelle,' and 'jacking down' have smaller contributions, corresponding to their shorter durations. Although these activities share similar fuel consumption rates, it is important to note that actual fuel consumption and emissions can vary depending on the specific nature of the task. Although the operational activities in this study are assumed to have equivalent fuel consumption rates due to a lack of specific data, it is important to recognise that actual fuel consumption and associated emissions may vary between different operational activities.

In this analysis of the activity-related emissions, only the core duration was used, which is an important aspect to verify. To validate the exclusive use of core duration, a comparison between activity-related outputs and vessel-related outputs was conducted. The results of this comparison are illustrated in table 5.7.

Table 5.7: Comparison of the total activity and total vessel emissions for the decommissioning of OWF Lincs Limited

	Total activity emissions [kg]	**Total vessel emissions [kg]**	**Difference [%]**
CO_2	3,393,988.62	3,530,488.66	3.87
CH_4	43.73	45.50	3.89
N_2O	174.05	180.58	3.62
CO_2-eq. (20 years)	3,445,175.58	3,583,609.93	3.86
CO_2-eq. (100 years)	3,442,805.30	3,581,144.08	3.86

In this table, total emissions from all activities under the perfect weather simulation are presented in the first column. The second column shows total emissions for all vessels under the same perfect weather conditions. Both the activity and vessel emissions exclude delays, though vessel emissions include those released during idling periods, whereas the activity script focuses solely on core durations. The third column highlights the differences between the outputs. The average difference across all emission types is 3.8%, indicating that emissions released from idling at sea are minimal. Therefore, using core duration is confirmed as a valid method for calculating activity emissions.

In conclusion, the analysis reveals that the majority of emissions are generated during operational activities, with transit contributing only a small portion. This distribution is primarily driven by the longer durations of operational activities. Therefore, strategies focused on reducing these durations could play a key role in mitigating overall emissions. Optimising the decommissioning concept and batch sizes could be part of these strategies. Additionally, further reductions in operational emissions can be achieved by improving fuel consumption rates, ultimately supporting a more sustainable decommissioning of OWFs.

5.3. Influence of weather conditions and transport strategy

This section presents two scenario analyses for the decommissioning of WT topsides at OWF Lincs Limited. These analyses investigate the influence of weather conditions and transport strategy on GHG emissions. Subsection 5.3.1 focuses on the impact of inter-annual weather variability on the vessel-related emissions. Subsequently, the impact of the campaign start date and the transport strategy on the total emissions is addressed in subsection 5.3.2. Both subsections critically evaluate the results and propose potential strategies for optimising decommissioning processes, with the aim of minimising vessel-related GHG emissions.

5.3.1. Inter-annual weather variability

This subsection investigates how inter-annual weather variability affect the direct vessel-related GHG emissions during the decommissioning of WT topsides OWF of Lincs Limited. First, the methodology for the weather assessment is introduced and explained in detail. Subsequently, the results are presented and analysed. Finally, conclusions are drawn from these results.

This subsection evaluates the impact of varying weather conditions on vessel-related emissions, using the deterministic methodology outlined in section 3.1. The baseline vessel emission analysis, presented in subsection 5.2.1, utilised average transit and idling/operating durations. These durations, presented in table 5.4 were obtained from 24 simulations of different weather years. Although these average durations provide insights into general trends, analysing other weather scenarios offers the opportunity to better understand the effect of weather variations on emissions. Due to the complexity of presenting the results for 24 distinct weather scenarios in a clear and organised manner, the analysis focused on the impact of minimum, average, and maximum conditions. Additionally, a perfect weather simulation was included as a separate scenario. The average values are summarised in table 5.4, while the minimum, maximum, and perfect weather durations are detailed in table 5.8.

Table 5.8: Durations ($T_{transit}$) and ($T_{idle/operate}$) with minimum, maximum and perfect weather for vessels during OWF Lincs Limited's decommissioning

Vessel type	**min**		**max**		**PW**	
	$T_{transit}$ [hr]	$T_{idle/operate}$ [hr]	$T_{transit}$ [hr]	$T_{idle/operate}$ [hr]	$T_{transit}$ [hr]	$T_{idle/operate}$ [hr]
TB1	24.19	1,018.90	171.37	1,379.40	24.19	980.65
TB2	23.57	917.30	119.33	1,198.23	23.57	880.43
WTIV	8.39	2,019.24	8.39	2,549.46	8.39	1,858.51

With the provided durations in table 5.8, the amount of CO_2, CH_4, N_2O and CO_2-equivalents over the 20- and 100-year time horizons were calculated for the TBs and WTIV under the different weather scenarios.

Figure 5.5 illustrates the CO_2-equivalent emissions over a 100-year time horizon for the TBs and WTIV under minimum, average, maximum and perfect weather conditions during the decommissioning of WT topsides of OWF Lincs Limited. The bar for the perfect weather scenario is shown with a dashed line to distinguish it from the generalised weather scenarios. In the perfect weather scenario, emissions are minimised due to the absence of delays, rendering it a hypothetical best-case scenario.

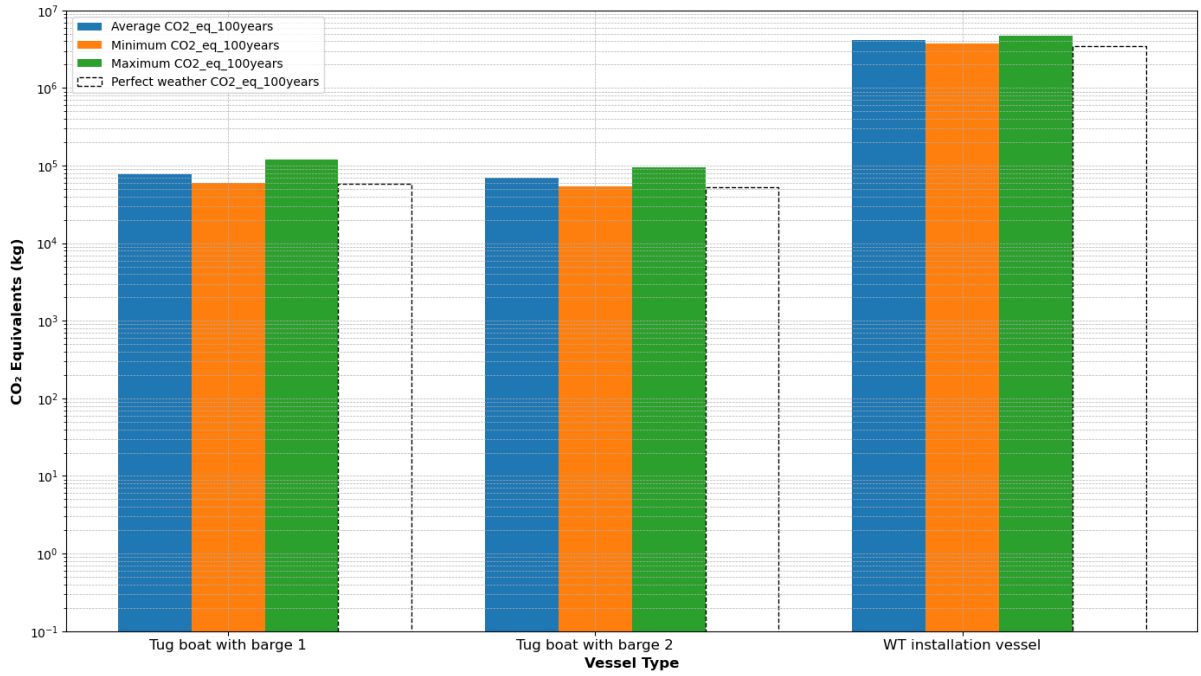

Figure 5.5: The amount of CO_2-equivalents over 100-year time horizon under minimum, average, maximum and perfect weather conditions released per vessel for the decommissioning of OWF Lincs

The figure indicates that the order of vessels contributing to emissions remains consistent across all weather scenarios, with the WTIV consistently being the largest emitter, followed by TB1 and TB2. The generalised weather scenarios from the years 1994 to 2017 - average, minimum, maximum - and perfect weather show a predictable trend in their impact on vessel-related emissions. The perfect weather scenario shows the lowest emissions for all vessels, as operations proceed without unnecessary fuel consumption caused by delays. These are followed by the minimum, average and maximum scenarios, ranked according to the respective transit and idling/operating durations, as shown in table 5.8.

To quantify the impact of weather delays on emissions, the total CO_2-equivalent emissions over a 100-year time horizon were compared between the perfect weather and maximum weather scenarios. In the perfect weather scenario, total CO_2-equivalent emissions amounted 3,581,144 kg, whereas in the maximum weather scenario, the emissions increased to 4,958,719 kg. This difference of 1,377,575 kg CO_2-equivalents represents approximately 27.8% of the emissions in the maximum weather scenario. These additional emissions are a result of extended transit and idling/operating durations. With extended transiting and idling/operating durations, fuel consumption increases, resulting in higher emissions. The extended transiting durations can be attributed to vessels reducing speed in response to adverse weather conditions. As explained in section 3.1, the idling/operating state consists of two components: immobile at sea and total transfer duration. In this case study, the total transfer duration has a negligible impact on emissions, making immobile at sea the dominant factor. The extended idling/operating durations are therefore caused by vessels remaining immobile at sea while awaiting improved weather conditions to resume operations or transit. As engines cannot be turned off while vessels are offshore, fuel consumption continues during these periods, leading to higher emissions. This confirms that the additional emissions in the maximum weather scenario result from delays caused by adverse weather conditions.

In conclusion, adverse weather conditions significantly increase GHG emissions from vessels due to extended transit and idling/operating durations. Reducing these emissions requires strategies to optimise operations under challenging weather conditions. Potential approaches include improved planning to avoid delays, deploying vessels that are less affected by adverse weather.

5.3.2. Campaign start date and transport strategy assessment

This subsection examines how the campaign start month and transport strategy affect the amount of direct GHG during the decommissioning of WT topsides of OWF Lincs Limited. First, the methodology of this analysis is discussed, followed by a presentation and analysis of the results. Finally, conclusions are drawn based on these results.

This subsection evaluates the impact of the campaign start month and transport strategy on total emissions, using the deterministic using the methodology described in section 3.1. The start months and transport strategies were analysed simultaneously, leading to an integrated conclusion. This analysis was conducted under conditions similar to those in TNO's study, as described in Dighe et al. (2024), where the impact of these factors on costs was examined. The campaign starting months include all 12 months of the year. Each of these months is simulated as the start month. For each starting month, the impact on the amount of GHG emitted by all vessels involved in decommissioning OWF Lincs Limited is assessed. In addition to the variation in starting months, this subsection also considers the impact of different transport strategies on GHG emissions. As discussed earlier in subsection 2.2.3, there are two transport strategies: the pendulum strategy and the feeder strategy. The pendulum strategy involves a WTIV shuttling between the port and the OWF to transport dismantled parts. In the feeder strategy, the WTIV remains on site while smaller support vessels, TBs, transport the components to the port. In the Lincs Limited case, two TBs are deployed to avoid the WTIV from waiting for one TB to return from port. As mentioned in section 5.1, this strategy is referred to as the double feeder concept. Besides the WTIV and TBs, already discussed in previous analyses, a CTV is also included in this analysis. The CTV is used in both strategies for preparatory work on the turbines before the actual removal takes place. The transiting and idling/operating durations for the different starting months and transport strategies were calculated and simulated by UWiSE for the decommissioning of 20 years, from 1995 to 2014. Unlike previous analyses, which used average, minimum, maximum or perfect weather values, this analysis included all 20 simulated values for the different years. These different transiting and idling/operating durations for the vessels - CTV, TBs and WTIV - over the years 1995 to 2014, results in 20 different outputs. These results will be presented using box plots to illustrate the variation across the years.

Figure 5.6 (a) and (b) respectively show the results of the total CO_2-equivalents over 100-year time horizon using the pendulum and double feeder strategies. Both figures contain 12 box plots, with each representing a starting month of the decommissioning campaign.

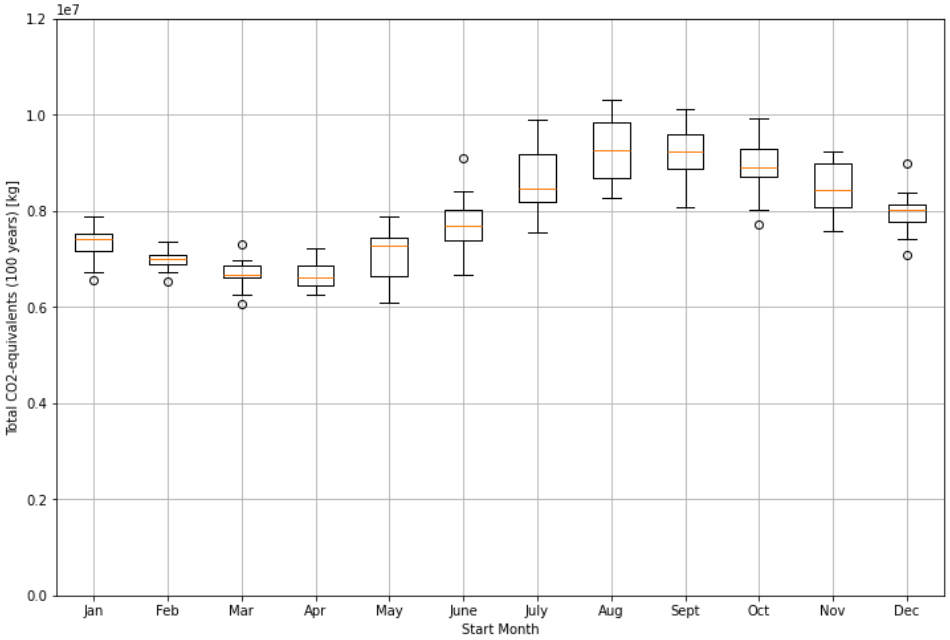

(a) Pendulum strategy

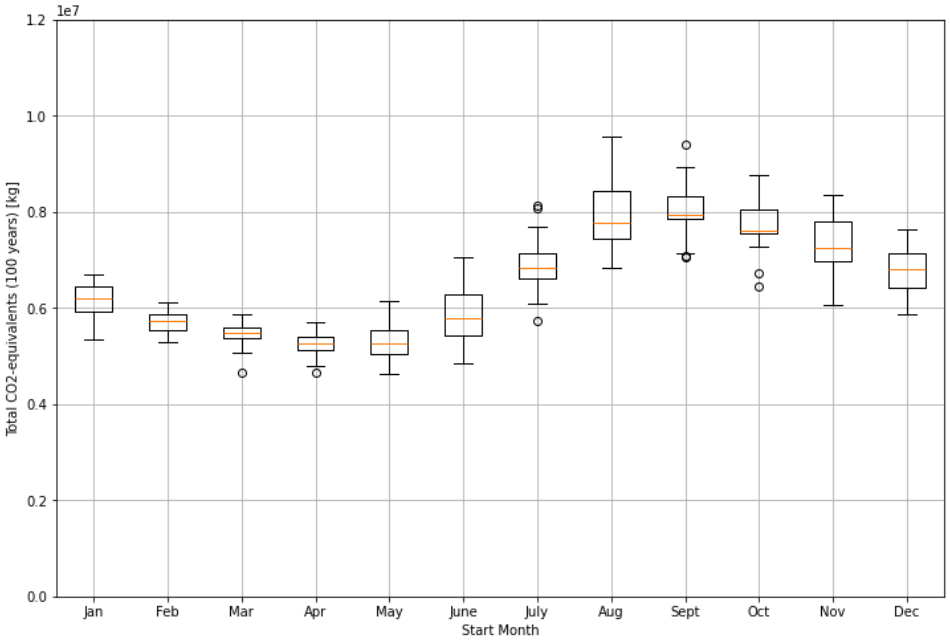

(b) Double feeder strategy

Figure 5.6: The amount CO_2-equivalents over 100-year time horizon for all starting months and both transport strategies during decommissioning of OWF Lincs Limited

The results of the pendulum strategy show that total CO_2-equivalents over 100-year time horizon are relatively low when decommissioning starts in the first months of the year, but begin to increase markedly for start dates in the summer months. Emissions reach their highest values when decommissioning begins in July and August, with a median of approximately 9.0 x 10^6 kg. In addition, a wider spread in emission results is visible for these months, indicating increased variability due to weather-related delays. The lowest emissions are observed for start dates in February and March.

The double feeder strategy follows a similar seasonal pattern, but generally shows consistently lower emission levels compared to the pendulum strategy. This reduction can be attributed to the use of TBs for transport, which allows the WTIV to remain on site and focus solely on dismantling operations. Given the high fuel consumption of the WTIV, especially in transiting mode, reducing its need for transport contributes significantly to the emission reductions. Although emissions also increase in the summer start months, they remain consistently lower than in the pendulum strategy, with a peak of approximately 8.0 x 10^6 kg in July and August. This strategy also shows a larger spread in emissions during the summer start months, but this variability is less pronounced than in the pendulum strategy. The lowest emissions are again registered for decommissioning starting in February and March, with a median of approximately 6.0 x 10^6 kg of CO_2-equivalents.

This seasonal pattern can be explained by the duration of the decommissioning campaign, which for the WT topsides of OWF Lincs Limited averages around five months. Therefore, when this specific decommissioning starts early in the year, it is completed before autumn, avoiding the period of more frequent and severe weather disruptions. In contrast, when this campaign begins in summer, it extends into autumn and early winter, when adverse weather conditions, such as storms and rough seas, are more prevalent. These conditions cause longer delays, particularly during transit and idling periods, as vessels must reduce speed or remain immobile at sea while waiting for safer conditions to resume operations. This explains the higher emissions observed in subsection 5.3.1. The increased variability in emissions seen during the summer months can be attributed to the unpredictability of the weather in the later stages of the project. Decommissioning that extends into autumn and winter is subject to more volatile weather patterns, increasing the likelihood of delays.

In conclusion, the double feeder strategy consistently generates lower emissions than the pendulum strategy, particularly due to the use of TBs for transport, allowing the WTIV to focus exclusively on dismantling operations. Additionally, this analysis revealed that the total duration of the decommissioning campaign plays a significant role in the total emissions produced. Furthermore, the seasonal variability observed in the start months is directly linked to the unpredictability of weather conditions. In summary, the effectiveness of decommissioning strategies varies by case study. For the decommissioning of the WT topsides of OWF Lincs Limited,it is recommended to implement the double feeder strategy and initiate the campaign early in the year, ideally in February or March, to minimise operational disruptions, and consequently emissions.

These results can be compared with the findings of of TNO's study, Dighe et al. (2024), which focused on costs. In that study, the pendulum strategy was identified as cost-efficient, noting similar seasonal variations in costs across different start months. However, this analysis emphasises the reduction in emissions associated with the double feeder strategy. While the double feeder strategy may involve higher costs, it demonstrates significant benefits in terms of emission reductions. This suggests a potential trade-off between cost efficiency and emissions reduction, inviting further investigation into how these factors balance, particularly given the offshore wind industry's growing focus on carbon reduction. Future studies could explore this trade-off more thoroughly, taking into account both sustainability targets and cost considerations.

5.4. Uncertainty analysis

This section presents an uncertainty analysis for vessel-related emissions released from the decommissioning of WT topsides at OWF Lincs Limited. An uncertainty analysis identifies which parameters have the most significant impact and evaluates how uncertainties in input parameters affect the output. First, subsection 5.4.1 covers a one-at-a-time sensitivity analysis for the deterministic model. Subsequently, a global sensitivity analysis for the probabilistic model is conducted in subsection 5.4.2. Finally, subsection 5.4.3 addresses the uncertainty propagation in emissions, providing insights into the reliability and robustness of the results.

5.4.1. One-at-a-time analysis

This subsection considers the OAT-based sensitivity analysis for decommissioning of WT topsides of OWF Lincs Limited. First, the methodology is outlined, followed by the presentation and analysis of the results. Finally, conclusions are drawn from the findings of this analysis.

As discussed in section 3.1, the aim of a deterministic sensitivity analysis is to evaluate how sensitive model results are to changes in input parameters. This differs from scenario analysis in that not the entire parameter set, but only individual values are modified. As described in section 3.1, the OAT approach is selected to perform the DSA. This method adjusts one input parameter at a time, while the others remain constant, in order to quantify the effect of this variation on the output. Performing an OAT analysis requires identifying the relevant input parameters and assigning specific variations.

First, the key parameters are selected. As outlined in subsection 3.2.2, the input parameters include fuel consumption, LCV, thermal efficiency, emission factors, and the GWP for CO_2, CH_4, and N_2O. Since GWP does not directly affect the quantities of CO_2, CH_4, and N_2O emitted, but only modifies their impact over 20 or 100 years, varying GWP would not provide meaningful insights into the emissions. Additionally, while the foundation of GWP is rooted in technical calculations that estimate impacts over a defined time horizon, the value is also shaped by policy considerations. The purpose of this analysis is to examine the impact of technical parameters on actual emissions, therefore GWP is excluded from the key parameters. The remaining parameters directly influence the amount of emissions, making them relevant for inclusion in the OAT analysis. For parameter variations, a uniform approach is applied, with each parameter increased and decreased by 5%, 10%, and 20%. This consistent variance set facilitates the comparability of the sensitivity of the different parameters and provides insight into their respective impact on the model outputs.
In addition, the average transiting and idling/operating durations for the TBs and WTIV, as provided in table 5.4, were utilised as case-dependent inputs in the OAT analysis for the WT topside removal at OWF Lincs Limited.

The percentage variations in the selected parameters are applied to the decommissioning of WT topsides of OWF Lincs Limited, and the results are presented in figures 5.7 to 5.10. Figure 5.7, 5.8 and 5.9, show the impact of these variations on CO_2, CH_4, and N_2O, respectively. In addition to the emissions of individual gases, CO_2-equivalents over 20- and 100-year time horizons are also depicted in figures 5.10 (a) and (b), providing the combined effects of GHGs. Although GWP is not directly included in the OAT analysis, changes in the emissions still influence the CO_2-equivalents. A consistent y-axis scale is maintained for CO_2 and CO_2-equivalents, while different y-scales are applied to CH_4 and N_2O to better visualise the sensitivity of these outputs to different input parameters. This ensures clarity and facilitates comparison across the different parameters. In the graphs, each parameter is assigned a unique colour for distinction. Fuel consumption, thermal efficiency, lower calorific value, CH_4 emission factors, CO_2 emission factors, and N_2O emission factors are represented in blue, green, red, turquoise, purple, and yellow, respectively. Numerical details are included in appendix D.

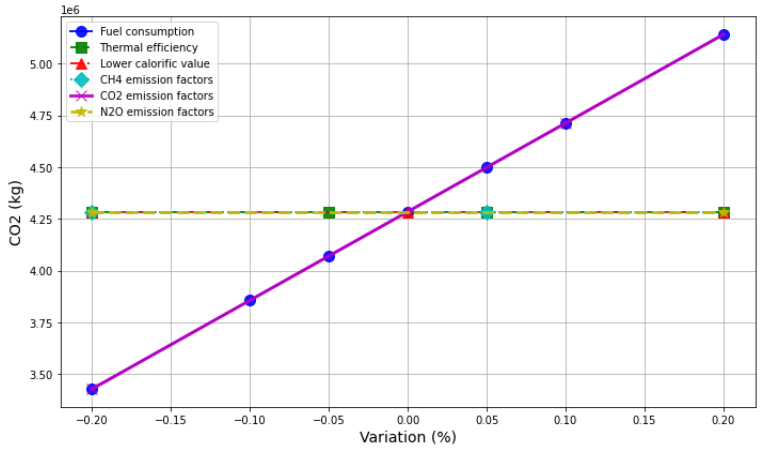

Figure 5.7: Impact of percentage variations in parameters on CO_2 emissions during the decommissioning of OWF Lincs Limited

Figure 5.7 demonstrates that both fuel consumption and the CO_2 emission factor have a direct and proportional impact on CO_2 emissions, with variations in these parameters linearly influencing the output due to their direct correlation with the amount of fuel burned. In contrast, parameters as LCV and thermal efficiency have no effect on CO_2 emissions. The linear sensitivity in this case is attributed to the proportional relationship between fuel burned and the amount of CO_2 released.

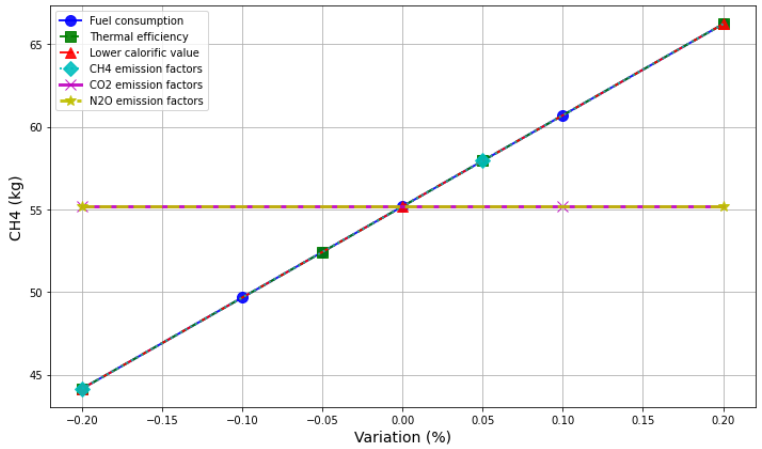

Figure 5.8: Impact of percentage variations in parameters on CH_4 emissions during the decommissioning of OWF Lincs Limited

Figure 5.8 demonstrates that CH_4 emissions are influenced by fuel consumption, thermal efficiency, LCV, and the CH_4 emission factor, each having a direct and proportional effect on the output. This linear sensitivity is expected, as these parameters directly affect the amount of fuel burned and emissions produced. The y-axis in this figure is scaled differently from that of CO_2 emissions due to the significantly lower quantities of CH_4 emitted. While this adjustment improves the visibility of trends in CH_4 output, it may obscure the fact that the absolute sensitivity is lower.

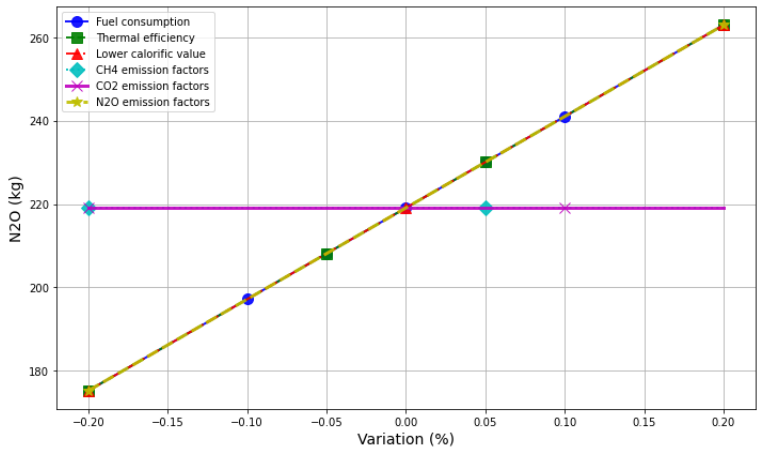

Figure 5.9: Impact of percentage variations in parameters on N_2O emissions during the decommissioning of OWF Lincs Limited

Figure 5.9 shows that N_2O emissions are influenced by the same parameters as CH_4, each having a direct and proportional effect on the output. This linear sensitivity is expected because the influencing parameters are directly related to fuel use and emissions production, resulting in proportional changes. The y-axis is also scaled differently from that of CO_2 emissions due to the lower quantities of N_2O emitted.

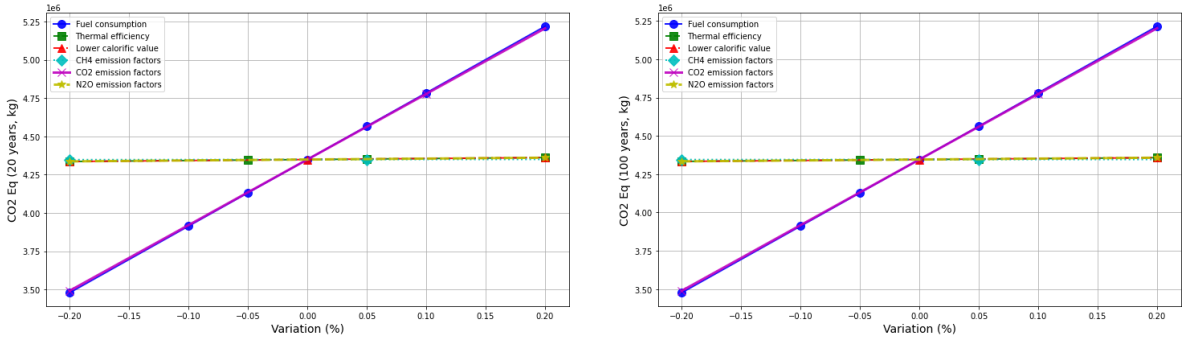

(a) 20-year time horizon

(b) 100-year time horizon

Figure 5.10: Impact of percentage variations in parameters on CO_2-equivalents during the decommissioning of OWF Lincs Limited

Figure 5.10 (a) and (b) illustrate that CO_2-equivalent emissions over both 20-year and 100-year horizons are primarily driven by variations in fuel consumption and the CO_2 emission factor, each showing a strong linear effect. This linear sensitivity is expected, as both fuel consumption and CO_2 emissions are directly proportional to the amount of fuel burned. In contrast, the other parameters have negligible influence on CO_2-equivalents, which is consistent with the fact that CH_4 and N_2O are emitted in smaller quantities. The y-axis in both figures is scaled consistently with CO_2 emissions, which may obscure the lower sensitivity of CH_4 and N_2O, reflecting their smaller overall contributions to the CO_2-equivalent totals.

The results of the OAT analysis for the decommissioning of WT topsides of OWF Lincs Limited indicate that fuel consumption has the most significant influence on all GHG emissions, causing a linear increase across outputs. This highlights the critical importance of optimising fuel consumption to effectively reduce GHG emissions. Regarding emission factors, CO_2 has a large and direct impact on emissions, while CH_4 and N_2O exhibit much smaller effects due to the lower quantities of these gases emitted. Variations in LCV and thermal efficiency show almost no impact on emissions in this model, suggesting that these parameters are less relevant for emission reduction within the current framework.

In conclusion, effective emission reduction strategies for OWF decommissioning should prioritise optimising fuel consumption and accurately modelling the emission factor for CO_2, as these have the most significant impact on emissions. While CH_4 and N_2O play a role, their contributions are far less critical than that of CO_2, offering fewer opportunities for effective reduction.

5.4.2. Global analysis

This subsection presents the GSA, conducted for the decommissioning of WT topsides of OWF Lincs Limited. First, the methodology applied will be described, followed by a detailed analysis of the results. Finally, conclusions will be drawn based on these findings.

As described in section 3.3, the objective of a GSA is to examine which input parameters have the largest impact on output variance. This is achieved by analysing how simultaneous changes in multiple parameters contribute to the model's output, including the interactions between these parameters. In contrast to a OAT sensitivity analysis, where only one parameter is varied at a time, a GSA examines the combined effects of variations across multiple parameters over their entire range. This approach provides insight into which parameters are most critical for the model outputs and how they interact with others. As described in section 3.3, the sobol analysis is utilised to perform the GSA.

The Sobol analysis was performed to investigate how input parameters influence emission variability, both individually (first-order) and in combination with other parameters (total-order). The first-order indices are expected to align with the results from the OAT analysis. In this case, the input parameters used in the OAT analysis were further refined by including the different vessel states. Specifically, parameters related to fuel consumption and thermal efficiency were adjusted to account for variations during transiting and idling/operating states of the vessels. This more detailed approach enhances the understanding of each parameter's contribution to emission variance and highlights potential areas for optimisation across various operational stages. In addition, the total-order Sobol indices provide information about the collective influence of parameters, including their interactions. When the total-order indices deviate from the first-order indices, it indicates interactions between parameters. This analysis therefore helps to identify the key factors that contribute to uncertainty in emissions during offshore wind farm decommissioning. The selected input parameters include fuel consumption (state 1 and 2), thermal efficiency (state 1 and 2), LCV, and emission factors for CO_2, CH_4, and N_2O. Additionally, GWP factors for 20 and 100 years were included to evaluate the models sensitivity to the selection of a specific time horizon for calculating CO_2-equivalents. To perform the Sobol analysis, the boundaries of the parameters are utilised. These boundaries were established by determining the range of variation for each input parameter. For normally distributed parameters, this range was calculated based on their respective means and standard deviations. In the case of lognormally distributed parameters, location and scale parameters were used to define the boundaries. The distributions, with values of μ and σ, are further detailed earlier in section 3.3. A total of 1024 simulations were conducted using the Monte Carlo method, followed by the application of the Sobol method to calculate the first-order and total-order Sobol indices.
In addition, the average transiting and idling/operating durations for the TBs and WTIV, as provided in table 5.4, were utilised as case-dependent inputs in the GSA for the WT topside removal at OWF Lincs Limited.

With the established boundaries of the selected parameters, simulations and calculations were performed for the decommissioning of the WT topsides at OWF Lincs Limited, and the results are presented in figures 5.11 to 5.15. The figures illustrate the first-order and total-order Sobol indices for CO_2, CH_4, N_2O, and CO_2-equivalents over both 20- and 100-year time horizons for the WTIV. The TBs exhibit identical trends, and therefore their results are omitted.

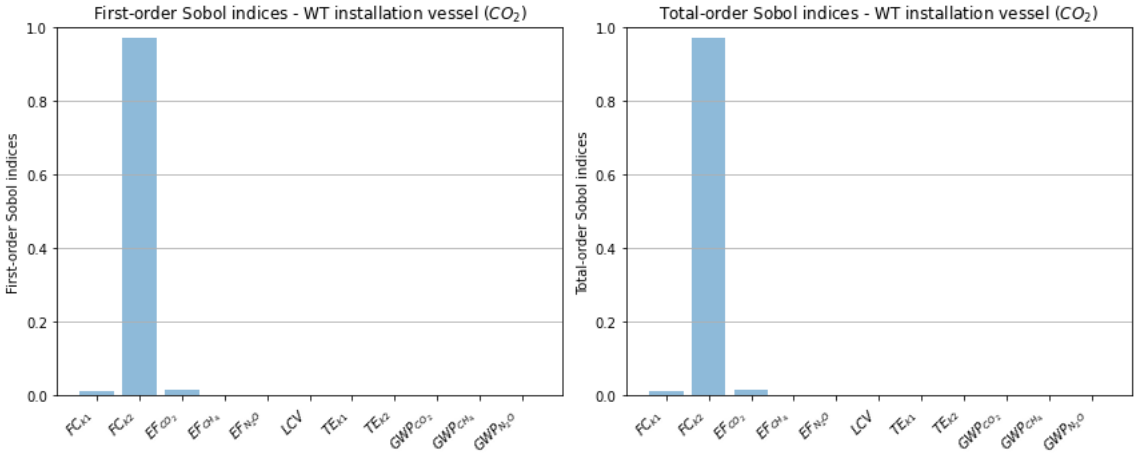

Figure 5.11: Sobol sensitivity indices for CO_2 during the decommissioning of OWF Lincs Limited

Figure 5.11, presenting the Sobol indices for CO_2, reveals that fuel consumption in state 2 has the largest influence on the variance of CO_2 emissions. Fuel consumption in state 1 and the emission factor for CO_2 contribute marginally to the variance. The first- and total-order indices are identical, indicating that no significant interaction between the parameters is present.

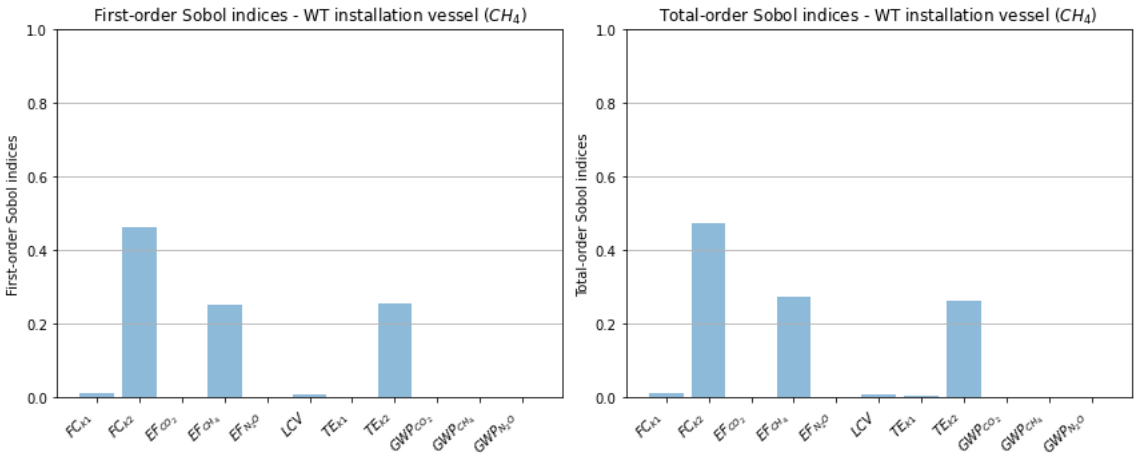

Figure 5.12: Sobol sensitivity indices for CH_4 during the decommissioning of OWF Lincs Limited

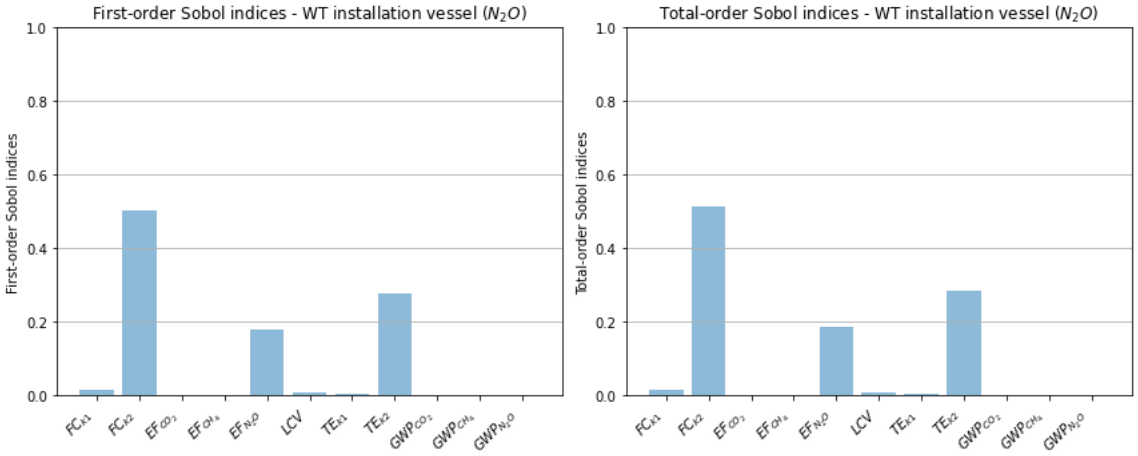

Figure 5.13: Sobol sensitivity indices for N_2O during the decommissioning of OWF Lincs Limited

Figures 5.12 and 5.13 demonstrate similar trends for CH_4 and N_2O emissions, respectively. In both cases, fuel consumption in state 2 is the dominant factor contributing to the variance in emissions, followed by thermal efficiency in state 2 and the respective emission factors for CH_4 and N_2O. Fuel consumption in state 1 has a negligible impact on the variance for both gases. Additionally, the alignment of the first- and total-order Sobol indices indicates that there are no significant interactions between the parameters in either case.

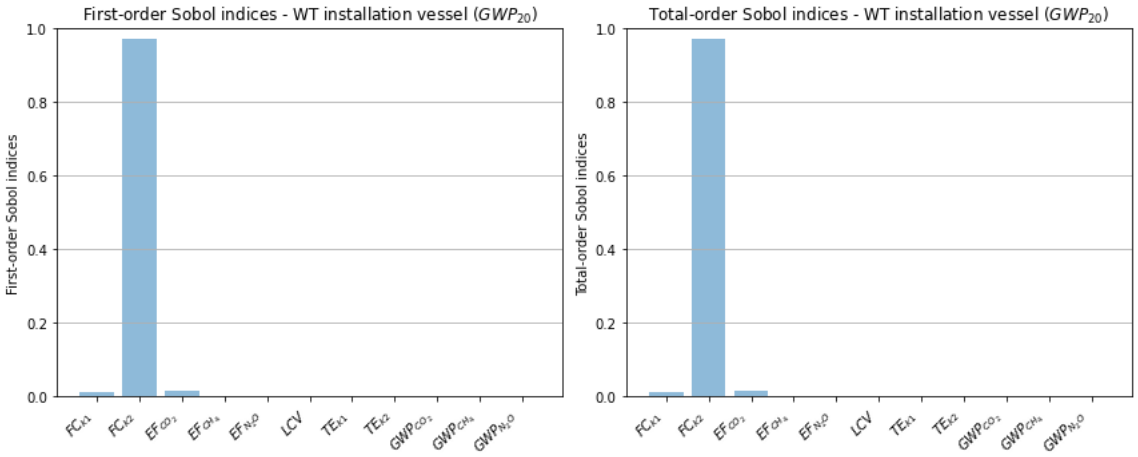

Figure 5.14: Sobol sensitivity indices for CO_2-equivalents over 20-years time horizon during the decommissioning of OWF Lincs Limited

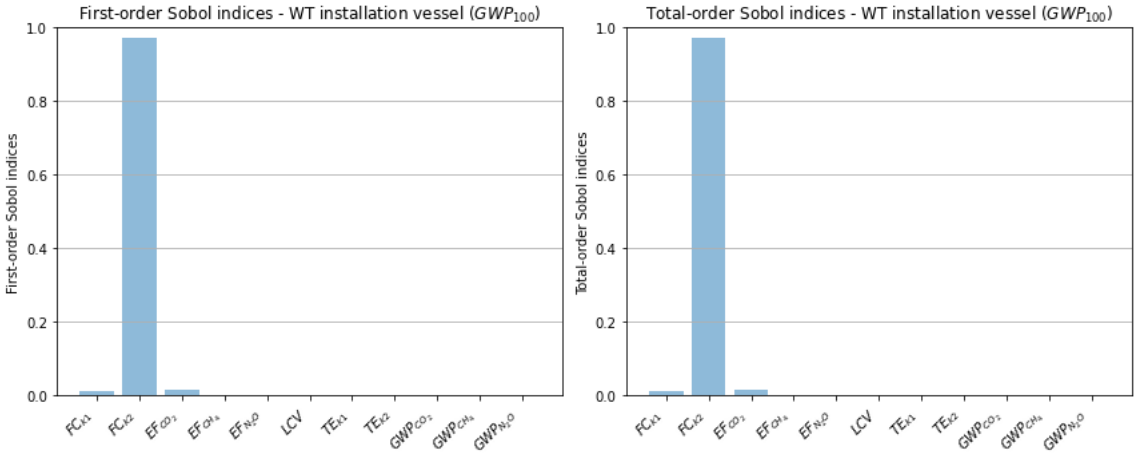

Figure 5.15: Sobol sensitivity indices for CO_2-equivalents for 100-year time horizon during the decommissioning of OWF Lincs Limited

Figures 5.14 and 5.15 show the Sobol sensitivity indices for CO_2-equivalents over 20- and 100-year time horizons, respectively. In both cases, a similar pattern can be observed. Fuel consumption in state 2 has the greatest influence on the variance in emissions, with thermal efficiency in state 2 and the CO_2 emission factor also contributing. The impact of fuel consumption in state 1 is minimal across both time horizons. Additionally, the GWP factors for 20- and 100-year time horizons have a relatively minor influence on the variance. This is because they only adjust the time horizon to express the evaluated emissions in terms of CO_2-equivalents, without affecting the actual emissions themselves. Moreover, the identical first- and total-order Sobol indices suggest there are no interactions between the parameters in either scenario.

First, the GSA reveals that fuel consumption in state 2 contributes the most to the variance in emissions of CO_2, CH_4, N_2O, and CO_2-equivalents over both 20- and 100-year time horizons. The emission factors, particularly for CH_4 and N_2O, and thermal efficiency in state 2 have a secondary influence on the variance. This partially confirms the results from the OAT analysis, as discussed in subsection 5.4.1, where fuel consumption was identified as the most influential parameter. However, the refined input parameters introduced in the GSA provided more detailed insights into which specific state contributes most to the variance for some parameters. In particular, the GSA revealed that fuel consumption and thermal efficiency during the operational state (state 2) have the greatest influence on emissions. This aligns with the findings from subsection 5.2.2, which demonstrated the dominant contribution of operational emissions in this decommissioning case. Thus, the GSA not only validates the main factors identified in the OAT analysis but also highlights the specific importance of state 2 in this decommissioning scenario. Thus, the GSA results not only confirm the key drivers of emissions identified in the OAT analysis, but also highlights the specific importance of state 2 within the context of decommissioning WT topsides of OWF Lincs Limited. Second, the GSA indicates that significant interactions between the parameters have been observed.

These results suggest that future decommissioning strategies should primarily focus on optimising fuel consumption during the idling/operating state, as this is the largest source of emission variability. Reducing fuel consumption during idling could lead to significant reductions in total emissions. However, it is important to emphasise that this analysis was conducted in the context of the OWF Lincs Limited case study. As described in subsection 5.2.2, both campaign duration and emissions in this particular case consisted mainly of the idling/operating state. However, the focus on this state does not automatically apply to all decommissioning projects, as the relative contribution of operational states may vary from one OWF decommissioning to another.

5.4.3. Uncertainty propagation in emissions

This subsection considers the uncertainties related to the vessel-related emissions for the decommissioning of WT topsides of OWF Lincs Limited. First, an explanation will be provided on how uncertainties are assessed. Subsequently, the vessel-related emissions and their associated uncertainties will be presented and analysed.

The vessel-related emissions in this subsection are calculated using the probabilistic GHG inventory tool, based on the methodology described in section 3.3. This methodology accounts for uncertainties in the fixed input parameters, which were included in the simulations to assess their effect on the output. In order to quantify the variation in the outputs, 1000 simulations were conducted using the Monte Carlo method, making both the input and output probabilistic in nature. Several methods can be used to visualise probabilistic results, such as histograms, box plots, density plots, and violin plots. Although box plots were initially considered, a decision was made to use violin plots for this study. The violin plots combine features of both box plots and density plots, presenting not only the median, quartiles, and extreme values but also the probability distribution of the data using symmetric density curves (Atlassian, 2024). This offers a more detailed visualisation of how CO_2, CH_4, and N_2O are distributed across the different vessel types, allowing for insights into how uncertainties in the input parameters propagate to the output. As the focus remains on vessel-related emissions from the decommissioning of WT topsides at OWF Lincs Limited, the average transiting and idling/operating durations for the vessels, presented in table 5.4, were used as case-dependent inputs.

Subsection 5.2.1 already revealed that emissions from TBs and WTIV differ approximately 10^2. Placing violin plots for these vessels in one graph makes the discrepancy less visible. In order to prevent this, violin plots for the different emission types and vessel types are presented separately. Moreover, the y-axes for the TBs and WTIV have been scaled separately, as these two types of vessels emit different quantities in this decommissioning scenario. This adjustment allows for a clearer visualisation of the specific shape of the violins. Figure 5.16 (a), (b) and (c) present the violin plots of CO_2 emissions from the TB, TB2 and WTIV, respectively. Subsequently, figure 5.17 (a), (b) and (c) show the CH_4 emissions, and finally, figure 5.18 (a), (b) and (c) the N_2O emissions. Subsection 5.2.1 indicated that CO_2-equivalents with time horizons of 20 and 100 years consisted mostly of CO_2. As a result, violin plots of the CO_2-equivalents were almost identical to those of CO_2. Therefore, the violin plots of the CO_2-equivalents for both time horizons of 20 and 100 years are not presented.

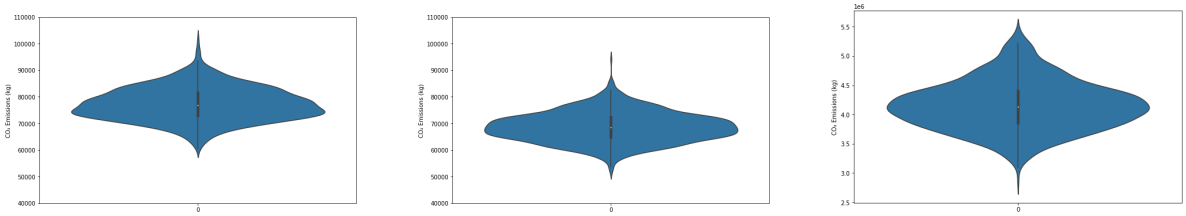

(a) Violin plot for TB1 **(b)** Violin plot for TB2 **(c)** Violin plot for WTIV

Figure 5.16: Violin plots of CO_2 emissions for all vessels during the decommissioning of OWF Lincs Limited

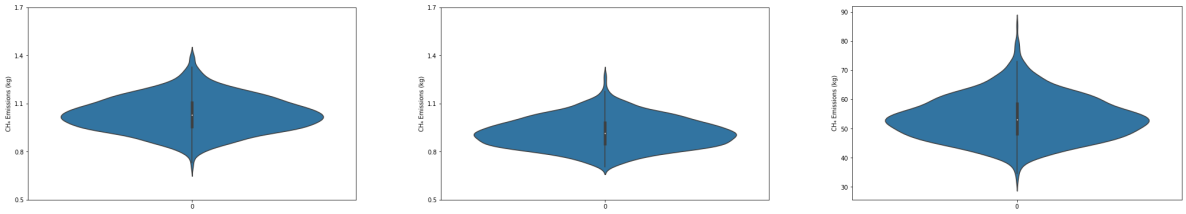

(a) Violin plot for TB1 **(b)** Violin plot for TB2 **(c)** Violin plot for WTIV

Figure 5.17: Violin plots of CH_4 emissions for all vessels during the decommissioning of OWF Lincs Limited

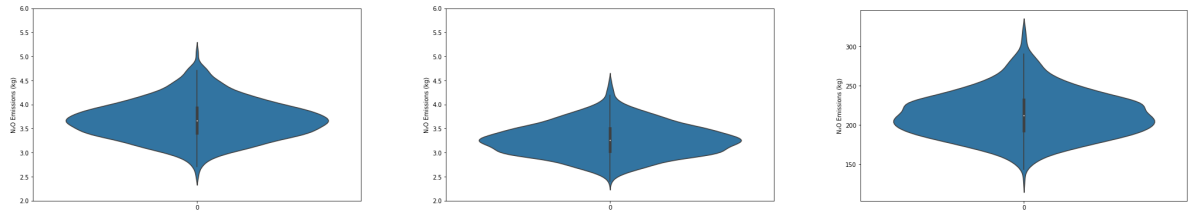

(a) Violin plot for TB1 **(b)** Violin plot for TB2 **(c)** Violin plot for WTIV

Figure 5.18: Violin plots of N_2O emissions for all vessels during the decommissioning of OWF Lincs Limited

The violin plots display the 1000 simulated outputs for CO_2, CH_4, and N_2O emissions, combining features of both box plots and density plots. The central box in the plot includes a thick line, a white circle, and smaller lines at the ends. The thick line represents the interquartile range, capturing the middle 50% of the data. The bottom and top edges mark the first and third quartiles, while the white circle indicates the median. The smaller lines extend to the maximum values within 1.5 times the interquartile range. In contrast, the density plot surrounding the box illustrates the distribution of the data points, providing insights into how input uncertainties influence the variability and spread of the outputs.

Figure 5.16 (a), (b) and (c) show the distribution of CO_2 emissions. Both TBs and the WTIV exhibit a nearly symmetrical shape around the median, suggesting a near-normal distribution. The narrow width of the violins implies that there is little variation within emissions, implying that the influence of uncertainties in the fixed input parameters for CO_2 emissions is relatively small. Figure 5.17 (a), (b) and (C) illustrate the distribution of CH_4 emissions The WTIV shows a slightly asymmetrical, upward-skewed shape, which may indicate a lognormal distribution. These shape could be the result of the uncertainty in the energy-based emission factors for CH_4. The TBs, in contrast, exhibit a more symmetrical distribution, though its broader width indicates a higher degree of uncertainty in the CH_4 emissions. Figure 5.18 (a), (b) and (c) present the distribution of N_2O emissions. The patterns for both the TBs and WTIV follow similar trends as their respective CH_4 distributions.

By analysing the shapes of the violin plots across different emission and vessel types, the influence of the input parameter distributions becomes clear. The lognormal distributions applied to fuel consumption and the energy-based emission factors for CH_4 and N_2O contribute to the skewness observed, particularly for the WTIV. Since fuel consumption is a factor in all emission calculations, its lognormal nature introduces a slight skew across all outputs. This effect is more pronounced in the CH_4 and N_2O distributions due to the lognormal distribution of their emission factors. In contrast, CO_2 exhibits narrower and more symmetrical distributions, reflecting the stability of its normally distributed emission factors.

In conclusion, CO_2 emissions show relatively small uncertainties and a more symmetrical distribution, making them more predictable. On the other hand, CH_4 and N_2O, especially for the WTIV, display greater variability due to uncertainties in their emission factors. While reducing CO_2 emissions remains a key strategy due to its lower variability, CH_4 and N_2O require additional focus when developing mitigation policies to address their higher uncertainty.

6

Conclusion and recommendations

This chapter provides the conclusion and recommendations of this research. In section 6.1, the conclusion will be presented, by addressing the research questions in subsection 6.1.1 and the main question in subsection 6.1.2. Subsequently, recommendations for future research will be elaborated in section 6.2, based on the findings of the case study results and the conclusion.

6.1. Conclusion

The objective of this study is to develop a model for quantifying and analysing GHG emissions generated during the large-scale decommissioning of OWFs.

6.1.1. Research questions

The aim of this subsection is to address the research questions, which are presented in a chronological manner.

1. *How can the decommissioning phase be characterised and how does the phase affect GHG emissions?*

   The decommissioning of OWFs can be characterised as a complex and diverse process that heavily depends on the specific characteristics of each wind farm. Each project presents its own challenges, with factors such as the technologies used, geographical location, and the scale of infrastructure playing key roles. Therefore, no standard decommissioning programme exists. Consequently, this variability in approaches leads to different emission profiles, as GHG emissions during the various sub-phases depend heavily on the scope of the decommissioning.

   In conclusion, the detailed characterisation of the decommissioning phase and its associated activities is essential for developing accurate GHG emission models. To enhance the predictive accuracy of these models, decommissioning processes should be formalised and standardised where possible. Identifying common operational patterns across different wind farm projects can streamline the modelling process, allowing for efficient and flexible models that can adapt to specific cases.

2. *What approaches can be utilised to measure GHG emissions based on the specified parameters during the decommissioning of an OWF?*

In order to accurately measure GHG emissions during OWF decommissioning, several methods are available. These methods can be categorised into four approaches: CEM, GHG inventory, process-based modelling and LCA. Each of these has its strengths and limitations.

The GHG inventory approach was identified with a multi-criteria decision analysis as the most suitable method for quantifying GHG emissions during OWF decommissioning. This due to its balance of accuracy, speed, robustness and relatively low data requirements. Although accuracy may be somewhat limited by the quality of available data, this method offers sufficient flexibility and applicability to be used effectively in large-scale projects such as OWF decommissioning. Furthermore, the approach can be easily adapted to incorporate new data and insights, making it a suitable method for future applications in an constantly evolving operational context.

3. *How could a tool designed to calculate emissions from various activities involved in decommissioning of an OWF be conceptualised, particularly in terms of its appearance and functional design features?*

   The tool designed for quantifying emissions from various activities involved in OWF decommissioning is conceptualised as a flexible and robust emissions modelling system. It integrates case-specific logistical data, such as vessel operations and fuel consumption, with a generic database of emission factors. This structure enables the accurate calculation of emissions per vessel or activity, ensuring consistent results across different decommissioning scenarios. The tool visualises both specific GHG emissions and CO_2-equivalents, allowing for comparisons of short- and long-term climate impacts.

   In terms of appearance and functional design, the tool is user-friendly and highly adaptable, providing both detailed and aggregate outputs to help identify key emission sources. The model incorporates both deterministic calculations and probabilistic analyses to account for uncertainties in input data, enhancing the reliability of the results. To verify the model, a consistency check and benchmark analysis were performed, demonstrating that the tool provides consistent and accurate emissions estimates across various scenarios. Additionally, sensitivity analyses are integrated to identify which input parameters have the greatest impact on emissions variance. Finally, uncertainty propagation further ensures the robustness of the results.

4. *What preliminary insights can be drawn from the tool in terms of its capability to assess GHG emission reduction strategies for future offshore wind farm decommissioning projects*

   The tool demonstrates significant potential in assessing GHG emission reduction strategies for future OWF decommissioning projects. The tool's ability to quantify GHG emissions per activity and vessel provides critical insights into the highest emission sources, helping stakeholders effectively prioritise reduction efforts. In particular, the tool's sensitivity analysis feature enhances its functionality by highlighting the input parameters that have the largest influence on emissions variance, making it easier to prioritise the most effective strategies for reduction. For the specific case of decommissioning WT topsides of Lincs Limited, the tool revealed that less than 2% of emissions originated from transport activities, whereas operational activities contributed over 98% of the total emissions. This suggests that optimisation efforts should focus on operational processes. Additionally, the sensitivity analysis showed that fuel consumption during idling/operating state is the most significant driver of emissions, indicating that improvements in fuel consumption could result in substantial reductions.

A crucial insight the tool offers is its ability to quantify the impact of factors, such as weather conditions, campaign timing and transport strategy. For example, it allows stakeholders to assess how starting the decommissioning campaign in different months and employing specific transport strategies could lead to emissions reductions. In the Lincs Limited case, the double-feeder strategy offered the most efficient emissions reduction, particularly when the campaign started in February or March. However, TNO's cost study, which implemented the exact same scenario, revealed that the double-feeder strategy involved higher costs compared to other methods. This resulted in a trade-off between cost efficiency and emissions reduction. This demonstrates the tool's capability to help stakeholders evaluate trade-offs between emissions, cost, and project duration.

In general, the tool's capability to break down emissions and assess the impact of external variables and decommissioning strategies makes it a powerful instrument for developing effective GHG emission reduction strategies. The preliminary insights drawn from the Lincs Limited case study demonstrate the tool's potential to inform sustainable decommissioning practices for future OWF projects.

6.1.2. Main question

The aim of this subsection is to address the main research question, presented below. This response constitutes the main conclusion of the study. Based on this conclusion, recommendations will be provided for the stakeholders of this research.

How can GHG emissions associated with the decommissioning of a large-scale OWF be effectively quantified and assessed?

GHG emissions during the decommissioning of an OWF can be effectively quantified using a comprehensive emissions modelling tool based on the GHG inventory approach. This method enables precise calculations of emissions per activity and vessel. To support the assessment, scenario and sensitivity analyses are conducted to identify key emission sources. This quantification provides stakeholders with a clear understanding of where emissions occur and offers insights into potential reduction strategies, making it a powerful tool for optimising decommissioning processes.

Based on results of the analyses, the following recommendations are proposed for stakeholders in future OWF decommissioning projects. First, investing in more efficient vessels is essential, as optimising fuel consumption is crucial for reducing emissions. In addition, flexible operational planning, supported by accurate weather forecasting, can help further minimise emissions. Furthermore, selecting the appropriate transport strategy can lead to additional emission reductions. Finally, carefully selecting the campaign's start month, aligned with the campaign duration and conditions, can also contribute to lowering overall emissions.

These conclusions and recommendations provide a framework for minimising CO_2, CH_4, N_2O, and CO_2-equivalents from OWF decommissioning. With a combination of improved planning, optimisation of vessel strategies, and investments in cleaner technologies, emissions can be significantly reduced in future OWF decommissioning projects.

6.2. Recommendations for future research

This subsection provides recommendations for the future development of the emission quantification tool, aimed at improving its accuracy and functionality. The recommendations are based on the assumptions made during the study and insights obtained from the verification and case study results.

First, a key recommendation concerns the improvement of fuel data. Throughout this study, simplified fuel consumption data was used due to limited availability of detailed information. Both the sensitivity and scenario analyses demonstrated that fuel consumption and emission factors are the primary drivers of total GHG emissions. To enhance the accuracy of emission calculations, future iterations of the tool should integrate more specific data. This includes fuel consumption data specific to the operational conditions and actual load profiles of the different vessels.

Second, it is recommended to further refine the modelling of CH_4 emissions. The benchmark analysis revealed that this emission type is sensitive to variations. Therefore, future iterations of the tool should improve the accuracy of this emission type, to enhance the overall GHG emissions estimate. However, as CH_4 emissions are released in very small quantities, this recommendation is of lower priority.

Third, expanding the scope beyond direct GHG emissions from offshore activities during OWF decommissioning is recommended. To start, it would be beneficial to consider also air pollutants instead of only GHGs, as both CH_4 and N_2O are emitted in small quantities. Including an assessment of other pollutants, such as NO_x, SO_x, and PM, could add significant value to the tool, as these pollutants are substantial contributors to environmental impacts. Additionally, the benchmark results indicated that indirect emissions, while smaller than direct emissions, still have a notable impact. Therefore, incorporating indirect emissions alongside direct emissions would be interesting. Moreover, including emissions from onshore activities would offer a holistic view of the total emissions related to OWF decommissioning. While this expansion would require more extensive data collection, especially for indirect emissions and onshore processes, it would provide a more complete and accurate quantification of the total environmental footprint of OWF decommissioning projects.

By implementing these recommendations, the emissions tool can be further developed into a powerful instrument for quantifying and optimising GHG emissions during OWF decommissioning projects, focusing on accuracy, flexibility, and future sustainability.

Finally, further research should explore the integration of the developed GHG emission assessment model into existing decommissioning tools. These existing tools, such as UWiSE Decommission, optimise the decommissioning process based on cost and time. By combining emission quantification and assessment with cost optimisation models, a powerful tool could be created for future large-scale OWF decommissioning projects. This would allow decision-makers to evaluate the most cost-effective strategies for reducing GHG emissions, thereby aligning both environmental and economic objectives in the decommissioning process.

References

4C Offshore. (2024). Global Offshore Renewable Map. https://map.4coffshore.com/offshorewind/

Adedipe, T., Shafiee, M., & Author(s), T. (2021). LCI METHODOLOGY AND DATABASES An economic assessment framework for decommissioning of offshore wind farms using a cost breakdown structure. *The International Journal of Life Cycle Assessment*, *26*, 344–370. https://doi.org/10.1007/s11367-020-01793-x

Ahmad, S., Jalagat, R., Alulis, I., & Aquino, P. G. (2021). BENCHMARKING FOR COMPETITIVE ADVANTAGE AND ORGANIZATIONAL PERFORMANCE: PROPOSED FRAMEWORK. *Vidyabharati International Interdisciplinary Research Journal*, *12*(1), 67–77. https://www.researchgate.net/publication/350441984

Ahmed, S. P. (2023, December). Use of marine auxiliary engine. https://www.merchantnavydecoded.com/use-of-marine-auxiliary-engine/#:~:text=A%20marine%20auxiliary%20engine%20is,ship's%20various%20systems%20and%20equipment

ALPHAMARINE. (2021). *Vessel and Equipment Data Sheets* (tech. rep.). https://assets.gov.ie/206916/aae7052f-5f88-4848-a90f-557829bcba97.pdf

Arvesen, A., Birkeland, C., & Hertwich, E. G. (2013). The Importance of Ships and Spare Parts in LCAs of Offshore Wind Power. *Environmental science technology*, *47*(6), 2948–2956. https://doi.org/10.1021/es304509r

Atlassian. (2024). A complete guide to violin plots. https://www.atlassian.com/data/charts/violin-plot-complete-guide#:~:text=Violin%20plots%20are%20used%20when,groups%20are%20similar%20or%20different.

Beinke, T., Alla, A. A., & Freitag, M. (2018, January). *Decommissioning of Offshore Wind Farms*. https://doi.org/10.1007/978-3-319-74225-0\{_}30

Bonou, A., Laurent, A., & Olsen, S. I. (2016). Life cycle assessment of onshore and offshore wind energy-from theory to application. *Applied energy*, *180*, 327–337. https://doi.org/10.1016/j.apenergy.2016.07.058

Brandt, A. R., Heath, G. A., & Cooley, D. (2016). Methane Leaks from Natural Gas Systems Follow Extreme Distributions. *Environmental Science Technology*, *50*(22), 12512–12520. https://doi.org/10.1021/acs.est.6b04303

Brightway. (2024). Brightway LCA Software Framework. https://docs.brightway.dev/en/latest/

Casati, D. B. (2013). Statistical challenges and approaches for the analysis and verification/validation of weather and climate extremes. https://www.cawcr.gov.au/projects/verification/Casati/statxtr.htm

Chen, J. (2024, March). Normal Distribution: What It Is, Uses, and Formula. https://www.investopedia.com/terms/n/normaldistribution.asp

Chirosca, A.-M., Rusu, L., & Bleoju, A. (2022). Study on wind farms in the North Sea area. *Energy Reports*, *8*, 162–168. https://doi.org/10.1016/j.egyr.2022.10.244

Climate Change Committee. (2017, November). *Quantifying greenhouse gas emissions*. https://www.theccc.org.uk/publication/quantifying-greenhouse-gas-emissions/

Dalgic, Y., Lazakis, I., Dinwoodie, I., McMillan, D., & Revie, M. (2015). Advanced logistics planning for offshore wind farm operation and maintenance activities. *Ocean Engineering*, *101*, 211–226. https://doi.org/10.1016/j.oceaneng.2015.04.040

Daniel P. Loucks, E. v. B. (2016). *Model Sensitivity and Uncertainty Analysis*.

Database, E. (2024). The ecoinvent database search. https://ecoquery.ecoinvent.org/3.9.1/cutoff/search

Davie, S., Minto, C., Officer, R., Lordan, C., & Jackson, E. (2014). Modelling fuel consumption of fishing vessels for predictive use. *ICES Journal of Marine Science*, *72*(2), 708–719. https://doi.org/10.1093/icesjms/fsu084

Dernotte, J., Dec, J. E., & Ji, C. (2015). Energy Distribution Analysis in Boosted HCCI-like / LTGC Engines - Understanding the Trade-Offs to Maximize the Thermal Efficiency. *SAE International Journal of Engines*, *8*(3), 956–980. https://doi.org/10.4271/2015-01-0824

Dighe, V., Bloothoofd, J., van der Mijle Meijer, H., Mancini, S., & AITIP. (2024). *Decommissioning Logistics of Wind Turbine Blades: Modelling and Analysis* (tech. rep.).

Dinh, V. N., & McKeogh, E. (2018, September). *Offshore Wind Energy: Technology Opportunities and Challenges*. https://doi.org/10.1007/978-981-13-2306-5_1

Doedee, V. (2021, April). How to Determine Vessel Emissions — Mr. Sustainability. https://www.mr-sustainability.com/guide/2020/how-to-guide-vessel-emissions

Eckardt, S. (2022, May). *Handbook of Offshore Wind Farm Decommissioning*. SeeOff.

EIA. (2022, July). Energy and the environment explained. https://www.eia.gov/energyexplained/energy-and-the-environment/greenhouse-gases.php

Energy, C. (2020, February). Heating value. https://www.clarke-energy.com/heating-value/

EPA, U. (2024, March). Understanding global warming potentials | US EPA. https://www.epa.gov/ghgemissions/understanding-global-warming-potentials

Faber, J., Hanayama, S., Zhang, S., Pereda, P., Comer, B., Hauerhof, E., van der Loeff, W. S., Smith, T., Zhang, Y., Kosaka, H., Adachi, M., Bonello, J.-M., Galbraith, C., Gong, Z., Hirata, K., Hummels, D., Kleijn, A., Lee, D. S., Liu, Y., … Lim, K. (2021). *Fourth IMO GHG Study 2020*. INTERNATIONAL MARITIME ORGANIZATION.

Floatels, C. (2007). *SERVICE SUPPORT VESSELS DP GEZINA DP GALYNA* (tech. rep.). https://www.cfbv.com/wp-content/uploads/2014/08/WalkToWorkVessels-DP-Gezina-DP-Galyna.pdf

Fujian. (2017). *Flag Dutch DP class Class 2* (tech. rep.). https://www.vroon.nl/uploads/vessels/Vessel-particulars/Vroon-Offshore-Services/Vessel-particulars_VOS-Start.pdf

Garg, A., Kainou, K., & Pulles, T. (2006). *2006 IPCC Guidelines for National Greenhouse Gas Inventories*. https://www.ipcc-nggip.iges.or.jp/public/2006gl/pdf/2_Volume2/V2_1_Ch1_Introduction.pdf

Gillenwater, M. (2005, June). *Calculation tool for direct emissions from stationary combustion* (tech. rep.).

Gillian Smits, C. G. G. G. (2015). Logistics and Cost Reduction of Decommissioning Offshore Wind Farms. https://www.researchgate.net/publication/274896458

Gjødvad, J., & Ibsen, M. D. (2016, January). *ODIN-WIND: An Overview of the Decommissioning Process for Offshore Wind Turbines*. https://doi.org/10.1007/978-3-319-39095-6\{_}22

GL, D. (2014, December). *Assessment Wind Measurement Program North Sea* (tech. rep. No. 14-2781, Rev. 1). KEMA Nederland BV. https://offshorewind.rvo.nl/file/download/fa117a7e-825c-4766-949c-5405c6ea779f/1425640012assessment%20wind%20measurement%20program%20north%20sea.pdf

Gray, A. (2021, February). *SETTING a BENCHMARK FOR DECARBONISING OM VESSELS OF OFFSHORE WIND FARMS* (tech. rep.). ore.catapult.org.uk

Hall, R., João, E., Knapp, C. W., Technology, Innovation Centre, U. o. S., of Civil, D., & Environmental Engineering, U. o. S. (2020). *Environmental impacts of decommissioning: Onshore versus offshore wind farms* (tech. rep.). https://doi.org/10.1016/j.eiar.2020.106404

Hall, R., Topham, E., & João, E. (2022). Environmental Impact Assessment for the decommissioning of offshore wind farms. *Renewable sustainable energy reviews*, *165*, 112580. https://doi.org/10.1016/j.rser.2022.112580

Hamby, D. M., & Society, H. P. (1994). *A COMPARISON OF SENSITIVITY ANALYSIS TECHNIQUES* (tech. rep.). Health Physics Society. https://web.engr.oregonstate.edu/~hambydm/papers/senscomparison.pdf

Hillers, M., Bentin, M., Kotzur, S., Schleuter, D., Klussmann, J., of Applied Sciences Emden/Leer, U., Bruns, A., Ring, H., & Schneider, J. (2023, January). *Simulation Analysis Comparison of various logistical concepts for offshore wind farm decommissioning* (tech. rep.).

Huang, Y.-C., Gan, X.-J., & Chiueh, P.-T. (2017). Life cycle assessment and net energy analysis of offshore wind power systems. *Renewable energy*, *102*, 98–106. https://doi.org/10.1016/j.renene.2016.10.050

IHC, R. (2023, July). *Subsea trenching* (tech. rep.). https://www.royalihc.com/sites/default/files/documents/%E2%80%A2RIHC%20Dredging%20Productsheet%20Beaver%2050_110569933.pdf

IMO. (2015). *Third IMO Greenhouse Gas Study 2014* (tech. rep.). International Maritime Organization. www.imo.org

INC., C. (2011, July). *Basic Engine Model Curve number* (tech. rep.). https://mart.cummins.com/imagelibrary/data/assetfiles/0055821.pdf

Institute, W. R., & for Sustainable Development, W. B. C. (2004). *A Corporate Accounting and Reporting Standard*. https://ghgprotocol.org/sites/default/files/standards/ghg-protocol-revised.pdf

IPCC. (2000). Good Practice Guidance and Uncertainty Management in National Greenhouse Gas Inventories — IPCC. https://www.ipcc.ch/publication/good-practice-guidance-and-uncertainty-management-in-national-greenhouse-gas-inventories/

IPCC. (2021). *The climate change 2021 The physical science basis* (tech. rep. No. AR6).

Jalili, S., Maheri, A., & Ivanovic, A. (2022). Cost and emission analyses of decommissioning of offshore wind farms using reverse installation method: Cases of lincs limited, gunfleet sands, and horns rev i wind farms. *Interreg North Sea Region Decom Tools*, *Interreg North Sea Region– Project Number: 20180305091606*.

Jalili, S., Maheri, A., Ivanović, A., Neilson, R. D., Bentin, M., Kotzur, S., May, R., & Sünner, I. (2023). Economic and Environmental Assessments to Support the Decision-Making Process in the Offshore Wind Farm Decommissioning Projects. *ELSEVIER*. https://doi.org/10.2139/ssrn.4415949

John. (2023, August). What is the EU Waste Framework Directive? https://www.superfy.com/eu-waste-framework-directive/

Joustra, J. J., van der Meulen, T. H., Bastein, T., Swamy, S. K., Saraswati, N., & of Technology, D. U. (2020). *Offshore wind farm decommissioning: An orientation of possible economic activity in the south holland region and the rotterdam port area* (tech. rep.).

Kaldellis, J., & Apostolou, D. (2017). Life cycle energy and carbon footprint of offshore wind energy. Comparison with onshore counterpart. *Renewable energy*, *108*, 72–84. https://doi.org/10.1016/j.renene.2017.02.039

Kleijnen, J. P., CentER, of Information Systems, D., & Auditing, T. U. (1994). *SENSITIVITY ANALYSIS VERSUS UNCERTAINTY ANALYSIS: WHEN TO USE WHAT?* (Tech. rep.). https://exampleurl.com

Kramel, D., Muri, H., Kim, Y.-R., Lonka, R., Nielsen, J. B., Ringvold, A. L., Bouman, E., Steen, S., & Strømman, A. H. (2021). Global Shipping Emissions from a Well-to-Wake Perspective: The MariTEAM Model. *Environmental science technology*, *55*(22), 15040–15050. https://doi.org/10.1021/acs.est.1c03937

Kumar, I., Tyner, W. E., & Sinha, K. C. (2016). Input–output life cycle environmental assessment of greenhouse gas emissions from utility scale wind energy in the United States. *Energy policy*, *89*, 294–301. https://doi.org/10.1016/j.enpol.2015.12.004

Kyrtatos, A., Spahni, M., Hensel, S., Züger, R., Sudwoj, G., & Diesel, W. G. (2016). *The Development of the Modern Low-Speed Two-Stroke Marine Diesel Engine* (tech. rep.).

Lee, S., Choi, Y. M., Woo, J.-C., Kang, W., & Jung, J. (2014). Estimating and comparing greenhouse gas emissions with their uncertainties using different methods: A case study for an energy supply utility. *Journal of the Air Waste Management Association*, *64*(10), 1164–1173. https://doi.org/10.1080/10962247.2014.930078

Lee, T., & Frey, H. C. (2012). Evaluation of Representativeness of Site-Specific Fuel-Based Vehicle Emission Factors for Route Average Emissions. *Environmental Science Technology*, *46*(12), 6867–6873. https://doi.org/10.1021/es204451z

Levy, P. E., Cowan, N., Van Oijen, M., Famulari, D., Drewer, J., & Skiba, U. (2017). Estimation of cumulative fluxes of nitrous oxide: uncertainty in temporal upscaling and emission factors. *European Journal of Soil Science*, *68*(4), 400–411. https://doi.org/10.1111/ejss.12432

Libretexts. (2024, March). 8.9: The First Law of Thermodynamics and Heat Engine Processes. https://phys.libretexts.org/Bookshelves/Conceptual_Physics/Introduction_to_Physics_(Park)/04%3A_Unit_3-_Classical_Physics_-_Thermodynamics_Electricity_and_Magnetism_and_Light/08%3A_Thermal_Physics/8.09%3A_The_First_Law_of_Thermodynamics_and_Heat_Engine_Processes

Licorn, G. (2007). *VESSEL PARTICULARS ENGINE/PROPULSION* (tech. rep.). https://www.gspoffshore.com/wp-content/uploads/2022/10/GSP_LICORN.pdf

Lindstad, E., Eskeland, G., Rialland, A. I., & Valland, A. (2020). Decarbonizing Maritime Transport: The Importance of Engine Technology and Regulations for LNG to Serve as a Transition Fuel. *Sustainability*, *12*(21), 8793. https://doi.org/10.3390/su12218793

LTD, C. M. S. (1980). *CASPIAN MARINE SERVICES LTD* (tech. rep.). https://www.caspmarine.com/_files/ugd/b7ad7b_3673e7e21619418f8807fa09f2b17379.pdf

Manageruser. (2023, February). IPCC Sixth Assessment Report Global Warming Potentials - ERCE. https://erce.energy/erceipccsixthassessment/

Mancini, S., Bloothoofd, J., Dighe, V., van der Mijle Meijer, H., Energy, T., & Materials Transition Unit. Wind Energy group. Westerduinweg 3, t. N., 1755 LE Petten. (2023). *Development and verification of a discrete event simulation tool for high-fidelity modelling of offshore wind and solar farm decommissioning campaigns* (tech. rep.). TNO.

Marelli, S., Lamas, C., Konakli, K., Mylonas, C., Wiederkehr, P., Sudret, B., Chair of Risk, S., & Quantification, U. (2024). *UQLAB user manual – Sensitivity analysis* (tech. rep. No. UQLab-V2.1-106). Chair of Risk, Safety; Uncertainty Quantification, ETH Zurich, Switzerland.

Mello, G., & Robaina, M. (2020). Wind farms life cycle assessment review: CO2 emissions and climate change. *Energy reports*, *6*, 214–219. https://doi.org/10.1016/j.egyr.2020.11.104

Milne, C., Jalili, S., Maheri, A., b, School of Engineering, U. o. A., & Centre for Energy Transition, U. o. A., School of Engineering. (2021, September). *Decommissioning cost modelling for offshore wind farms: A bottom-up approach* (tech. rep.). https://doi.org/10.1016/j.seta.2021.101628

Mohareb, E. A., MacLean, H. L., & Kennedy, C. A. (2011). Greenhouse Gas Emissions from Waste Management—Assessment of Quantification Methods. *Journal of the Air Waste Management Association*, *61*(5), 480–493. https://doi.org/10.3155/1047-3289.61.5.480

MULTICAT - GRS. (2024, February). https://grs.group/grs-offshore-renewables/3d-vessel-portfolio/multicat/

NAEI. (2022, August). Overview Air pollutants. https://naei.beis.gov.uk/overview/ap-overview

NationalGrid. (2023, June). What are scope 1, 2 and 3 carbon emissions? https://www.nationalgrid.com/stories/energy-explained/what-are-scope-1-2-3-carbon-emissions#:~:text=Definitions%20of%20scope%201%2C%202,owned%20or%20controlled%20by%20it.

Nations, U. (1998). *Kyoto Protocol to the United Nations Framework Convention on Climate Change* (tech. rep.). https://unfccc.int/resource/docs/convkp/kpeng.pdf

Nations, U. (2024). The Paris Agreement. https://unfccc.int/process-and-meetings/the-paris-agreement

Pavlovic, M. (2024). Log-normal Distribution - A simple explanation - Towards Data Science. https://towardsdatascience.com/log-normal-distribution-a-simple-explanation-7605864fb67c

Perveen et al. (2014). Off-shore wind farm development: Present status and challenges. *29*, 780–792. http://dx.doi.org/10.1016/j.rser.2013.08.108

Piasecka, I., Tomporowski, A., Flizikowski, J., Kruszelnicka, W., Kasner, R., & Mroziński, A. (2019). Life Cycle Analysis of Ecological Impacts of an Offshore and a Land-Based Wind Power Plant. *Applied sciences*, *9*(2), 231. https://doi.org/10.3390/app9020231

Serraris, J.-J., McNaughton, J., TNO, MARIN, Dighe, V., Huang, L., & Hernandez Montfort, J. (2024, February). *Floating Offshore Wind Turbine Transportation, Installation, Maintenance Operations (FOWT IOM) - Work Package 1: Literature and Market Review* (tech. rep.).

Sówka, I., Bezyk, Y., of Ecologistics, U., Environmental Risk Management, W. U. o. S., Faculty of Environmental Engineering, & Technology. (2017). *Quantifying and reporting greenhouse gas emissions at local level* (tech. rep.). EDP Sciences. https://doi.org/10.1051/00084

Spielmann, V., Brey, T., Dannheim, J., Vajhøj, J., Ebojie, M., Klein, J., & Eckardt, S. (2021). Integration of sustainability, stakeholder and process approaches for sustainable offshore wind farm decommissioning. *Renewable Sustainable Energy Reviews*, *147*, 111222. https://doi.org/10.1016/j.rser.2021.111222

Steubing, B., De Koning, D., Haas, A., & Mutel, C. L. (2020). The Activity Browser — An open source LCA software building on top of the brightway framework. *Software Impacts*, *3*, 100012. https://doi.org/10.1016/j.simpa.2019.100012

Submarine, K. (1999). *PARTICULARS OF CABLE SHIP RESPONDER* (tech. rep.). https://www.gob.mx/cms/uploads/attachment/file/467794/ficha_t_cnica_RESPONDER.pdf

Tatsuo Takaishi, R. N., Akira Numata, & Sakaguchi, K. (2008, March). *Approach to High Efficiency Diesel and Gas Engines* (tech. rep. No. Technical Review Vol. 45 No. 1). https://www.mhi.co.jp/technology/review/pdf/e451/e451021.pdf

Team, W. (2024, January). Multi-Criteria decision analysis. https://www.wallstreetmojo.com/multi-criteria-decision-analysis/#Multi-Criteria-Decision-Analysis-Explained

The University of Edinburgh. (2003). *Model Validation and Verification*. https://www.inf.ed.ac.uk/teaching/courses/ms/notes/note14.pdf

TNO. (2023, November). TNO UWiSE tool. https://www.tno.nl/nl/newsroom/2023/11/uwise-ontmanteling-windparken/

Topham, E., Gonzalez, E., McMillan, D., & João, E. (2019). Challenges of decommissioning offshore wind farms: Overview of the European experience. *Journal of physics. Conference series*, *1222*(1), 012035. https://doi.org/10.1088/1742-6596/1222/1/012035

Topham, E., & McMillan, D. (2017). Sustainable decommissioning of an offshore wind farm. *Renewable Energy*, *102*, 470–480. https://doi.org/10.1016/j.renene.2016.10.066

Topham, E., McMillan, D., Bradley, S., Hart, E., Advisory, D. G. R., Wind, Marine Energy Systems CDT, U. o. S., Eletronic, Electrical Engineering Department, U. o. S., & Energy Systems Catapult, B. (2019, March). *Recycling offshore wind farms at decommissioning stage* (tech. rep.). https://doi.org/10.1016/j.enpol.2019.01.072

United. (2004, June). *Information on Global Warming Potentials* (tech. rep. No. FCCC/TP/2004/3). https://unfccc.int/resource/docs/tp/tp0403.pdf

van Lieshout, T. P., de Jonge, V., Verbeek, R., Vredeveldt, A., Finner, S., & TNO. (2020). *Green Maritime Methanol: WP3 factsheet and comparison with diesel and LNG* (tech. rep. No. TNO 2020 R11822).

Vis, I. F., Ursavas, E., University of Groningen, F. o. E., & Business, D. o. O. (2016, January). *Assessment approaches to logistics for offshore wind energy installation* (tech. rep.). http://dx.doi.org/10.1016/j.seta.2016.02.001

VLmaritime. (2017, July). 100 pax Fast Supply Crewboat / Utility vessel - Van Loon Maritime Services B.V. https://www.vlmaritime.com/product/e0033-fast-supply-crewboat/

Vroon. (2022, March). *AHTP Vos Thalassa* (tech. rep.). https://www.vroon.nl/uploads/vessels/Vessel-particulars/Vroon-Offshore-Services/Vessel-particulars-VOS-Thalassa.pdf

Wang, Y., & Wright, L. A. (2021). A Comparative Review of Alternative Fuels for the Maritime Sector: Economic, Technology, and Policy Challenges for Clean Energy Implementation. *World*, *2*(4), 456–481. https://doi.org/10.3390/world2040029

Wątróbski, J., Jankowski, J., Ziemba, P., Karczmarczyk, A., & Zioło, M. (2019). Generalised framework for multi-criteria method selection. *Omega*, *86*, 107–124. https://doi.org/10.1016/j.omega.2018.07.004

Wikipedia. (2023, November). List of offshore wind farms in the North Sea. https://en.wikipedia.org/wiki/List_of_offshore_wind_farms_in_the_North_Sea

Windcarrier. (2021). *JACK-UP INSTALLATION VESSEL BLUE TERN*. https://windcarrier.com/media/gdhexjgm/blue-tern-29102021.pdf

WindEurope. (2019). Our energy, our future. https://windeurope.org/wp-content/uploads/files/about-wind/reports/WindEurope-Our-Energy-Our-Future.pdf

Winkler, L., Kilic, O. A., Veldman, J., University of Groningen, F. o. E., & Business, D. o. O. (2022). *Collaboration in the offshore wind farm decommissioning supply chain* (tech. rep.). https://doi.org/10.1016/j.rser.2022.112797

Yard, F. S. E. S. (2015). *Vessel Specifications Brochure* (tech. rep.). https://vortexoffshore.com/wp-content/uploads/2019/04/AHTS-DP2-6509-BHP-88-TBP.pdf

Yin, C., & McKay, A. (2018). Introduction to modeling and simulation techniques. *ResearchGate*. https://eprints.whiterose.ac.uk/135646/

Zhang, K., Peng, C., Wang, M., Zhou, X., Li, M., Wang, K., Ding, J., Zhu, Q., for Ecological Forecasting, C., Change, G., College of Forestry, N. A. U., & Institute of Environment Sciences, U. o. Q. a. M., Department of Biology Sciences. (2017). *Process-based TRIPLEX-GHG model for simulating N2O emissions from global forests and grasslands: Model development and evaluation* (tech. rep.). https://doi.org/10.1002/2017MS000934-T

A

OWF components

Table A.1: Overview of the systems, sub-systems, components, and materials in OWFs

System Level	Sub-system Level	Component Level	Material Level
Wind turbine	Rotor	Hub	Spheroidal graphite cast iron
		Nose cone	Steel/aluminium structure + GFRP cover
		Pitch system	Alloy steel gears/bearing + cast iron casing + copper windings
		Blades	Composite material / glass reinforced plastics
	Nacelle	Gearbox (not for direct drive WT)	Cast iron, high-alloy steel
		Generator	Copper, electrical steel
		Main frame	Cast iron, low-alloy steel
		Main shaft	Low-alloy steel, high-alloy steel
		Transformer	Copper, electrical steel
		Housing	
		(Mechanical brake)	
		(Yaw system)	
	Tower	Tower structure	Low-alloy steel
		Internals	Aluminum
	Support structure	Foundation	S355 Steel
		Transition piece	S355 Steel
		Cable tuning and protection	HDPE
Offshore substation	Topside	Several decks	Cast iron
		Switch equipment	
		Transformer	
		Compensation coils	
		Protection control	
		Communication technology	
		Auxiliary power generation	
		Emergency power supply	
		Surge protection	
		Control systems	
		Cooling systems	
	Support structure	Foundation	S355 Steel
		Transition piece	S355 Steel
		Cable tuning and protection	HDPE
Meteorological mast	Support structure	Foundation	S355 Steel
		Transition piece	S355 Steel
		Cable tuning and protection	HDPE
Transmission system	Inter-Array cables	33kV submarine cables	Copper, steel, lead
		Cable protection	HDPE
	Export cable	66 kV/155 cable	Copper, steel, lead
		Cable protection	HDPE
	(Converter system)		
Scour protection	Scour protection layer	Scour protection layer	Concrete, natural stone, gravel sand

Wind turbine

First, the system called the WT will be explained. This system consists of several sub systems, namely the rotor, nacelle, tower and support structure. The first sub-system of the WT is the rotor, which then consists of several components, namely the hub with nose cone and the blades. The hub contains the pitch and control system, which can adjust rotor blades. The rotor blades are made of a composite material of synthetic resin and fibers. The most commonly used fiber material is glass fiber (GRP - Glass Fiber Reinforced Composite Material). Carbon fiber reinforced plastic (CP) is also used to reinforce heavily loaded parts of the rotor blade (Eckardt, 2022). The second sub-system of the WT is the nacelle, which also consists of several components, namely the gearbox, generator, main frame, main shaft, transformer, converter and housing. The gearbox is an important part of the nacelle. In fact, offshore wind turbines (OWTs) can be categorized by this in two groups, turbines with gearbox and turbines without gearbox. Turbines without gearbox are also referred to as direct-drive. New larger OWTs are appearing on the market as direct-drive because of the various advantages associated with them. This is because these gearless OWTs reduce the weight of the nacelle, since the gearboxes are the heaviest part of it. It also reduces the number of technical failures as there are fewer moving parts, which in turn reduces O&M costs. However, the direct drive turbine is currently the minority of in the industry (Topham, McMillan, et al., 2019). The generator is another important component of the nacelle. There are different types of generators, variable-speed and fixed-speed. To make maximum use of the available wind energy, a variable-speed generator is preferred. This is because it provides constant power under varying wind conditions. Various types of alternating current (AC) machines are double-fed induction generators, wound rotor induction generators, synchronous generators or permanent magnet synchronous generators. Of these, DIFGs are the most widely used because of low cost and their modular, compact and standardised construction (Perveen et al., 2014). However, the type of generator that can be used depends on whether the turbine is geared or not. As such, the DGIGS and squirrel-cage asynchronous generators can only be used for indirect drive turbine, where the permanent magnet synchronous generators can be used for both direct and indirect drive. The third sub-system of the WT is the tower, it consists of its own structure and internals. The transformer and inverter of the converter, if not placed in the nacelle, will be located in the tower. In addition, the power, instrumentation and control cables ducts will run through the tower (Eckardt, 2022). The final sub-system of the WT is the support structure, it consists of the foundation and a transition piece. The foundation of an OWT can have a fixed or floating structure. The fixed platform types cause high-frequency vibrations from rotating blades and flexibility of the tower prevent resonances at natural frequencies. This significantly reduces fatigue life as water depth increases. The floating supported structures are more flexible in terms of construction and installation procedures. In addition, the floating structures can be easily removed from the OWF (Perveen et al., 2014). Scotland developed the first commercial floating OWF, Hywind (Jalili et al., 2023). Figure A.1 provides an overview of the different fixed and floating foundation types, and corresponding water depth

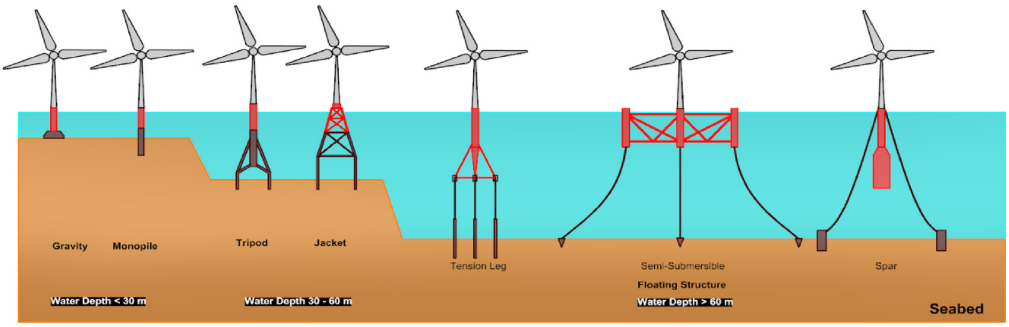

Figure A.1: Foundation types with corresponding water depth [m] (Chirosca et al., 2022)

As shown in figure A.1, the type of foundation depends on the depth of the water. The different types of fixed foundations are gravity-based structures (GBS), monopiles, tripods, tripiles, suction buckets and jackets. For shallow water of depths less than 30m, GBS and monopiles can be used. The GBS has a large surface area and weight, which protects the turbines from the forces of waves and wind (Piasecka et al., 2019). This foundation is usually used for seabeds with high bearing capacity, however, a prepa-

ration of the seabed is still needed (Eckardt, 2022). Monopiles are most commonly implemented due to their adaptability to different types of seabeds, easy fabrication and low cost (Topham, McMillan, et al., 2019). For slightly deeper water, between 30m and 60m, the tripods, tripiles, suction buckets, and jackets can be installed as foundations. The tripods and triple foundation types are attached to three poles so that they can be used in deeper what. These foundations are usually used on a relatively flat seabed because they are not suitable for rocky substrates. The jacket foundation consists of a large four-legged structure placed symmetrically off the main axis of the entire structure. This foundation is usually used for the OSS (Eckardt, 2022). When the water gets even deeper than 60m, problems arise with the foundations mentioned above. A solution to this are floating foundations. In this type of foundation, the entire structure is held in place by ropes/chains that are the connection between the structure and the seabed. The main types of floating foundations are the tension-leg platform (TLP), semi-submersible type, spar-buoys and pontoon (Chirosca et al., 2022). The TLP foundation are often rectangular floats that are pulled slightly underwater and tensioned by taut lines or chains. The advantage of these foundations is that they can be set up and tested in a drywell on shore. The semi-submersible type foundation are usually triangular or square scaffolds made of concrete or steel that promise a particularly low slope of chain. The spar-buoys foundation are large hollow concrete/steel cylinders that require about 200m of water depth and are therefore very expensive to install (Eckardt, 2022). Using the information in table B.1, different information can be obtained from. In terms of foundations types, it is clear that the most implemented structure in the North Sea is monopiles, accounting for 78%. The other 22% of the implemented foundations in the North Sea are jackets, tripods, tripiles, suction buckets, gravity and floating-based. The second component of the subsystem the support structure is the transition piece. A transition piece is placed on top of the foundation, connecting the foundation to the WT tower. On the outside of the transition piece is a boat jetty, the access system, between platforms and a railing. On the inside of the transition piece is the transformer, medium voltage switch gear system and corrosion protection system. It varies by type of foundation how and where the transition piece is connected. For jackets, tripods and tripiles foundations, the transition piece is connected to the foundation on land. For monopile foundations, the transition piece is connected to the foundation element via a screw or grout connection. Grouting is the process of filling the gap between the monopiles and the transition piece with concrete that cures under water. It is a relatively inexpensive connection since it does not require flanges. However, before degradation, this joining technique is irreversible. Conversely, a flange connection involves high material costs due to the prefabrication of flanges with large diameter and wall thickness, but subsequent dismantling is easy (Eckardt, 2022).

Offshore substation

Second, the system the OSS will be discussed. This itself consists of several sub systems, namely the topside of the OSS and support structure. The OSS is one of the largest interconnected components and is another important subsystem of the OWF. This is where the electricity enters the OSS through the inter-array (IA) cables from the OWF at a voltage of 33kV usually, then the transformation occurs at the OSS to 66/155kV, where after the electricity leaves the OSS towards the land (grid) with the export cables (EC) (Eckardt, 2022). Whether an OSS is necessary depends on the total installed capacity of an OWF and its distance from the coast. At the time when the total installed capacity is less than 30 MW, an OSS is not needed. If the total installed capacity is more than 30 MW but less than 120 MW, an OSS would only be needed if the OWF is more than 10km from the coast. However, if the total installed capacity is more than 120MW, an OSS is needed regardless of the distance between the OWF and the coast (Huang et al., 2017). The topside of the OSS consists of several decks on which components are located that are required for the high transformation from an input voltage of typically of 33kV to an output voltage of 66 or 155 kV for the EC. For this transformation, the following main electrical components and sub-components must be present; switch equipment on the input and output side, a transformer, compensation coils, protection control, and communication technology, auxiliary power generation and distribution systems, emergency power supply, surge protection, control systems, and cooling systems. The support structure of the OSS is the same as that of the WT. Most OSS are built on jacket foundations anchored to ground piles. However, jacket foundations with suction buckets or monopiles can also be used (Eckardt, 2022).

Meteorological mast
The next system is the MM, also called Met Mast (MM). This system is used for measuring wind speeds in the wind energy sector (GL, 2014). The MM consists of the same sub systems as the OSS, namely the topside of the MM and support structure. However, both the topside and support structure of the MM are a lot smaller and lighter in weight than those of OSS (Jalili et al., 2023).

Transmission system
The subsequent system is the transmission system. This consists of several subsystems, namely the inter array cables (IAC), the EC and possibly a converter system. Two factors determine the connection type of the transmission system. The first factor is the distance between the OWF and the technically possible connection point on land, and the second is the amount of electricity being transmitted. Depending on these two factors, two different transmission systems are possible. For the first type of transmission system, both collection and transmission are done by a three-phase cable for a 50 Hz AC system. Until now, 33kV connections are usually used. Then the electricity in the OSS is transformed from 33kV to 66 / 155 kV and then transported to the mainland. For this transmission system, a maximum cable length of about 60-80km is possible. For the second type of transmission system, only the collection is done by a three-phase cable for a high voltage direct current (HVDC) system on land. After the OSS, the electricity is first transmitted to a converter station, where the electricity is converted to direct current (DC) and then transmitted to another converter station on land via a DC submarine cable where it is converted to alternating current (AC) and then delivered back to the grid. For this transmission system, distances between 100-200km make sense as they are more cost effective and less transmission losses over long distances (Eckardt, 2022). High voltage alternating current (HVAC) and HVDC are the two different ways of high voltage power transmission. HVAC has undersea transmission limitations in terms of transmission distance, high power losses and resonance problems. Due to these drawbacks, HVDC transmission systems are preferred. Especially for relatively large OWFs at a distance of more than 50 km, the most economical solution is an HVDC connection (Perveen et al., 2014). The first sub-system of the transmission system are the IA cables. These are usually 33kV three-phase cables. The individual cable strands to which the WTs are connected converge at the OSS. The cross-sectional area of the IA cables increases toward the OSS as more electricity runs through them. The cross-sectional area of the IA cables varies between 300-400mm2. The length of the cables depend on the OWF layout and the number of WTs in the OWF. The IA cables are buried in the seabed usually at a burial depth of 1-2m. The second sub-system of transmission is the alternating current export cable. This cable connects the OSS of the OWF to the converter platform or onshore substation. These cables are usually 155kV three-phase cables. Depending on the connected load, there are one or more EC. The length of EC depends on the distance between the OSS of the OWF and the converter platform or substation. Similar to the IAC, EC are buried in the seabed. The third optional sub-system of the transmission system is a converter station. A converter station consist of a topside, substructure and cable access tower. Depending on the size of the OWF, the collected electricity may or may not be routed to an offshore converter station. In this converter station, the power is transformed to 320 kV by the transformer, then it is rectified and smoothed in the rectifiers to allow transmission via HVDC to shore (Eckardt, 2022).

Scour protection
The last system discussed is SP. Scour is caused by the interaction of the substructure and water. The development of scour is influenced by several factors such as current velocity and soil conditions. Several systems exist to counteract scour. The most common systems are concrete mattress placed around the foundation pile, riprap based on natural stone, gravel or sand and geocontainers (Eckardt, 2022).

B

Overview OWFs in North Sea region

Wind Farm Name	Turbines	Commissioned	Decommissioning	Distance to shore [km]	Foundation type
Horns Rev I	80 × Vestas V80-2MW	2002	By 2030	18	Monopiles
Scroby Sands	30 × Vestas V80-2MW	2004	By 2030	2.5	Monopiles
Kentish Flats	30 × Vestas V90-3MW	2005	By 2030	10	Monopiles
Beatrice Demonstration Project	2 × REpower 5M	2007	By 2030	10	Monopiles
Egmond aan Zee	36 × Vestas V90-3MW	2008	By 2030	13	Monopiles
Princess Amalia	60 × Vestas V80-2MW	2008	By 2030	26	Monopiles
Lynn and Inner Dowsing	54 × Siemens SWP-3.6-107	2009	By 2030	5	Monopiles
Hywind	1 x Siemens SWP-2.3-82	2009	By 2030	10	Floating - spar
Horns Rev II	91 × Siemens SWP-2.3-93	2009	By 2030	32	Monopiles
Alpha Ventus	6 × Multibrid M5000, 6 × REpower 5M	2010	By 2040	56	Tripod
Gunfleet Sands 1 & 2	48 × Siemens SWP-3.6-107	2010	By 2040	7	Monopiles
Thanet	100 × Vestas V90-3MW	2010	By 2040	11	Suction bucket jacket
Belwind	55 × Vestas V90-3.0MW 55 × Alstom Haliade 150-6MW	2010	By 2040	46	Monopiles
Sheringham Shoal	88 × Siemens SWT-3.6-107	2012	By 2040	17	Monopiles
Greater Gabbard	140 × Siemens SWT-3.6-107	2012	By 2040	23	Monopiles
Thorntonbank	6 × REpower 5M, 48 × Senvion 6M	2013	By 2040	27	GBS and Jackets
Lincs	75 × Siemens SWT-3.6-120	2013	By 2040	8	Monopiles
BARD Offshore 1	80 × BARD 5.0	2013	By 2040	100	Tripile
London Array	175 × Siemens SWT-3.6	2013	By 2040	20	Monopiles
Teesside	27 × Siemens SWT-2.3	2013	By 2040	1.5	Monopiles
Meerwind Süd/Ost	80 × Siemens SWT-3.6-120	2014	By 2040	53	Monopiles
Northwind	72 x Vestas V90-3MW	2014	By 2040	37	Monopiles
Riffgat	30 x Siemens SWT-3.6-120	2014	By 2040	15	Monopiles
Amrumbank West	80 × Siemens SWT-3.6-120	2015	By 2040	40	Monopiles
Borkum Riffgrund I	78 × Siemens SWT-4.0-120	2015	By 2040	55	Suction bucket jacket
Butendiek	80 × Siemens SWT-3.6	2015	By 2040	35	Monopiles
DanTysk	80 × Siemens SWP-3.6-120	2015	By 2040	70	Monopiles
Global Tech I	80 × Multibrid M5000	2015	By 2040	110	Tripod
Eneco Luchterduinen	43 x Vestas V112/3000	2015	By 2040	24	Monopiles
Humber Gateway	73 x Vestas V112-3MW	2015	By 2040	10	Monopiles
Nordsee Ost	48 × Senvion 6.2M126	2015	By 2040	55	Four-legged jacket
Trianel Windpark Borkum	40 × Areva M5000-116	2015	By 2040	45	Tripod
Westermost Rough	35 × Siemens SWT-6.0	2015	By 2040	8	Monopiles
Gode Wind 1 & 2	97 × Siemens SWT-6.0-154	2016	By 2050	42	Monopiles
Dudgeon	67 × Siemens SWT-6.0-154	2017	By 2050	32	Monopiles
Gemini	150 × Siemens SWT-4.0	2017	By 2050	55	Monopiles
Hywind (United Kingdom)	5 × Siemens SWP-6.0-154	2017	By 2050	29	Floating - spar
Nobelwind	50 × Vestas V112-3.3MW	2017	By 2050	47	Monopiles
Nordergründe	18 × Senvion 6.2M126	2017	By 2050	15	Monopiles
Nordsee One	54 × Senvion 6.2M126	2017	By 2050	40	Monopiles
Sandbank	72 × Siemens SWT-4.0-130	2017	By 2050	90	Monopiles
Veja Mate	67 × Siemens SWT-6.0-154	2017	By 2050	95	Monopiles
Borkum Riffgrund II	56 × MHI Vestas V164	2019	By 2050	54	Monopiles and Suction bucket jackets
Deutsche Bucht	31 × MHI Vestas V164-8.0MW	2019	By 2050	95	Monopiles
Hohe See	48 × Siemens SWT-7.0-154	2019	By 2050	90/100	Monopiles
Horns Rev III	49 × MHIVestas V164-8.3MW	2019	By 2050	30	Monopiles
Merkur	66 × GE Haliade 150-6MW	2019	By 2050	45/47	Monopiles
Norther	44 × Vestas V164-8.4MW	2019	By 2050	23	Monopiles
Albatros	16 × Siemens SWT-7.0-154	2020	By 2050	95	Monopiles
Borssele I–II	94 × Siemens SWT-8.0-154	2020	By 2050	22	Monopiles
Northwester 2	23 x Vestas V164-9.5MW	2020	By 2050	52	Jacket
Rentel	42 x Siemens SWT 7.0-154	2020	By 2050	34	Monopiles
Mermaid	28 x Siemens SWP 8.4MW	2020	By 2050	54	Monopiles
Seastar	20 x Siemens SWP 8.4MW	2020	By 2050	40	Monopiles
Borssele III–IV	77 × MHI Vestas V164 9.5MW	2021	By 2060	22	Monopiles
Borssele V	2 × MHI Vestas V164 9.5MW	2021	By 2060	24	Monopiles
Kaskasi	38 × Siemens Gamesa SG 8.0-167DD	2022	By 2060	35	Monopiles
Hywind Tampen	11 × Siemens SG 8.0-167 DD	2023	By 2060	140	Floating - spar
Hollandse Kust Noord	69 x Siemens Gamesa 11.0-200DD	2023	By 2060	18.5	Monopiles

Table B.1: Decommissioning timeline of OWFs in the North Sea region, with distance to shore and foundation type

C

Description of vessels utilised in OWF decommissioning

- Anchor handling tug supply
  An anchor handling tug supply (AHTS) is a large vessel, supplying both tugs and anchors to oil rigs and freight ships. Because of this, the AHTS has a key function in the installation of floating WTs. In fact, they provide the deployment and retrieval of anchors and mooring lines which keep the floating turbines in place (Serraris et al., 2024).
- Barge
  Barges are transport vessels, and cannot perform crane operations. It's a vessel with a large deck and flat hull, and has no propulsion of its own and therefore must be pulled and held in place by tugs. As a result, this vessel suffers from wave motion, and is therefore of limited use. The barge is used during OWF decommissioning to transport components, constructions, cables or even bulk materials (Eckardt, 2022).
- Cable laying barge
  The cable laying barge (CLB) is a vessel used for a specific process within OWF decommissioning, namely to remove IAC and EC. These types of vessels are equipped with large drums for pulling and storing the cables (Gjødvad & Ibsen, 2016). Similar to the barge, the CLB does not have its own propulsion. Therefore the CLB must be pulled and held in place by tugs. As a result, this vessel suffers from wave motion, and is therefore of limited use.
- Cable laying vessel
  The CLV has the same specifications as the CLB. However, the only difference is that a CLV actually has its own propulsion system. They also use sophisticated speed and positioning control systems to prevent the cable from being damaged during removal. (Eckardt, 2022).
- Crane vessel
  Crane vessels have powerful cranes for lifting large components. Some crane vessels are semi-submersible vessels and therefore reduce the impact of waves. For safe and accurate positioning, crane vessels also have GPS-controlled dynamic positioning. These mobile floating cranes are also sometimes used for transportation. The crane vessel is mainly used during OWF decommissioning to lift large components of the OSS onto a transport vessel or to dismantle foundations (Eckardt, 2022).
- Deck carrier
  Deck carriers are also transport vessel. However, the type of vessel does have its own propulsion. It is further equipped with safety systems and equipment for safe operations in conjunction with JUVs. The deck carrier is used during OWF decommissioning to transport OWTs components or foundations using a feeder concept (Eckardt, 2022).
- Derrick crane barge
  The DCBV can also be used for the removal of the SPL. When using this vessel, the removed SP will be transported to land on a barge pulled by tugs. This since the DCBV is basically a floating crane. The use of an ROV is relevant for inspection and support for offshore operations (Jalili

et al., 2023). The DCBV does not have its own propulsion since it is a barge and not a vessel. As a result, the removed components of the OWF will be transported to shore by a transport vessel. As a result, this type of vessel uses the feeder concept as its transportation strategy.

- Dredger
  The dredger is also used for a specific process within OWF decommissioning, namely the removal of the SPL. The type of dredger varies with the operational water depth. The dredgers are equipped with dynamic positioning and, in some cases, an ROV to control the removal work (Eckardt, 2022).
- Heavy lift vessel
  Heavy lift vessel (HVL) are designed to lift large components. There are different types and variations of this vessel, namely floating sheerlag cranes, monohull crane vessel, catamaran cranes and semi-submerging vessels lifting without cranes (Gjødvad & Ibsen, 2016). The HVL is generally used during the WT topside and substructure removal (Topham & McMillan, 2017).
- Jack-up barge
  The jack-up barge (JUB) is a specialized barge equipped with a jack-up system, of 4 or 6 legs, for stable operation in water depths up to 40m. In addition, the JUB has a main crane, which has a capacity of 1,500 tons. Other components of the JUB include GPS-controlled dynamic positioning, accommodation for crew and sometimes a helideck. The JUB does not have its own propulsion since it is a barge and not a vessel. As a result, the removed components of the OWF will be transported to shore by a transport vessel (Gjødvad & Ibsen, 2016). This makes the JUB automatically part of the the transport strategy called feeder concept, where it executes the feeder vessel's operations. The JUB is used during OWF decommissioning for dismantling the WT topside, but also sometimes for WT substructure, OSS and MM (Jalili et al., 2023).
- Jack-up vessel
  The JUV has the same specifications as the JUB, but additionally has its own propulsion. Therefore, this type of vessel transports the removed components to shore (Gjødvad & Ibsen, 2016). As a result, the JUV is often part of the so-called shuttle concept transportation strategy. Therefore it is characterized by sufficient deck space for transporting parts from multiple WT topsides (Eckardt, 2022). The JUV, similarly to the JUB, is used during OWF decommissioning for dismantling the WT topside, but also sometimes for WT substructure, OSS and MM (Jalili et al., 2023). A jack-up vessel exists in various sizes. The most commonly used can be categorized into two groups, medium or large JUVs. Besides OWF decommissioning, JUVs are also often used during installation of the OWTs. Therefore, these vessels are also called wind turbine installation vessels (WTIV) (Gjødvad & Ibsen, 2016).
- Multicat vessel
  A Multicat is a multi-purpose vessel used primarily for offshore operations. It is equipped with powerful winches, cranes and a spacious deck, making it ideal for tasks such as towing, anchor handling and dredging support ("MULTICAT - GRS", 2024).
- Rock dumping vessel
  A rock dumping vessel (RDV) can be used during the SPL removal stage. In this stage, the RDV is then in fact used to fill the voids where the foundation has been removed. Therefore, this vessel is only used during complete removal (Jalili et al., 2023).
- Semi-submersible crane vessel
  Semi-submersible crane vessels (SSCVs) consist of a platform and six or eight supporting columns evenly spaced. Each side is stabilized by a single pontoon, providing a robust foundation (Serraris et al., 2024). Because of this increased stability, this type of vessel has a very large crane capacity (Gjødvad & Ibsen, 2016). A SSCV with proper lifting height, reach and loading capacity, is used for topside installation, and hence decommissioning, on site.
- Other smaller (support) vessels
  - Crew transport vessel
    This is a transport vessel for personnel and baggage. Crew transport vessels (CTVs) are relatively small vessels, fitting up to 24 men. They are used during all phases of an OWF. There are several types of CTVs, of which the three most commonly used are the monohull, catamaran and small waterplane are twin hull (SWATH). The monohull is single-hull and

thereby offers flexibility, which results in a variety of tasks. The catamaran, on the other hand, is double hulled. Which provides improved stability for safe and effective transfer of crew personnel to floating WTs. Finally, a SWATH, also double-hulled, offers minimal contact with water surface in addition to a stable platform. This design is ideal for crew operations in challenging weather conditions at sea (Serraris et al., 2024).

- Offshore support vessel
  An offshore support vessel (OSV) provides multifunctional support including transportation of crew and equipment, and operational assistance in removal processes. The lease of an OSV is much cheaper than that of a JUV. Therefore, the foundation preparation stage, among others, is often performed by an OSV (Jalili et al., 2023).
- Remotely operated vehicle
  A ROV is an underwater robot, which has no propulsion of its own, used for inspections and support of subsea activities. These vehicles are controlled from the surface, equipped with a camera, tools and sometimes sensors, allowing detailed operations. They are used for precise tasks such as cutting underwater cables and inspecting substructures (Jalili et al., 2023).
- Service operation vessel
  A service operation vessel (SOV) serves as the primary base for executing tasks, in the different life cycle phases of an OWF, on offshore installations. They are equipped with machinery needed to perform these tasks. In addition, the vessel provides accommodation and work and storage space for personnel (Serraris et al., 2024). Using an SOV has a number of advantages over using a CTV. These include the ability of this vessel to carry more personnel, as well as the stable walk-to-work platform (Gray, 2021).
- Survey / Research vessel
  These vessels examine the seabed or marine environment, among other things. They are designed and equipped according to the respective task and are mainly used during OWF decommissioning for monitoring and documenting the cleanliness of the seabed (Eckardt, 2022).
- Tug boats
  Tug boats (TBs) are smaller vessel, which are mainly used for transporting large components. Those components are stored on barges. They pull and hold barges in place. The most commonly used can be categorized into two groups: lead or assist TBs.
- Walk-to-work-vessel
  A W2WV is designed to safely transfer personnel and equipment from the vessel to offshore platforms or wind turbines via a motion-compensated walkway (Eckardt, 2022). Generally, the vessel is used for removing the IAC, and when removing but also when leaving the EC in situ.

D

Detailed results of OAT sensitivity analysis

Table D.1: Results for changing fuel consumption in OAT sensitivity analysis for the decommissioning of OWF Lincs Limited

[%]	CO_2 [kg]	CH_4 [kg]	N_2O [kg]	CO_2-eq. (20 years) [kg]	CO_2-eq. (100 years) [kg]
-20	3.427e+06	44.15	175.27	3.479e+06	3.477e+06
-10	3.856e+06	49.67	197.18	3.914e+06	3.911e+06
-5	4.070e+06	52.43	208.13	4.131e+06	4.128e+06
0	4.284e+06	55.19	219.09	4.349e+06	4.346e+06
5	4.499e+06	57.95	230.04	4.566e+06	4.563e+06
10	4.713e+06	60.71	241.00	4.784e+06	4.780e+06
20	5.141e+06	66.22	262.90	5.219e+06	5.215e+06

Table D.2: Results for changing LCV in OAT sensitivity analysis for the decommissioning of OWF Lincs Limited

[%]	CO_2 [kg]	CH_4 [kg]	N_2O [kg]	CO_2-eq. (20 years) [kg]	CO_2-eq. (100 years) [kg]
-20	4.284e+06	44.15	175.27	4.336e+06	4.333e+06
-10	4.284e+06	49.67	197.18	4.342e+06	4.340e+06
-5	4.284e+06	52.43	208.13	4.346e+06	4.343e+06
0	4.284e+06	55.19	219.09	4.349e+06	4.346e+06
5	4.284e+06	57.95	230.04	4.352e+06	4.349e+06
10	4.284e+06	60.71	241.00	4.355e+06	4.352e+06
20	4.284e+06	66.22	262.90	4.362e+06	4.358e+06

Table D.3: Results for changing thermal efficiency in OAT sensitivity analysis for the decommissioning of OWF Lincs Limited

[%]	CO_2 [kg]	CH_4 [kg]	N_2O [kg]	CO_2-eq. (20 years) [kg]	CO_2-eq. (100 years) [kg]
-20	4.284e+06	44.15	175.27	4.336e+06	4.333e+06
-10	4.284e+06	49.67	197.18	4.342e+06	4.340e+06
-5	4.284e+06	52.43	208.13	4.346e+06	4.343e+06
0	4.284e+06	55.19	219.09	4.349e+06	4.346e+06
5	4.284e+06	57.95	230.04	4.352e+06	4.349e+06
10	4.284e+06	60.71	241.00	4.355e+06	4.352e+06
20	4.284e+06	66.22	262.90	4.362e+06	4.358e+06

Table D.4: Results for changing EF_{CO_2} in OAT sensitivity analysis for the decommissioning of OWF Lincs Limited

[%]	CO_2 [kg]	CH_4 [kg]	N_2O [kg]	CO_2-eq. (20 years) [kg]	CO_2-eq. (100 years) [kg]
-20	3.427e+06	55.19	219.09	3.492e+06	3.489e+06
-10	3.856e+06	55.19	219.09	3.920e+06	3.917e+06
-5	4.070e+06	55.19	219.09	4.135e+06	4.132e+06
0	4.284e+06	55.19	219.09	4.349e+06	4.346e+06
5	4.499e+06	55.19	219.09	4.563e+06	4.560e+06
10	4.713e+06	55.19	219.09	4.777e+06	4.774e+06
20	5.141e+06	55.19	219.09	5.206e+06	5.203e+06

Table D.5: Results for changing EF_{CH_4} in OAT sensitivity analysis for the decommissioning of OWF Lincs Limited

[%]	CO_2 [kg]	CH_4 [kg]	N_2O [kg]	CO_2-eq. (20 years) [kg]	CO_2-eq. (100 years) [kg]
-20	4.284e+06	44.15	219.09	4.348e+06	4.345e+06
-10	4.284e+06	49.67	219.09	4.348e+06	4.346e+06
-5	4.284e+06	52.43	219.09	4.349e+06	4.346e+06
0	4.284e+06	55.19	219.09	4.349e+06	4.346e+06
5	4.284e+06	57.95	219.09	4.349e+06	4.346e+06
10	4.284e+06	60.71	219.09	4.349e+06	4.346e+06
20	4.284e+06	66.22	219.09	4.350e+06	4.346e+06

Table D.6: Results for changing EF_{N_2O} in OAT sensitivity analysis for the decommissioning of OWF Lincs Limited

[%]	CO_2 [kg]	CH_4 [kg]	N_2O [kg]	CO_2-eq. (20 years) [kg]	CO_2-eq. (100 years) [kg]
-20	4.284e+06	55.19	175.27	4.337e+06	4.334e+06
-10	4.284e+06	55.19	197.18	4.343e+06	4.340e+06
-5	4.284e+06	55.19	208.13	4.346e+06	4.343e+06
0	4.284e+06	55.19	219.09	4.349e+06	4.346e+06
5	4.284e+06	55.19	230.04	4.352e+06	4.349e+06
10	4.284e+06	55.19	241.00	4.355e+06	4.352e+06
20	4.284e+06	55.19	262.90	4.361e+06	4.358e+06